UNIVERSITY OF LJUBLJANA

Faculty of Mechanical Engineering

APPLICATION OF NUMERICAL METHODS AND COMPUTATIONAL SIMULATIONS TO PLASMA–SHEATH CONDITIONS FOR VIRTUAL CATHODES UNDER HIGH EMISSION CURRENTS

Master Thesis

Submitted to the Faculty of Mechanical Engineering
of the University of Ljubljana
for the acquirement of a scientific degree of Master of Science

Janez Krek

Mentor: Doc. dr. Leon Kos

Co-mentor: Prof. dr. Jožef Duhovnik

Ljubljana, June 2015

Univerza v Ljubljani
Fakulteta za strojništvo

Aškerčeva cesta 6
1000 Ljubljana, Slovenija
telefon (01) 47 71 200
faks (01) 25 18 567
dekanat@fs.uni-lj.si

Naš znak: 0/10-11/15
Tekoča štev.: **M/1089**
Datum: 19.1.2015

ODLOČBA

Komisija za podiplomski oz. doktorski študij Fakultete za strojništvo v Ljubljani je na svoji seji, dne 17.11.2003 in s spremembami dne 5.9.2008, 10.2.2014 ter 12.1.2015

sklenila:

Janez Krek, univ.dipl.inž.
je slušatelj podiplomskega študija in se mu:

1. odobri dokončanje študija po vpisanem programu **do 30. 9. 2016**, tj. vključno z zagovorom magistrskega dela.

2. odobri tema magistrskega dela z naslovom:
Aplikacija numeričnih metod in računalniških simulacij za določanje pogojev pojava navidezne katode v plinskih diodah ter karakterizacijo pri velikih emisijskih tokovih

3. potrdi mentor: *doc.dr. Leon Kos*
4. in somentor: *prof.dr. Jožef Duhovnik*

5. priznajo izpiti iz predmetov: Variacijski račun (dr. Krušič)
Linearna algebra (dr. Krušič)
Teorija konstruiranja z uporabo računalnika (dr. Duhovnik)
Metode umetne inteligence (dr. Bratko)

6. potrdi komisija za zagovor seminarjev, in sicer:
   1. seminar: prof.dr. Jožef Duhovnik, prof.dr. Siegbert Kuhn, Austria, izr.ddr. Tomaž Gyergyek, (UL, FE)
   2. seminar: doc.dr. Leon Kos, prof.dr. Jožef Duhovnik, izr.prof.ddr. Tomaž Gyergyek (UL, FE)

7. odobri pisanje magistrske naloge v angleškem jeziku z naslovom:
Application of numerical methods and computational simulations to plasma-sheath conditions for virtual cathodes under high emission currents

S to odločbo se anulirata prejšnji odločbi pod štev. 0/10-15/14 z dne 14.2.2014 in 1401/03 z dne 26.11.2003 ter sklep komisije pod štev. 3010/08 z dne 5.9.2008.

UNIVERZA V LJUBLJANI • FAKULTETA ZA STROJNIŠTVO •

Prof.dr. Mitjan Kalin,
prodekan za pedagoško dejavnost
II. in III. stopnje

Dostavljeno:
- kandidatu
- mentorju
- somentorju

Acknowledgments

First, I would like to express my sincere gratitude to my colleague and friend, dr. Nikola Jelić, without whom this thesis would never have become a reality. It is his great unselfishness and persistence in unfolding the mysteries of plasma physics that dragged me towards finishing this thesis.

To my supervisor, doc. dr. Leon Kos, who was an almost endless source of wisdom and knowledge that helped me evolve from a curious student to a colleague. I will be always indebted to prof. dr. Jožef Duhovnik, who offered me the possibility to be part of his research group, to encourage and support my development as researcher in various fields. I would like to thank prof. John P. Verboncoeur for advice on research in the early stages of this thesis.

I thank my fellow lab mates in LECAD, who, each in their own way, helped me during all those years.

Last but not least, I would like to thank my wife for her support and encouragement in times when the end seemed far, far away.

koda: M/1089 UDK 004.942:519.876.5(043.2)

Janez Krek

APLIKACIJA NUMERIČNIH METOD IN RAČUNALNIŠKIH SIMULACIJ ZA DOLOČANJE POGOJEV POJAVA NAVIDEZNE KATODE V PLINSKIH DIODAH TER KARAKTERIZACIJO PRI VELIKIH EMISIJSKIH TOKOVIH

Ključne besede:
plazemski plašč, računalniške simulacijske metode, razelektritev v diodi, virtualna katoda, Particle-In-Cell (PIC) metoda, brezmrežna treecode metoda

PACS:
52.25.Dg, 02.60.Nm, 52.40.Kh, 52.65.-y, 94.20.Fg, 95.75.Pq, 02.70.-c, 52.58.-c

Izvleček:
Plašč plazme volumsko predstavlja majhen, vendar zelo pomemben, del industrijskih, laboratorijskih ali fuzijskih plazemskih naprav. V plašču se dogajajo velike časovne in prostorske spremembe parametrov plazme (električno polje, potenciali, itd.). V magistrskem delu je za modeliranje plazemskega plašča in pogojev nastanka virtualne katode uporabljen model planarne diode. Predstavljeni so teoretični (fizikalni) modeli popisa nastanka virtualne katode ter primeri simulacije njenega nastanka s preizkušenim simulacijskim programom XOOPIC v 2D prostoru. V XOOPIC, ki 2D Particle-In-Cell (PIC) koda, so bile za ugotovljene pomanjkljivosti dograjene izboljšave. Kot nov prispevek je bila dograjeno določanje gradientov električnih polj. Pomanjkljivosti odpravlja predstavljena brezmrežna metoda treecode (TC), ki je bila dodana v obstoječo 1D simulacijsko kodo. Predstavljeni so rezultati simulacij s PIC in TC programi kot tudi primerjava rezultatov obeh simulacijskih programov.

Code nr: M/1089 UDC 004.942:519.876.5(043.2)

Janez Krek

APPLICATION OF NUMERICAL METHODS AND COMPUTATIONAL SIMULATIONS TO PLASMA–SHEATH CONDITIONS FOR VIRTUAL CATHODES UNDER HIGH EMISSION CURRENTS

Keywords:
plasma sheath, computer simulation methods, discharge in diode, virtual cathode, Particle-In-Cell (PIC) method, gridless treecode method

PACS:
52.25.Dg, 02.60.Nm, 52.40.Kh, 52.65.-y, 94.20.Fg, 95.75.Pq, 02.70.-c, 52.58.-c

Abstract:
A plasma sheath, in terms of volume, represents a small but very important part of industrial, laboratory or fusion plasma devices. In a plasma sheath one can observe the large time and space changes of the plasma parameters, e.g., the electric field, potential, etc. In this thesis, a planar diode was used to model the plasma sheath and the conditions for the creation of a virtual cathode. Theoretical (physics) models and simulations in 2D space with the well-known simulations application XOOPIC are presented. For XOOPIC, which is a 2D Particle-In-Cell (PIC) code, the shortcomings and improvements are presented. One of the improvements was the computing of the electric field gradients. Some of the shortcomings are addressed with the presented gridless treecode (TC) method that was used in a new, stand-alone simulation code and also added to the existing 1D simulation code OOPD1, alongside the existing PIC method. The results acquired with the PIC and TC simulation codes are presented, together with a comparison of the results of both codes.

Contents

Acknowledgments **v**

Izvleček **vii**

Abstract **ix**

Notation **xix**

1 Introduction **1**
1.1 Scientific/engineering problem identification and methodological approach . . . 1
1.2 Overview of the investigations related to virtual cathode appearance . 2
1.2.1 Physical background . . . 2
1.2.2 Simulation methods background . . . 8
1.3 Thesis overview . . . 9

2 Plasma physics and computer simulations **11**
2.1 Plasma background . . . 11
2.1.1 Basic plasma properties and equations . . . 12
2.2 Computer-simulation methods . . . 12
2.2.1 Fluid model for plasma description . . . 13
2.2.2 Kinetic model for the plasma description . . . 14
2.3 Particle-In-Cell (PIC) method . . . 15
2.4 The treecode (TC) method . . . 17
2.4.1 Building a tree . . . 19
2.4.2 Multipole Acceptance Criteria (MAC) . . . 23
2.4.3 Use of treecode (TC) method in simulation code . . . 25

3 Comparison of the PIC and TC methods in simple plain diode **27**
3.1 Theoretical model of a plain diode . . . 28
3.2 Particle-In-Cell (PIC) method . . . 29
3.3 Treecode (TC) method . . . 31
3.4 Results . . . 31
3.4.1 Phase-space comparison for TC from MatLab and C programs 31
3.4.2 Two species diode scenario . . . 34

4 Theory and simulations of thermionic emissions in a simple diode 37
4.1 Langmuir exact solution (theoretical solution) 38
4.2 Semi-approximation solutions 39
4.3 Simulations 39
4.4 Results 40

5 PIC simulations on the plasma-sheath boundary in collisionless plasmas with warm ion sources 43
5.1 Defining the position of the plasma-sheath boundary 44
5.2 Numerical (PIC) simulation 46
5.2.1 Changing the ion source profile during the simulation 47
5.3 Results 49
5.3.1 Influence of strength factor α on the particle distribution . . . 49
5.3.2 Influence of the strength factor α on the particle distribution . 54
5.3.3 Comparing running times of two BIT1 versions 55

6 Gradients in a gas-filled diode during electrical breakdown 57
6.1 Numerical simulation parameters 58
6.2 Results of numerical simulations 60

7 Discussion and conclusion 65

Bibliography 69

A Slovenski povzetek 77
A.1 Uvod 77
A.2 Izvleček vsebine 77
A.3 Sklepi 80

Vita 83

Author's statement 85

List of Figures

1.1 Optional electric circuits in research and applications, shown together with a schematic drawing of a diode with the developed plasma. . . . 3

1.2 Working regimes of gas-filled diode. 4

1.3 Potential profile in diode in different diode regimes. 5

2.1 Simple flowchart of PIC-simulation program with possible Monte Carlo Collisions (PIC-MCC). 16

2.2 Example of tree representation (a) of square domain (b) (image taken from [1]). 18

2.3 Individual steps in generation of tree and dividing domain into subdomains. Node marked as "0" is the "root" node. 20

2.4 Global flowchart for creating tree. 21

2.5 Division of the domain at each stage (level) and the associated trees. 22

2.6 Schematic presentation of different acceptance criteria (MAC). *cm* is the center of mass for a given cluster, s is the max. external dimension of a cluster and b_{max} is the max. distance from the centre of mass to the edge. 24

2.7 Schematic diagram of a particle, cluster and MAC variables in 1D (a) an 2D (b) system. 24

2.8 General flowchart of TC method. 25

2.9 Simplified simulation code snippet presenting main decision in TC method. 26

3.1 Theoretical potential profiles for diode. 29

3.2 Number of "super-particles" in diode in relation to time (a) and potential profiles (b) in various simulation steps in PIC simulation. . . . 30

3.3 Comparison of phase-space diagrams at same simulation time (t=0.45ns) from MatLab (a) and our program in C (b). 32

3.4 Potential (a1, a2), phase-space (b1, b2) and particle density (c1, c2) in one cycle. Left column when the potential is increasing and right column when it is decreasing. 33

3.5 Illustration of the onset of oscillations (T_{onset}) and the oscillation period (T_{osc}) for various ratios of electrons and ions (R) as injected on the left- and right-hand side, respectively, with equal mass, charge and initial velocity. 35
3.6 Illustration of T_{onset} and T_{osc} change depending on electrons and ions injection ratio R ranging from 0% to 100%. 36

4.1 Simplified presentation of plain diode with global coordinate system $(x - \Phi)$ and coordinate system of introduced variables $(\xi - \eta)$. 38
4.2 Universal potential profiles acquired from exact (equation 4.1) and approximate methods (equations 4.4, 4.5 and 4.6). 41
4.3 Comparison of simulation results acquired with PIC and TC methods with the exact solution (equation 4.1) - potential profiles for case with high potential difference between cathode and anode. 41

5.1 The geometry of the system with the position of the coordinate system and a sketch of the potential profile. 47
5.2 Graphical representation of how the area under function is calculated and divided into strips. The total length of the strips (L'_{total}) is used as the upper limit from which new particle positions are randomly selected. 48
5.3 The electron density profile on a logarithmic scale as a function of the local plasma potential Φ as normalised to the electron temperature. 50
5.4 Velocity distribution as a function of the distance from the centre for the case of the smallest density that was simulated (i.e., $\varepsilon = 3.513 \times 10^{-2}$). The shape of the velocity distribution at the plane of symmetry of the system is compared with with the results obtained by Scheuer and Emmert. 50
5.5 The ion temperature profiles (a) and the corresponding local values of γ_i (b) for various ε as functions of the local plasma potential. It is evident that the maximum of γ_i is strongly dependent on the value of ε. 51
5.6 Determination of the plasma-sheath potential as a point in which the ion fluid velocity u_i equals the ion sound velocity $\sqrt{1 + \gamma T_i}$. 53
5.7 Illustration of the method for determining the plasma sheath physical locations from $\Phi(x)$ curves with values Φ_s determined from Fig. 5.6. . 53
5.8 Comparison of our PIC simulation results with the results of Scheuer and Emmert. 54
5.9 Comparison of the potential profile from PIC simulations and theoretical results. 55
5.10 Comparison of simulation computer times needed to run for various simulation steps for $S_i = const$ and $S_i = e^{\Phi(x)}$. 56

6.1 Number of electrons (first column) and ions (second column) during several characteristic moments (times) of the discharge development. Due to the azimuthal symmetry only the upper half of the disk cross-section in the central $z-r$ plane is shown and the system is visually stretched in the z-direction for a better visual resolution of the obtained results. 59
6.2 Total number of ions and electrons (a), ion and electron conduction electric currents to cathode and anode (b), cathode potential (c) and total conduction electric current at electrodes. 61
6.3 Profiles of electric fields $E_r(z,r,t)$ (first column) and $E_z(z,r,t)$ (second column) at times t_3 (first row) and t_4 (second row). 62
6.4 Estimation of radial and axial displacement current density distributions $\varepsilon_0 \partial E_r(z,r,t)/\partial t$ and $\varepsilon_0 \partial E_z(z,r,t)/\partial t$ in (z,r)-plane, done within the time-interval from t_3 to t_4. 62
6.5 Approximate $\varepsilon_0 \partial \vec{E}(z,r,t)/\partial t$ vector-field (between times t_3 and t_4). . 64

A.1 Predstavitev različnih delovnih režimov plinskega odvodnika. 78
A.2 Primer kvadratne računske domene (a) in predstavitev celic v drevesni strukturi (slika iz [1]). 79
A.3 Predstavitev enostavne planarne diode z zunanjim tokokrogom. . . . 80

List of Tables

2.1 Different multipole acceptance criteria and the required condition to be fulfilled for the criteria to be accepted; the parameters are presented in Fig. 2.6. 23

4.1 Simulation case parameters. 40

5.1 Plasma densities (at the plane of symmetry of the discharge), Debye lengths at the centre of the plasma and the corresponding smallness ε-parameters used. 49

Notation

Symbols and abbreviations

A	Atomic number
DC	Direct-Current
e	Elementary charge ($1.60217 \cdot 10^{-19} C$)
E	Strength of the electric field
ε_0	Vacuum dielectric constant ($8.85418 \cdot 10^{-12} F/m$)
ε	Smallness parameter (λ_D / L)
$f_{e,i}$	Electron, ion velocity distribution function (VDF)
$\Gamma_{i,e}$	Ion, electron flux
γ_i	Ion polytropic coefficient
k	Boltzmann constant ($1,38064 \cdot 10^{-23} m^2 kg/s^2 K$)
L	Half length of the system
λ_D	Debye length ($\lambda_D = \sqrt{\frac{\varepsilon_0 k T_e}{n_e e^2}}$)
$m_{e,i}$	Electron, ion mass ($m_e = 9.10938 \cdot 10^{-31} kg$, $m_i \approx A$ 1386.12 m_e)
$n_{i,e,n}$	Ion, electron, neutral number density
PIC	Particle-In-Cell
Φ	Electrostatic potential
R	Ionization rate
TC	TreeCode (method)
$T_{i,e}$	Ion, electron temperature
T_n	Temperature of the neutral gas
θ	Multipole acceptance criteria (MAC)
VDF	Velocity distribution function

Chapter 1

Introduction

1.1 Scientific/engineering problem identification and methodological approach

When designing and operating a plasma device one has to understand its main working principles and the underlying physical laws in detail, which include a description of the volume, surface and plasma boundary conditions, external electric circuit processes and system elements. This highly demanding task requires that one adequately defines *each* necessary parameter or variable at *each* point of the system (device) in space and time, which is a rather demanding task that is seldom completely solved by theoretical means. On the other hand, in a laboratory experiment a large number of parameters for such highly non-linear, self-consistent systems (including the experimental uncertainties originating from measurements, gas-composition properties, material impurities and physical imperfections, etc.) usually offers the scientist the opportunity to clearly distinguish the degree of importance for each parameter compared to other system/discharge parameters. However, in a numerical simulation this is possible simply by introducing or ignoring individual parameters in a series of numerical "experiments". Unfortunately, a plasma as a circuit element is still a complicated element to simulate with a numerical simulation due to the intrinsic presence of several space and time scalings, such as system travelling times and oscillations for light versus heavy particles, various lengths (Debye, plasma and collisional/ionisation length), etc. The thesis first presents the identification of some such characteristic times and lengths in several discharges, with special attention given to the regions of localised strong electric/magnetic fields and their gradients. The investigations include their behaviour in time, looking for special cases when these structures are stable or unstable (monotonic or non-monotonic). The reason for this research originates from the need to keep these structures under control in order to achieve the desired plasma parameters. The

appearance and location of such structures are closely related to the charged particles that originate from outside the quasi-neutral plasma (e.g., due to secondary, field-induced, temperature-emission-caused, intentional beam injections, etc.). The most typical example of such a structure is the so-called virtual cathode. In order to prevent or support their existence, one has to carefully investigate the conditions for its creation or removal. This thesis presents an investigation of the plasma and sheath properties in several discharge scenarios. These scenarios are very different from each other for the purposes of obtaining the necessary information about how to update existing or build new numerical simulation codes. The simulation codes will be developed in such a way that they will be used in a large variety of future investigations/applications of such localised structures (related to high plasma/field gradients). The state of the art of the investigations and numerical simulations are as follows.

1.2 Overview of the investigations related to virtual cathode appearance

1.2.1 Physical background

The gas-filled diode [2, 3] is one of the oldest and one of the most exhaustively investigated problems in the history of plasma physics. It is employed in a wide range of applications: as a basic component in electronic circuits, high-power electric devices, lasers, new material production, nuclear reaction chamber for new isotopes, x-rays, neutron and ion beams' production or as a nuclear fusion device's main chamber [4, 5, 6, 7, 8, 9]. In any of these applications a gas-filled diode essentially transforms and releases an externally stored electrical energy "bank" into a new, physical state: electrical/electromagnetic energy, gas, liquid, material, or even nuclear state and energy. For this reason, a diode must always be part of a closed external electric circuit and should be properly designed and tuned for each particular kind of transformation. A few of the simplest options for an external power supply are shown in Fig. 1.1 and are used in the following: pure DC discharge tube/diode-experiments and applications (G_A), Dense Plasma Focus (DPF) devices (G_B) and the industrial testing of lightening discharges protectors (G_C). Option G_A is the basic experimental device for tuning simultaneously both the current and the potential on a classic direct-current (DC) current-voltage characteristic, where the external resistor R plays an essential role, while the auxiliary capacitor represents a bypass for any AC perturbation (e.g., [10]). Option G_B is employed in processes that require extremely fast transferring of the capacitor bank's electrostatic energy into a highly localised region (e.g., in DPFs [7]). The physical processes therein assume simultaneous imploding electric, magnetic and particle kinetic energy in a self-consistent manner. The

discharge characteristics also depend on the diode geometry, the electrode material, the gas properties, the capacitor bank (C_0), the switch (sw) characteristics, and the "parasitic" impedance (L_0 and Z_{D0}). Option G_C is most frequently designed with specially constructed "ideal" current generators I(t), where the basic requirement is that a diode (such as the surge protectors of a Gas Discharge Arrestor type) should act as a short-cut for the extremely high currents and voltages within a short interval (e.g., several tens of μs after a certain prescribed voltage is detected), otherwise it should behave as an infinitely high resistance. Thus, in contrast to option G_B, the external energy should be released to the ground as soon as possible, with the minimum internal dissipation.

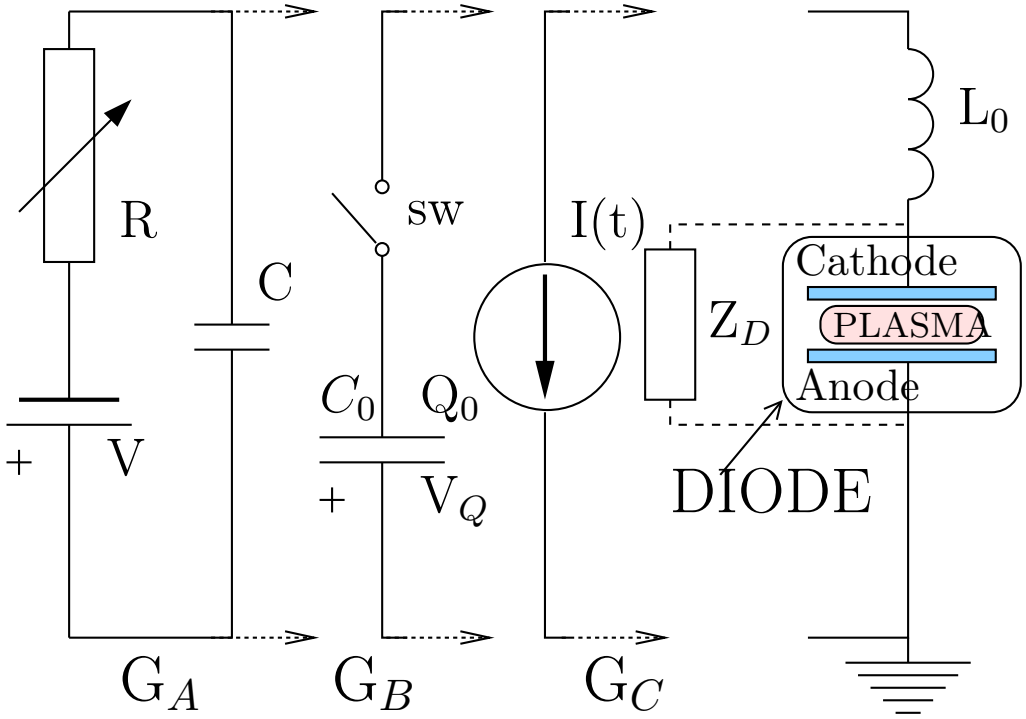

Figure 1.1: Optional electric circuits in research and applications, shown together with a schematic drawing of a diode with the developed plasma.

Although, on one hand, the above experiments and applications work well, the progress towards the optimisation of their performance is relatively slow. Not only have substantially new solutions and designs not appeared for years, but even some fundamental physical aspects within discharges in many widely used and commercially produced devices are not understood and remain unexplained. This is because the processes in gases, materials, and plasma in such devices not only have a complex physical background, but are also so numerous that their effects may considerably mask each other.

The current-voltage characteristic of a diode is a basic indication of its performance, but it is highly dependent on a particular application. The typical experi-

mental DC current-voltage characteristic of the apparently most simple case (a diode within a glass tube) is presented in Fig. 1.2. While it is relatively easy to obtain such a curve under (low-cost) laboratory-setup conditions, its description and understanding requires the identification of a large number of parameters that might be responsible for each of the regimes (as indicated therein). These regimes are essentially related to the degree of ionisation of the so-called "working" gas. It is assumed that the negative electrode (cathode) is capable of emitting a certain number of electrons that can travel to the opposite electrode (anode), either due to their initial kinetic energy or due to their extraction and acceleration in the electric field that is established between the electrodes. If the ionisation can be completely ne-

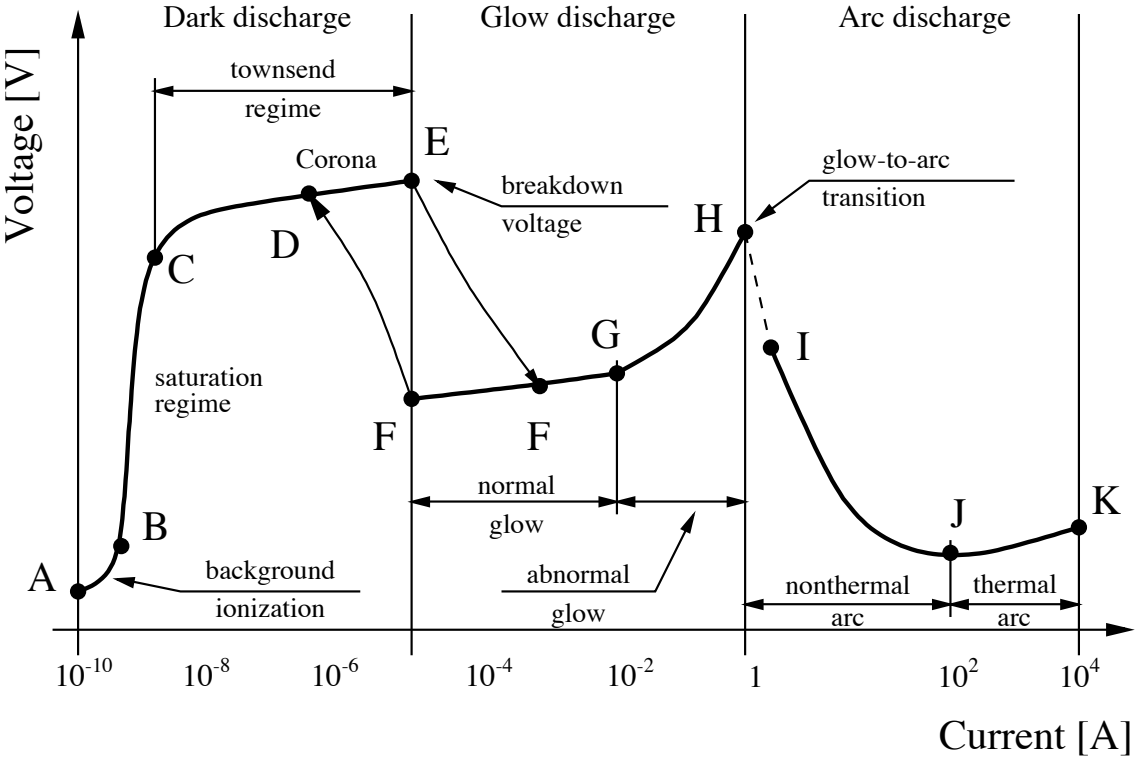

Figure 1.2: Working regimes of gas-filled diode.

glected, the diode is in a plasma-free regime, which corresponds to the section A-B in Fig. 1.2. While the volume ionisation might be neglected, i.e., the between-electrode space (gap) is free of positive charges (ions), the electron density can be built by electrons extracted from the cathode due to various mechanisms (increased cathode temperature, secondary-electron emission, possible beta radiation, etc.). The possible effects of the electron space-charge presence with respect to the potential profile are sketched in Fig. 1.3. The black curves A-D correspond to various electron emissions/currents: vanishing (A), small but non-vanishing (B), co-called "critical" (C) and rather high (D) electron emission/currents. The electron emission/current (space charge effects) for the curves A to D (Fig. 1.2) are obtained along section A-B of the current-voltage characteristics from Fig. 1.2.

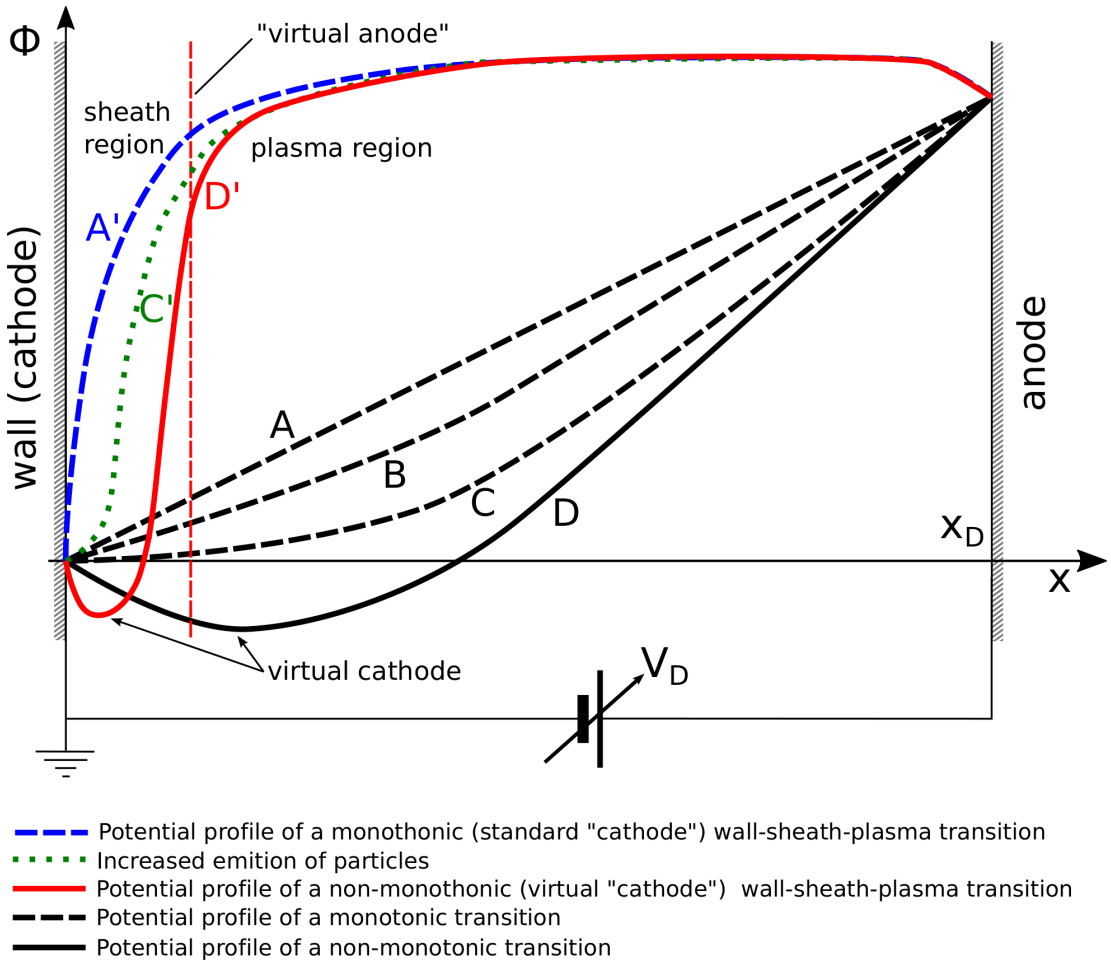

Figure 1.3: Potential profile in diode in different diode regimes.

When the potential profile is monotonic (curves A to C on 1.3) the current-voltage characteristic is described using the Child-Langmuir formula [11]:

$$J = \frac{4\varepsilon_0}{9}\sqrt{\frac{2e}{m_e}}\frac{V_a^{3/2}}{d^2} \tag{1.1}$$

where V_a is the potential on the anode, d is the distance between the anode and the cathode, e is the basic charge ($1.60217 \cdot 10^{-19}C$) and m_e is the electron mass ($9.10938 \cdot 10^{-31}kg$). When the electron emission increases (hot electrode emission, electric field-induced emissions), a *virtual cathode* is formed (curve D in Fig. 1.3). The theoretical current-voltage characteristic within the "D-sub-regime" is, however, much more complicated [12, 13] (see Sec. 4). An additional problem, which increases the complexity of the "D-sub-regime" is that the virtual cathode is not necessarily a stable structure [14, 15]. This makes it difficult to fully describe it using the analytic method from [12, 13] (and references therein), and therefore a computational simulation method is used (see Sec. 3).

It should also be noted that the virtual cathode forms provided that a high-density electron current is emitted from the physical cathode. High electron densities

are frequently desirable for maintaining a DC discharge, i.e., maintaining the plasma with "designed" parameters. This is especially the case in some so-called collisionless and low-collisional plasmas. This is usually achieved by auxiliary heating of the cathode so that the electrons (with a current density J_G) are emitted in accordance with the Dushman-Richardson formula [16]:

$$J_C = A_C T^2 e^{-\frac{W}{kT}} \tag{1.2}$$

where W is the "work function" (the material-specific threshold energy for thermo-electron emission; a typical value for tungsten is $W \approx 4.5eV$) and $A_C \approx 6 \cdot 10^5 A/m^2K^2$. Providing that the energy of such electrons is above the ionisation threshold (e.g., 13.59 eV for hydrogen, 15.76 for argon) and the diode length is sufficient, the so-called collisionless electrical gas breakdown can be achieved and a steady plasma is maintained, even at relatively low gas pressures (of the order of several Pa or lower).

In the past, starting from the beginnings of plasma physics, both collisionless and collisional plasmas have been thoroughly theoretically investigated. Tonks and Langmuir [17] defined the so-called plasma-sheath equation and divided this problem into two parts, each described with its own equation(s): the plasma equation and the sheath equation. The sheath equation is intended for use in the area near the system boundary (wall) that is several Debye lengths (λ_D) long, and the plasma equation is used in the rest of the system (of size L). The plasma equation, which corresponds to strict plasma quasi-neutrality ($n_e = n_i$), is today known as the Tonks and Langmuir (T&L) model [11] and is still far from being satisfactorily solved, unless considerable simplifications of the physical processes within the plasma are assumed. The gradually increased complexity of the investigation over time is presented in a series of articles [18, 19, 20, 21, 22, 23, 24, 25]. The sheath equation corresponds to the electric-field-dominated region and its description is also rather complex, primarily due to the difficult-to-define boundary conditions [26, 27, 28, 29]. In the present work the effects of a non-negligible ion temperature on the plasma sheath boundary, as well as the criteria for identifying such a boundary, are presented [30] (see also Chapter 5) The T&L-model intrinsically corresponds to the curve A' in Fig. 1.3. However, computational simulations of a T&L-model, which correspond to a non-monotonic sheath (such as the ones in the experiments of [31]), are still missing.

It should be noted that the T&L-model was originally developed for modelling the F-G region (normal discharge) in Fig. 1.2, within which the potential profile near the cathode is monotonic (curve A' in Fig. 1.3). It is still applicable to collisionless discharges, for which the current-voltage characteristic does not coincide with that from Fig. 1.2. Besides this similarity, both plasmas are macroscopically stable, i.e., time independent. While the diode's potential profile is evolving from a "B",

"C" or "D"-shape ("empty" diode) to a A'-shape ("normal" plasma), the physical-temporal-spatial processes within the inner-electrode space are extremely complex and numerous. This is especially true for a collision-dominated system, i.e., a system with a relatively high pressure (several tens of mbar). The mentioned temporal-spatial evolution is in fact a process known as the transition to breakdown, which is still the subject of in-depth investigations for a variety of applications. This was elaborated in detail in a recent review [5] on Townsend's mechanism, Paschen's law, possible streamers/filaments/arcs formations in spite of the fact that these structures are experimentally known and have been investigated for more than a century [32, 33, 34, 35]. Such a breakdown via the numerical simulation method (see Chapter 6 and Ref. [36]) was investigated. A common observation is that a variety of non-monotonic potential structures are formed during the transition to breakdown in both collisionless and collision-dominated diodes. Once a steady state is achieved, such structures usually become neutralised, i.e., virtual cathode regions are filled by the plasma ions. Nevertheless, once the plasma is ignited, a new source of external electrons might appear spontaneously due to the secondary-electron emission caused by the plasma-cathode interaction/bombardment. One such possible source of secondary emission is related to the high electric field strength appearing in the sheath region, which can lead to so-called field-induced electron emission, according to the Fowler-Nordheim equation:

$$J(x) = A\frac{(\beta E)^2}{\Phi_w}e^{-\frac{B\Phi^{3/2}}{\beta E}} \tag{1.3}$$

where Φ_w is the material's "work function" (representing the minimum necessary energy to extract a particle from a surface; for copper, $\Phi_w \approx 4.4$), $A = 1.5414{\cdot}10^{-6+\frac{4.52}{\sqrt{\Phi}}}$, β is factor of field enhancement and depends on the surface shape ($\beta = 300$) and $B = 6.53 \cdot 10^9$. According to the theoretical predictions and experimental observations (e.g., [37, 31]), in cases when the plasma ions are incapable of compensating for the space charge of the electrons emitted from the cathode or another surface, a virtual cathode may appear, even in a steady plasma (curves C' and D' in Fig. 1.3).

It is clear that the appearance of a virtual cathode might prevent the emitted electrons from penetrating into the plasma region efficiently and may lead to an undesirable plasma-density decrease and even to the disappearance of the plasma. In order to investigate the possibility of such a scenario, it is necessary to investigate the plasma parameters under various production conditions, i.e., both with and without external electrons, as is partially the case throughout the present work. However, the state-of-the-art numerical simulation codes do not allow simulations for this task to be pursued sufficiently reliably and cost-effectively at the same time.

1.2.2 Simulation methods background

Numerical simulations, as oposed to experiments, offer the important possibility to include relevant physical mechanisms (models) in a step-by-step manner and provide an ideal diagnostic tool at both the microscopic and macroscopic levels [38].

Diode investigations essentially require microscopic simulations with an extreme spatial-temporal resolution, especially during the initial and transient stages. Despite the availability of huge computing power through the utilisation of computer clusters and advanced simulation methods, these required higher spatial-temporal resolutions still represents a major factor in choosing the simulation method(s) for performing research. Namely, for simulating a single point at a direct current (DC) current-voltage characteristic of a steady plasma in a cylindrical tube, regardless of the regime (dark, glow or arc discharge), a tedious process of trial and error needs to be be pursued (e.g., [39]). The task for obtaining the whole characteristic sounds like an impossible mission. In contrast, in experiments a single point in the DC current-voltage characteristic can be repeated any time almost instantly. The transition stage towards the breakdown situation, in comparison to pure DC discharges in the steady state, represent a much harder problem, which is rather poorly investigated via kinetic codes, especially in cases when it leads to a extremely dense plasmas.

The available non-commercial program packages turned out to be insufficiently equipped with even some basic physical mechanisms, such as the feedback effects of particle-generated fields back to charged particle dynamics (see [36], and Chapter 6 below and the corresponding references therein). Such basic physical mechanisms in diodes, when used as gas-discharge arresters/tubes or dense plasma focus devices, are unavoidably related to electron emission (mainly at cathode). This emission could increase to strong, localized space-charge effects (high field and charged particle gradients), before and after a targeted degree of volume plasma production is achieved.

Thus, in the present work, the adequacy of the available kinetic codes (Particle-In-Cell: PIC) in the presence of strong field/particle gradients, has been questioned (Chapter 6) and the plasma parameters in a "conventional" plasma-sheath transition problem were investigated. The investigations were performed with a Particle-In-Cell (PIC) code (see [40], and Chapter 5 below and corresponding references therein) which showed that the relevant quantities are not changed sharply enough during the particle flows to the boundaries, as expected in accordance with the theoretical description.

A new simulation approach in the field of plasma simulations, the so-called *treecode* (TC) method, has been employed and benchmarked under more elemen-

tary physical scenarios: in a 1D electrically short-cut plain diode with cold electrons emitted from the cathode and with a disregarded volume plasma-creation (see [30], and Chapter 5 below and corresponding references therein). The treecode (TC) method [41, 42, 43] is a grid-free method that is, compared to grid-based (PIC) methods, more suitable for utilisation in simulations where high gradients of simulation quantities occur. In an investigation under elementary physical scenarios, the results obtained with the PIC and treecode simulation codes fit each other well, as well as with the theory [44]. In a more realistic (and in terms of utilized physical models, more demanding) diode scenario with an electrically biased DC-cathode with the strong emission of Maxwellian electrons, where the whole space charge is located near the cathode (thus forming a potential-deep known as the "virtual cathode"), the result of the PIC code does not fit the theoretical prediction, while the grid-independent treecode method does (see [44], and Chapter 4 below and the corresponding references therein). This indicates the necessity of preparing the treecode method for dealing with a rather dense plasma.

The treecode simulation codes cannot, and should not, be directly compared to the PIC and fluid simulation codes solely on supported (utilised) processes in codes (ionisation, collisions, etc.), but also based on the quality of the results from various "standard" simulations, so-called "benchmark" cases. It was suggested to the author by international collaborators to add the treecode method into some of the previously used (and available) PIC codes as an alternative method. This would enable users to select the desired simulation method from the input file prior to the start of the simulation and to simply compare the results from available methods or to select a method that is better suited to current research. The first step in the integration would be to integrate the treecode method in the 1D simulation code (e.g., OOPD1 or PyPD1) and later into 2D codes, e.g., XOOPIC. It is expected that only after that could the localised electrodynamic structures, densities and currents in more complex discharge scenarios (like that from Ref [36] and Chapter 6) be simulated, and hopefully successfully resolved, using the treecode method.

1.3 Thesis overview

The description of the objectives, the simulations and the results in the thesis are structured as follows. Chapter 2 presents an overview of the physical background, the simulation models and the codes that are later used for the research. Chapter 3 presents the research on a virtual cathode in a gas-evacuated diode with "cold" electron beam emissions from the cathode, shortcut bias and with comparison of 1D Particle-In-Cell (PIC) and 1D treecode (TC) [30] results. Chapter 4 presents the research on a diode with an arbitrary voltage applied to electrodes and with warm electrons (half-Maxwellian) [44]. In Chapter 5, a diode with a specified rate of vol-

ume ionisation is investigated, without secondary electrons for formulating plasma boundary conditions in the limiting case of vanishing electron emission [45]. Chapter 6 presents the results from investigating the sudden spacial-temporal evolution of plasma parameters within a cylindrically shaped gas-discharge tube by applying a 2D-PIC code [36] to illustrate the complexity of the full kinetic-Maxwell problem. Chapter 7, discussion and conclusion, summarises the presented work and outlines the plans for the future research and the development of simulation code(s).

Chapter 2

Plasma physics and computer simulations

2.1 Plasma background

Plasma, or the plasma state, is often referred to as the fourth state of matter, as an ionised gas is, on average, considered neutral and consists of an equal number of ions and electrons. The difference between an ordinary gas and plasma is that plasma contains enough free charged particles for its dynamics to be dominated by electromagnetic forces. Research on the phenomena in plasma is not a new field, and the beginnings of the research go way back to the start of the 20^{th} century. The physics of plasmas has developed from many roots, which include solar physics and in the wider sense from cosmic electrodynamics (with magnetohydrodynamics - MHD) and the physics of gas discharges (light sources and arcs for welding and cutting). Plasma research covers many areas, from thermonuclear fusion, astrophysical and space plasmas, energy-efficient lighting, metal and waste recycling, surface engineering, to the medical and health fields and the semi-conductor industry.

On the macroscopic scale, one can observe the following plasma properties:

1. plasma is a neutral gas

$$n_e = n_i, \tag{2.1}$$

2. any strong electric field is localised to distances λ_D, that are short compared with the characteristic system dimension L,

$$\lambda_D \ll L, \tag{2.2}$$

3. the particle density is high,

$$n \gg 1/\lambda_D^3, \tag{2.3}$$

2.1.1 Basic plasma properties and equations

Plasmas can be defined with a variety of properties or parameters. Here are some of the basic parameters and equations that have to be fulfilled for plasma to exist.

Debye length

The Debye length is the minimum scale length over which a plasma can be considered neutral and is a fundamental property of all plasmas. It is defined as:

$$\lambda_D = \sqrt{\frac{\varepsilon_0 k T_e}{n_0 e^2}} \tag{2.4}$$

where ε_0 is the vacuum dielectric constant, $k = 1.38 \cdot 10^{-23}$ J/K is the Boltzmann constant, T is the absolute temperature of the gas, n_0 is the number density of neutral particles and e is the elementary particle charge.

2.2 Computer-simulation methods

Computer simulations are an efficient design tool for providing accurate performance predictions in plasma-physics applications. Computer simulations are based on various models that describe the plasma and the processes in the plasma, experimental parameters and the simulation system geometry in different ways. The models generally describe the conservation of mass, energy, charge and also transformations among the chemical species. Equations for such models can be derived fundamentally from the general Boltzmann equation describing the probability distributions of individual species in velocity space, subject to collisions and external forces and from the set of Maxwell equations describing electromagnetic field interactions.

There are many different models for computer plasma simulations, which can incorporate various features, such as the model dimensionality (complexity, 1D, 2D or 3D), the use of a kinetic or fluid approach to describe the plasma-governing equations, etc. Computer simulations of the plasma can be divided into two main areas, based on how they describe the plasma and the processes inside the plasma [46, 38]: (1) fluid description (MHD model, wave equations) and (2) kinetic description (Vlasov, Fokker-Planck codes; particle codes).

The two main simulation-model descriptions differ in the way they describe plasma and how they are trying to approach problems in plasma descriptions. Many modern simulation programs incorporate both the fluid and kinetic models in plasma simulations [47]. Hybrid models may treat electrons as a fluid, using the fluid model to simulate them, and treat ions as particles, using the kinetic model for the simulation of the ions.

2.2.1 Fluid model for plasma description

The fluid plasma model, in contrast to the kinetic model, represents a *macroscopic* model of the plasma description and processes in the plasma. The main focus of the fluid model's representation is to describe the external features of the plasma, the parameters/features that can be observed. This is very similar to experiments, as in an experiment one seldom makes measurements at the microscopic level and no attention is given to small details/internal processes inside the plasma, for example, motion and forces on a single particle in the plasma. The aim of the fluid model is to represent plasma independently of what happens on the molecular level - one assumption is that the velocities of the particles inside the volume element can be neglected. With this, the fluid variables are functions of the position and time. It is similar to a fluid representation of the neutral gas and fluids, extended to include the specific behaviour of the plasma and the processes inside the plasma. Fluid (or continuum) plasma models reduce the computational complexity by averaging the velocity-space effects.

In many cases, plasma could be modelled as a one-fluid model with the use of *magnetohydrodynamic (MHD) equations*. The fundamental assumption is that the fields and fluid fluctuate on the same time and length scales - on the scale of the slower and heavier ions. In more advanced models, to support rapid wave fluctuations in plasma (due to the fact that electrons are much faster than ions), plasma is treated as a two-fluid model in *plasma wave equations*. Like MHD equations, these are also macroscopic equations, but the assumption underlying them is quite different.

In the fluid model of plasma description, one tries to numerically solve the magnetohydrodynamics (MHD) equations of the plasma by assuming transport coefficients. The fluid (or continuum) equations consist of three main equations, which describe the conservation of particles, momentum and energy for particular particle species. These equations work with quantities that are averages over all the particle velocities in a small volume element. Plasma-fluid calculations are often valid even though the main free path of the plasma particle is larger than the volume element of the fluid.

2.2.2 Kinetic model for the plasma description

The kinetic model is the most fundamental way to describe plasma - it describes plasma from the *microscopic* level, starting with a description of the motion of a single particle. Because they are dealing directly with various particles in the plasma, they are potentially the most powerful models for studying the processes in plasma. Depending on the processes taken into account in the simulation, those equations can become quite complex and difficult to solve. With a large number of particles usually present in the plasma, kinetic models require huge computational resources regarding memory requirements, CPU power and also in computational time.

Kinetic models utilise six-dimensional space (positions and velocities) and time to describe the processes in plasma in greater detail compared to fluid models. Instead of defining the density of the particles at a given position and time, the *distribution function* is defined as $f(\vec{r}, \vec{v}, t)$ - number of particles with a given velocity at a given position in the system at a given time.

With a given distribution function f_a, one can solve short- and long-range particle interactions in plasma, either with or without the presence of an external electric and magnetic field. In an electrostatic 1D system without a magnetic field present, the energy-conservation equation (2.5) and the Poisson equation (2.6) describe the basic set of equations.

$$n_0 u_0 = nu \quad ; \quad \frac{mu^2}{2} - e\Phi = \frac{mu_0^2}{2} \tag{2.5}$$

$$\frac{d^2\Phi}{dx^2} = \frac{e}{\varepsilon_0} n \tag{2.6}$$

where x is the coordinate in the system ($0 < x < L$; L is the system length), m is the mass of a particle, e is the charge of the particle, Φ is the electrostatic potential and n is the number of particles.

The Vlasov-Poisson equations in a time-dependent, non-relativistic, zero-magnetic field limit give:

$$\frac{\partial f_a}{\partial t} + \vec{v}\frac{\partial f_a}{\partial \vec{x}} + \frac{q_a \vec{E}}{m_a}\frac{\partial f_a}{\partial \vec{v}} = 0 \tag{2.7}$$

$$\nabla \vec{E} - 4\pi\rho = -\frac{\partial^2 \Phi}{\partial x^2} \tag{2.8}$$

where f_a is the distribution function, $\vec{x}$ is the position, $\vec{v}$ is the velocity, $\vec{E}$ is the electric field, m_a is the particle mass, Φ is the potential and ρ is the space charge.

2.3 Particle-In-Cell (PIC) method

Particle-in-Cell (PIC) simulation programs employ the kinetic model of the plasma description as a base for the simulations. The PIC techniques grew from electron-trajectory simulations in the 1950s, with capabilities to take into account just a few particles. But later, in the 1960s, scientists in universities and national laboratories developed PIC schemes that employed thousands of particles and normally used one-dimensional systems. The main focus of the research (software-code development) was on validating the physical and numerical models used in the PIC schemes. Between 1960 and 1980 [46], the self-consistent PIC method was formalised and put into computer code. Theoretical limitations and methods to overcome those limitations were developed and described more formally. In the 1980s the first device models and Monte-Carlo collisions were developed. These models were extended with a self-consistent circuit model and an improved Monte-Carlo model in the 1990s. One path of development for the PIC simulation codes (computer codes) is directed into developing object-oriented techniques and second in using PIC methods on computer clusters. The object-oriented approach [48] would enable scientists (and users at the same time) to write their own implementations of individual parts of the simulation system (device, physical models, transport models, collisions, ionisation models, etc.). Developing PIC code for computer cluster would utilize the parallel computing and thus shorten necessary computer simulation times.

Particle-in-Cell (PIC) codes, as presented by [46], found applications in a wide range of plasma investigations. They are based on the use of computer particles (particles in the computer simulation), i.e., so-called "super-particles", instead of "real" particles (particles in the read system). The use of computer particles in simulations is a solution to a problem where a huge number of real particles is required in simulations that require huge computational resources. Thus, a single "super-particle" contains as many as 10^6 "real" particles. Despite this method, in many applications, especially in fusion-related investigations, PIC simulations still take a long time to run. New parallel-computing techniques recently used in PIC (and similar) simulation codes can reduce this time dramatically; however, the costs of performing simulations are still very high. Another drawback of PIC codes is the requirement for defining the grid in advance (uniform grid or self-adaptive grid).

Typical simulation (computer) times for a single iteration of a common simulation case are in the range 1-10 seconds. This may seem short, but considering that the real time step in a single iteration is often in the range of 10^{-8} s (or even 10^{-11} s) and that usually simulations require up to $1.5 \cdot 10^6$ iterations to achieve a "steady state", the total simulation times can be up to 50-60 days. All the PIC simulation applications (programs, computer codes) that are based on PIC techniques have a similar main loop - a loop that forms the basis of a program/application. The basic

steps in every PIC simulation code are shown in Fig. 2.1.

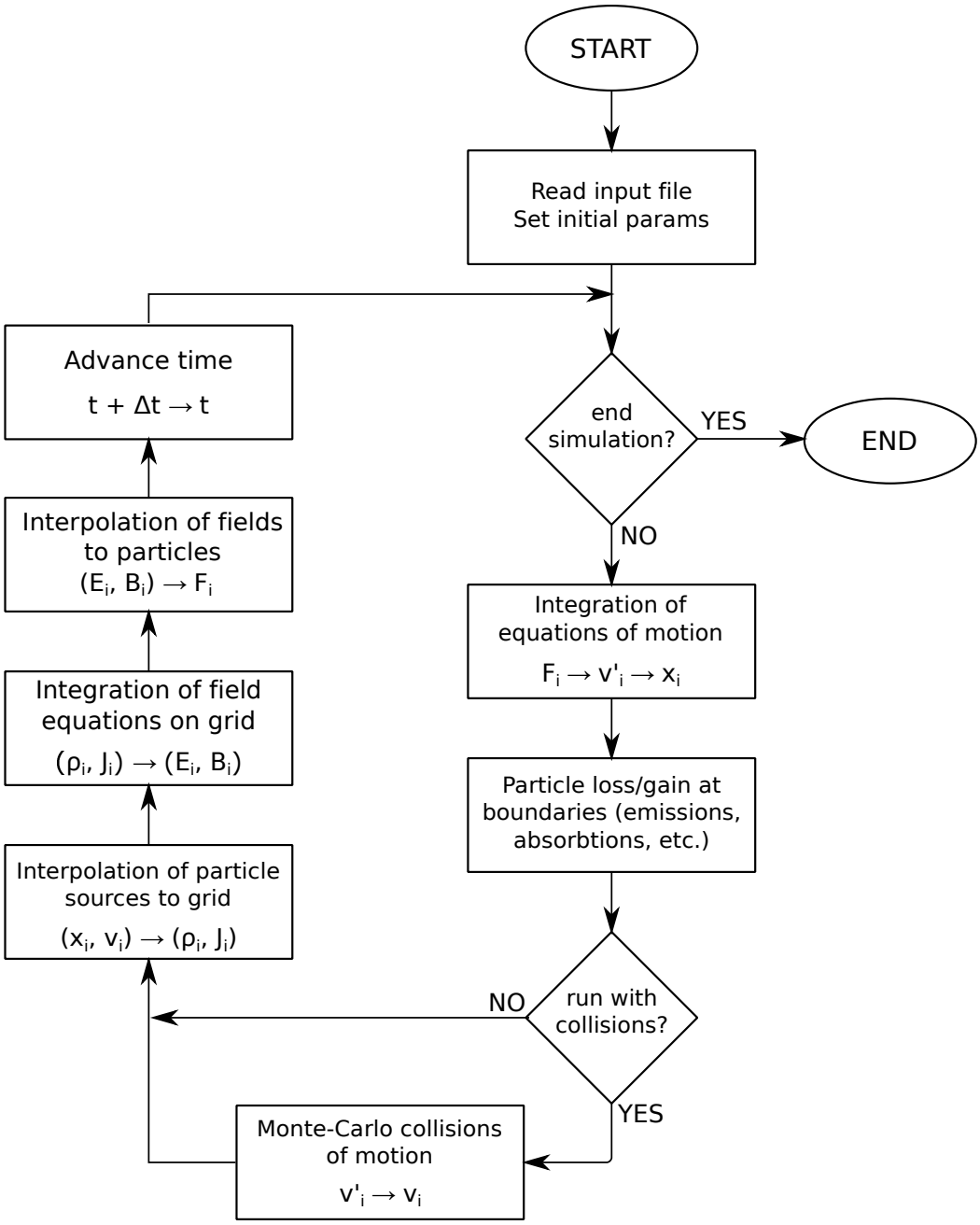

Figure 2.1: Simple flowchart of PIC-simulation program with possible Monte Carlo Collisions (PIC-MCC).

In addition to these basic steps, PIC simulation codes often offer the possibility to simulate collisions inside the plasma, which is a necessity when the simulation is performed with high-density plasma (where collisions between particles are more likely to occur).

2.4 The treecode (TC) method

The basic idea behind the treecode (TC), as presented by [41], is to replace particle-to-particle interactions with particle-to-cluster interactions in such a way that the number of necessary calculations is reduced without influencing the accuracy of the method too much. By grouping particles into clusters, with each cluster replacing many particles, the number of clusters is smaller than the number of particles. This results in a smaller number of required interactions (and thus the required simulation time) is reduced. The number of calculations for calculating the interaction between the particles (particle-to-particle interactions; number of particles is defined by N) are scaled according to $\mathrm{O}(N^2)$. With the use of the TC method, the number of interactions, now particle-to-cluster interactions, are scaled according to $\mathrm{O}(N \log N)$ - this is a huge reduction in the number of required calculations. In current plasma simulations, where the number of particles is of the order of 10^{22} (or 10^{17} of super particles), the number of particle-to-particle interactions represents a huge load, even for today's super computers, or at least computers that are normally used to run simulations. One of the advantages of the TC method is its scalability, which makes it a good candidate for running on parallel computers [49].

The TC method is simplest in 1D space, but it can also be extended in a way that it can be used in 2D or 3D space, as presented by [50]. The difficult part in extending the TC into dimensions higher than 1D is not the TC method itself, but the underlying equations that are used for solving the physics of the simulation. Due to the nature of the TC method, the TC method gives precisely the same results in 1D space as the direct summation method, see [14]. The method introduces another level of approximation to the PIC simulation, in addition to the already widely used approximation using super-particles instead of "real" particles. With a smart selection of the parameters for the TC method, as explained later, one can minimise the impact of the TC approximation on the simulation results. The TC method is gridless [51]; for running the simulation one does not need to define a grid for calculating the values of interest, the "temporary" grid in the form of clusters is automatically generated during each simulation step. The main computation of the particle interactions (positions, velocities) are made using a generated tree and without any grid. The grid is needed just as an auxiliary tool in the post-processing (computing the values of the potential, etc.).

The most striking property of the TC method is the tree, which is the basis for all the calculations and divides the computational domain into smaller parts. The TC method could be used in the 1D, 2D or 3D domains. The purpose of building the tree is the ability to represent the relations between the particles in simulating the domain. With the generated tree, the positions of the particles in the nodes and the relations between the nodes in the tree, the simulation method can perform a

faster calculation of the forces between the particles. The force on a particle is then used to compute the values of all the other relevant variables in the system, i.e., velocities, positions, fields, etc.

The tree is a hierarchical representation of particle positions in a simulation system (an example of a 2D system is shown in Fig. 2.3). Because the tree depends on particle positions, it is necessary to build the tree in each simulation step. The tree is composed of nodes, links between nodes and leaves (Fig. 2.2a), where each node can have zero or more children. The maximum number of children in each node of a tree is defined by the dimensionality of the domain for which the tree is created, and can be up to: 2 children for a 1D domain (also called binary trees), 4 children for a 2D domain (also called quad-trees) and 8 children for a 3D domain (also called octrees).

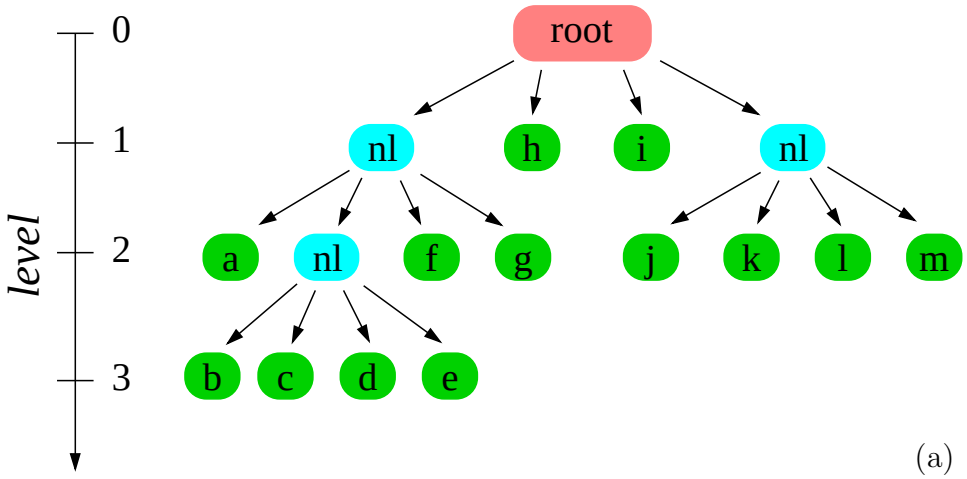

(a)

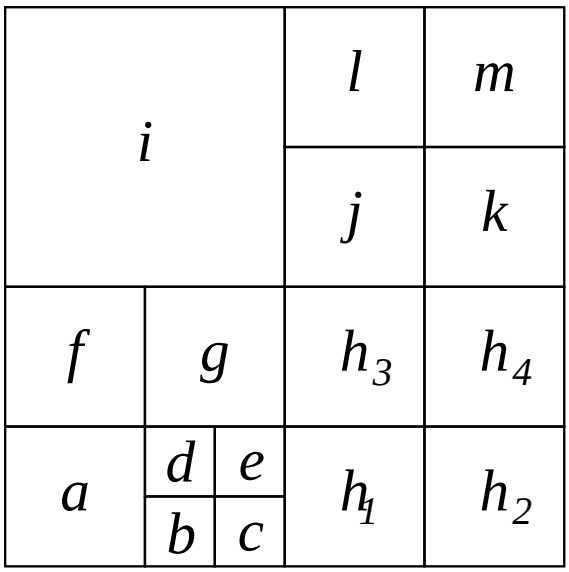

(b)

Figure 2.2: Example of tree representation (a) of square domain (b) (image taken from [1]).

There are nodes in a tree that have special names: nodes without children are called leaves (nodes named *a*, *h*, *i*, etc. in Fig. 2.2) and a node without a parent is called a root node (node named *root* in Fig. 2.2). The tree can be asymmetrical and does not need to be full - there can be nodes in a tree that have fewer children than the maximum number (for example: 1 child instead of a maximum of 4 children for a 2D system) - see Fig. 2.2a.

2.4.1 Building a tree

Building a tree always starts with dividing the whole computational domain (see Fig. 2.3, "level 0") into equal sub-domains (parts): 2 parts for a 1D system, 4 parts for a 2D system (as shown on Fig. 2.3) and 8 parts for a 3D system. Each of the newly generated sub-domains is further checked against the "dividing conditions" (e.g., the number of particles in the node, the size of the domain compared to the system size) and, if conditions are right, it is subdivided further, creating a new level in the final tree. The process of dividing the domains is repeated, usually via recursion, until there are no sub-domains to divide (see Fig. 2.3, dividing the area from level 2 to level 3). The selection of the "dividing conditions" greatly influences the generated tree size, which then makes a difference in the computation part of the method. A larger tree results in a slower simulation time and less gain from the treecode method - the TC method is similar to the direct-summation method. A smaller tree results in faster simulation times, but on the other hand, it incorporates more approximation: using a particle-to-cluster interaction instead of a particle-to-particle interaction brings to the simulation a certain error (this is not valid for 1D systems, see [14]).

Fig. 2.4 presents a simple flowchart explaining the process of converting particle positions in the simulation domain into a tree representation, as required by the TC method. Fig. 2.3 presents an overview of the domain and the associated tree for a simple 2D simulation domain.

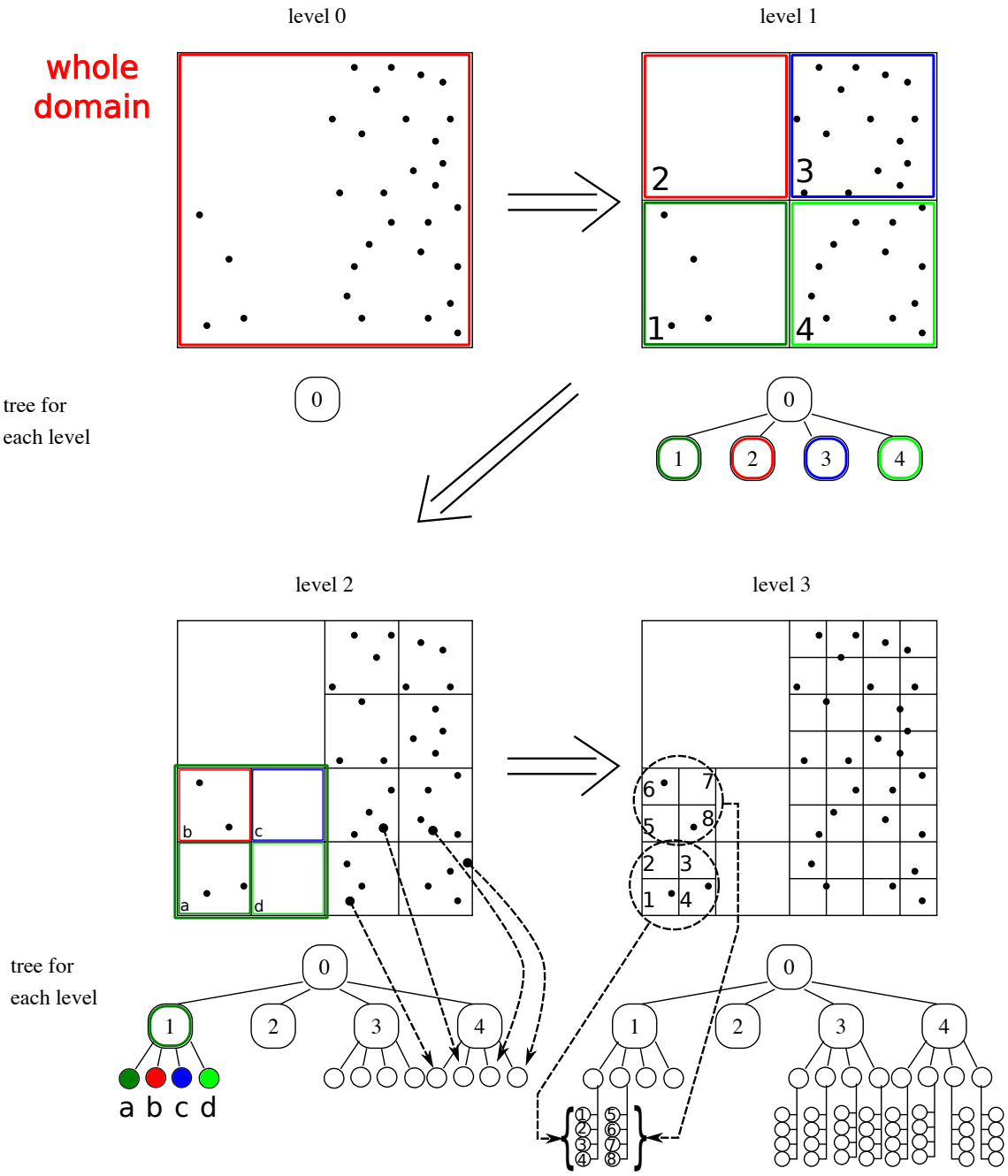

Figure 2.3: Individual steps in generation of tree and dividing domain into subdomains. Node marked as "0" is the "root" node.

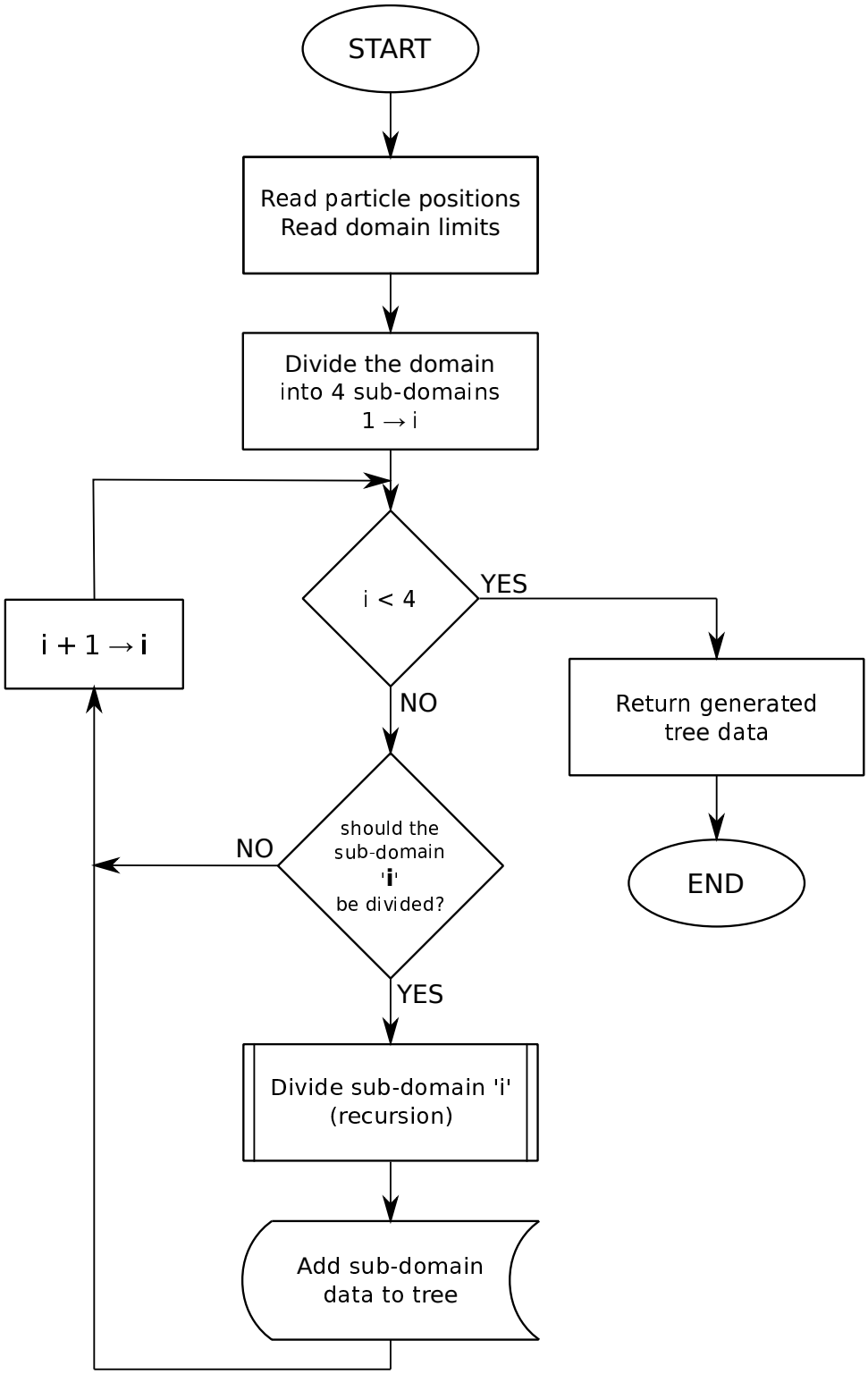

Figure 2.4: Global flowchart for creating tree.

The necessary individual steps to divide the simulation domain into the tree representation can be demonstrated on a simple square 2D domain with a few particles, as displayed in Fig. 2.5.

Level 0
The whole simulation domain, containing all the particles in the system, is considered. The "root" nodes created in the tree - containing all the particles in system.

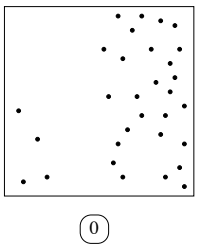

Level 1
The whole domain is divided into 4 equal sub-domains, each containing particles inside the sub-domain. In the tree, level 1 is created and 4 nodes are added to the "root" note, representing 4 newly created sub-domains.

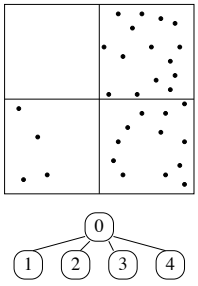

Level 2
Each sub-domain, created on "level 1" **that contains particles**, is further subdivided into smaller domains. Empty domains are not subdivided. In the tree, newly created domains are added to an appropriate node in the tree - to the "parent" node in the tree.

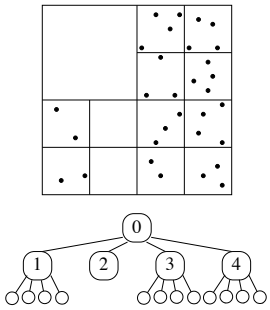

Level 3
In this step, the same procedure as in step 2 (on level 2) is repeated. The procedure is repeated until there are no more domains to be divided further and depend on the "dividing condition".

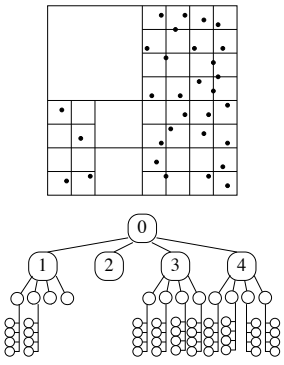

Figure 2.5: Division of the domain at each stage (level) and the associated trees.

2.4.2 Multipole Acceptance Criteria (MAC)

Another characteristics of the treecode method is the definition of the Multipole Acceptance Criteria (MAC) - the rule when a particle-to-particle (PtC) interaction will be used instead of particle-to-particle (PtP) interactions. A Particle-to-cluster (PtC) interaction is an advantage of the treecode method and brings a significant speedup of the simulation compared to PtP interactions. The criteria, called Multipole Acceptability criteria (MAC), are evaluated when the electrical field (or force) is computed on a current particle. The force (or electric field) on each particle in the system can be calculated using the following deduction (for the code implementation, see Fig. 2.9):

a) PtC interaction (utilising a Taylor approximation) if the MAC criteria is OK

b) if the current cluster has clusters on the next level in the tree, repeat the procedure with everyone of them

c) if the cluster does not have any clusters on the next level (in the tree), use the direct summation (particles that are close to a current particle - maybe in the same cluster)

The criteria, often denoted as θ, is considered one of the more important TC-method parameters and is defined, according to [52], as displayed in Table 2.1 and schematically presented in Fig. 2.6.

Name of criteria	Condition
Barnes-Hut MAC (BH MAC)	$r_1 > s/\theta$
min-distance MAC (MD MAC)	$r_2 > s/\theta$
Bmax MAC	$r_1 > b_{max}/\theta$

Table 2.1: Different multipole acceptance criteria and the required condition to be fulfilled for the criteria to be accepted; the parameters are presented in Fig. 2.6.

Fig. 2.7 presents (in 1D and 2D system) the necessary values needed to make a decision according to the MAC: particle locations, current particle x_i, cluster C, centre of cluster x_C, cluster size (radius of cluster) r_c and R as the distance between the current particle and the cluster centre. The error-tolerance parameter θ, with values in the interval $0 < \theta \leq 1$, is used when making a decision, as presented in Fig. 2.9 and as a simple *if-else* condition:

- use PtC interaction if: $R > r_c/\theta$
- otherwise use PtP interaction

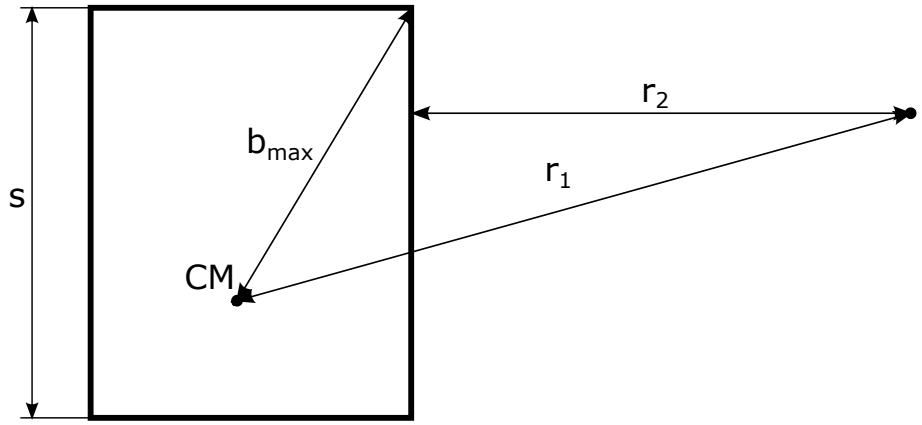

Figure 2.6: Schematic presentation of different acceptance criteria (MAC). *cm* is the center of mass for a given cluster, *s* is the max. external dimension of a cluster and b_{max} is the max. distance from the centre of mass to the edge.

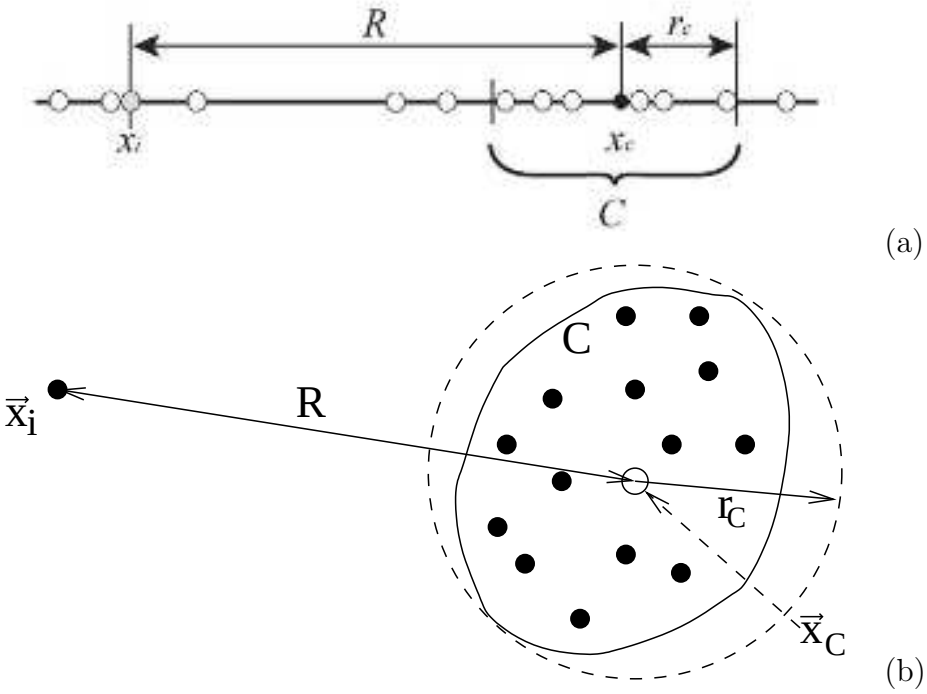

Figure 2.7: Schematic diagram of a particle, cluster and MAC variables in 1D (a) an 2D (b) system.

2.4.3 Use of treecode (TC) method in simulation code

The treecode (TC) method is used in computer-simulation codes in a similar manner to the PIC method. The main difference is the part where the actual computation is performed, while other "support", but required, activities (e.g., input-file reading, exporting data for post-processing, etc.) are the same. This suggests that one simulation code could utilise both methods and the user could select the desired simulation method in the input file and thus the TC method could be added to the current simulation codes. The simplified flowchart for a complete simulation using the TC method is presented (Fig 2.8).

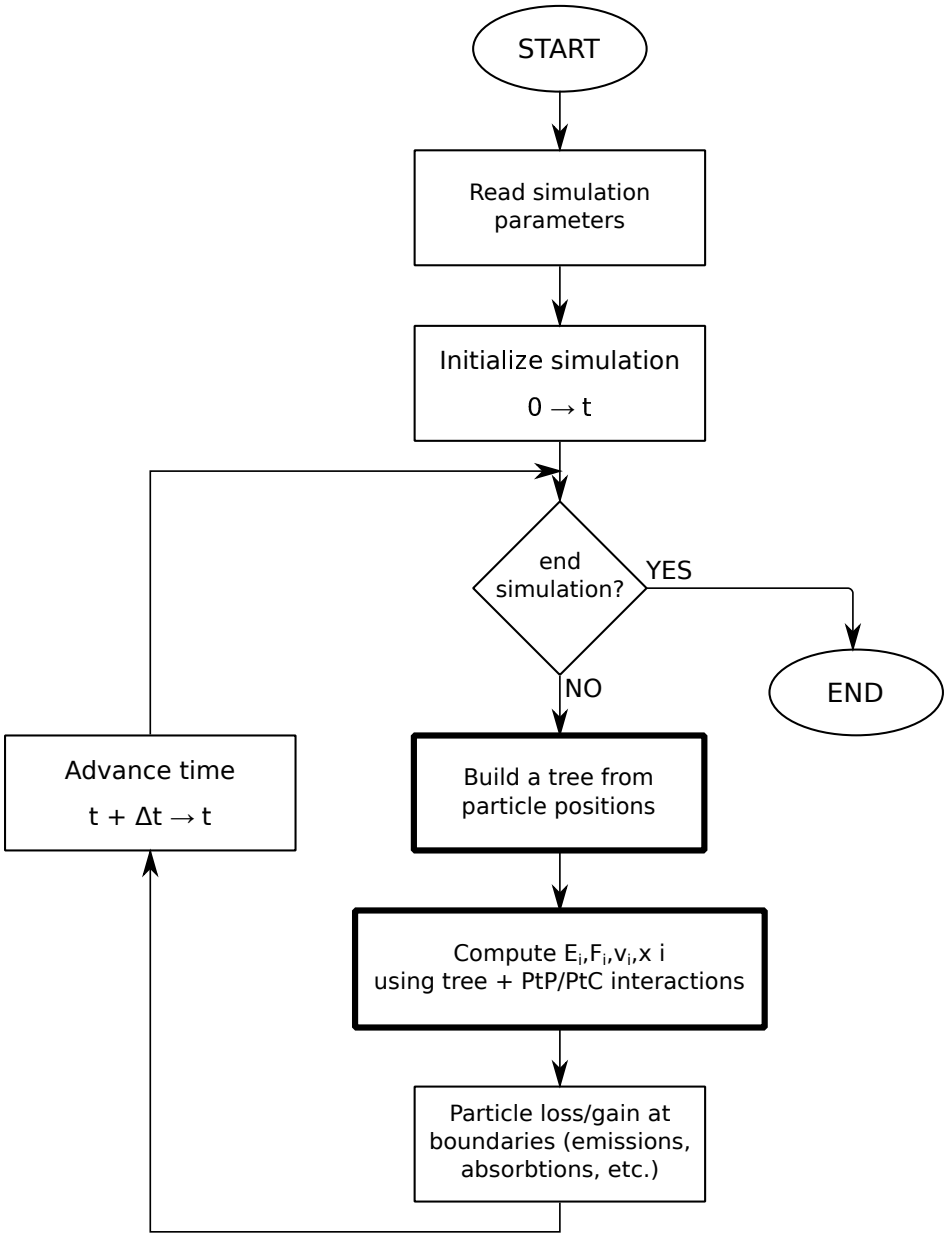

Figure 2.8: General flowchart of TC method.

The C++ code snippet in Fig. 2.9 is a simplified computer code and shows how the tree traverse is implemented, i.e., how the decision is implemented as to whether to use the PtC, PtP interactions or continue the calculation on the next level in the tree.

```
..
..
..
/* calculate distance between current particle and the centre of the cluster */
l = node->getDistanceFromCenter(pt_pos->e1());
/* calculate radius of tree node (cluster)*/
r = node->getRadius();

if( r < fabs(l) * theta ) {
  /* compute using particle-to-cluster interaction: particle is "far" from cluster
     (node) */
  Ec = compute_Ec_single( node->getQc(), l );

} else {
  if( node->getLeaf1() == NULL && node->getLeaf2() == NULL ) {
    /* this is last tree node and we have to compute the force with direct sum */
    Ec = compute_Ec_directSum( pl, node, pt_pos );

  } else {
    /* decent one level down the tree and try computing using particle-to-cluster
    interaction on sub-clusters (leafs) of current cluster. The method calls
    itself (recursion)! */
    Ec = 0;

    if( node->getLeaf1() != NULL ) {
      /* compute for first leaf of a node */
      Ec += compute_Ec_tc( pl, node->getLeaf1(), pt_pos);
    }

    if( node->getLeaf2() != NULL ) {
      /* compute for second leaf of a node */
      Ec += compute_Ec_tc( pl, node->getLeaf2(), pt_pos);
    }
  }
}

/* return computed value (in this case value of electric field) to given
particle */
return Ec;
```

Figure 2.9: Simplified simulation code snippet presenting main decision in TC method.

Chapter 3

Comparison of the PIC and TC methods in a shortcut plain diode[1]

In their historical article, Barnes and Hut [41] presented the treecode (TC) method as a way of reducing the number of necessary calculations when describing the interactions between bodies (i.e., particles) in various systems. The basic idea of the method is to replace, whenever possible, particle-to-particle (P-to-P) interactions with particle-to-cluster (P-to-C) interactions. The conditions when clusters can be used instead of particles mainly depend on the "size" (diameter) of a cluster and the distance between the particle and the cluster's centre point. In terms of accuracy and speed, the treecode method can be positioned between the so-called "direct summation" (known also as "direct integration"), with a typical process of $\mathrm{O}(N^2)$, and the PIC method ([46, 53, 54, 55]), with a typical process of $\mathrm{O}(N \log N)$. However, the main advantage of the TC method is its ability to deal with simulations where the calculated values have high gradients. Namely, while resolving short-scale structures in plasmas via a simulation method, like sheaths [56] and double layers, the proper selection of a grid is of decisive importance. For resolving the sheath via a numerical method with a sufficiently high accuracy, Kos et al. [57] employed a non-uniform grid where the length of the grid cells closer to the wall was less than 10^{-7} of the total length of the system. In the stationary state, obtaining the solution required several days of calculations for a single case. Obtaining results with high-resolution grids in non-stationary simulations appears to be a much more demanding and expensive task than was expected and the treecode should carry out these tasks more efficiently.

[1] Original/full text of this chapter was published in [30]

3.1 Theoretical model of a plain diode

The theoretical model of a plain diode with mono-energetic electrons emitted from the left-hand side of the system is used as a simulation model. This system may be described via energy-conservation equations (2.5) and Poisson's equation (2.6), already presented in Chapter 2.2.2, where the equations can be transformed into:

$$\frac{d^2\Phi}{dx^2} = \frac{e}{\varepsilon_0}\frac{n_0}{\sqrt{1+\frac{2e\Phi}{mu_0^2}}} \tag{3.1}$$

It is, furthermore, convenient to introduce dimensionless variables:

$$\eta = \frac{2e\Phi}{mu_0^2} \quad ; \quad \eta(\Phi_m) = \eta_m = \frac{2e\Phi_{min}}{mu_0^2} \tag{3.2}$$

$$\xi = \frac{x}{\lambda} \quad ; \quad \xi_m = \frac{x(\Phi_{min})}{\lambda} \tag{3.3}$$

where λ is defined as:

$$\lambda = \sqrt{\frac{mu_0^2\varepsilon_0}{2n_0e^2}} \tag{3.4}$$

With dimensionless variables from equations (3.2) and (3.3), equation (3.1) becomes:

$$\frac{d^2\eta}{d\xi^2} = -\frac{1}{\sqrt{1-\eta}} \tag{3.5}$$

with the solution:

$$\xi - \xi_m = \pm\frac{2}{3}\left(\sqrt{1-\eta}+2\sqrt{1-\eta_m}\right)\left(\sqrt{1-\eta}-\sqrt{1-\eta_m}\right)^{(1/2)} \tag{3.6}$$

The solution of equation (3.6) is shown in Fig. 3.1, where the potential profiles for various values of η_m in stationary states are shown. The potential profile in the stationary solution is symmetrical about the centre of the diode and by increasing the density, the maximum possible potential depth ($\eta_m = -3/4$) is gradually obtained. By increasing the density above a certain critical density, the maximum potential profile depth jumps to $\eta_m = -1$. A further increase in the density does not lead to a further potential depth increase (as is obvious for physical reasons, the maximum potential depth cannot be greater than the initial electron energy), but the position of the potential minimum is shifted closer to the cathode. A detailed inspection shows that the way the potential depth depends on the history of the beam density, i.e., shows a clear hysteresis behaviour. This is known to be related to instability, which cannot be modelled by the present stationary equations. This is one of the basic motivations for using this model for resolving the non-stationary behaviour via simulation codes, as follows in the sections below.

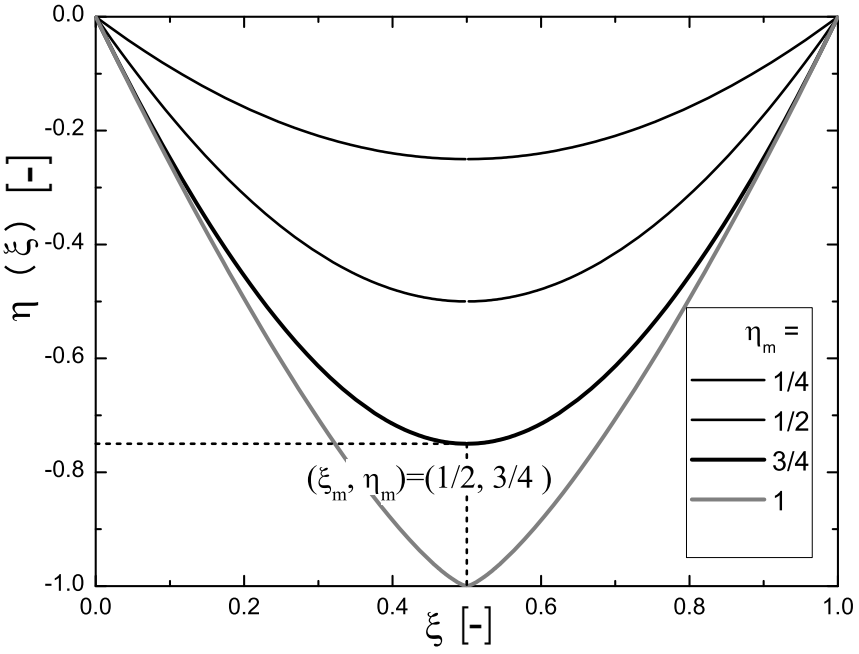

Figure 3.1: Theoretical potential profiles for diode.

3.2 Particle-In-Cell (PIC) method

The results for the short-cut diode in plane geometry were obtained using the PIC simulation code BIT1 (Berkeley-Innsbruck-Tbilisi-1D PIC-MCC code) and are presented in Fig. 3.2.

The simulation system length $l = 0.01m$ was divided into 100 cells, both walls grounded, vacuum inside the diode, system cross-section area $A = 10^{-4}m^2$, simulation time step was $dt = 10^{-11}s$, 10^4 particles in one computer particle $nc2p = 10^4$ and injecting 5 computer particles per simulation step. The injected particles are cold, mono-energetic electrons that are injected from the left-hand side wall with an initial velocity of $v_0 = 4.2 \times 10^5 m/s$ (velocity corresponds to $1eV$ energy). As seen in Fig. 3.2a, during the initial stage of several ns the system is filled with particles, leading to an increased space charge that produces a potential depth, as shown in Fig. 3.2b. Once the space charge is high enough, the potential depth becomes sufficiently strong and prevents new electrons from overcoming the potential barrier, and they are repelled back to the emitting electrode. This leads to a movement of the potential barrier and a consequent decrease in the density and the strength of the potential barrier. A weaker potential barrier enables deeper penetration of the emitted electrons into the diode. As a result, a periodic oscillation of the entire system is established, as expected from the theoretical analysis.

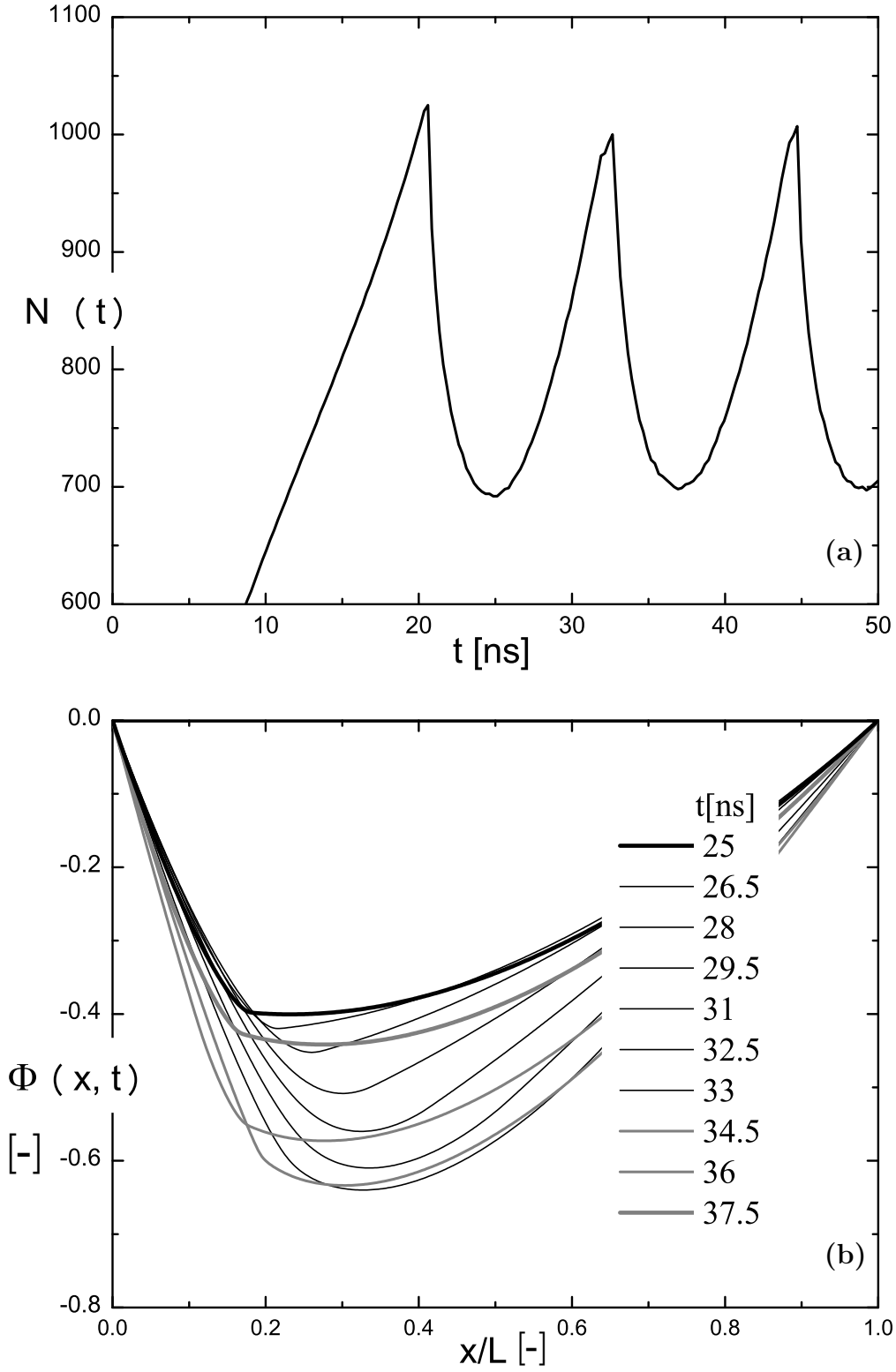

Figure 3.2: Number of "super-particles" in diode in relation to time (a) and potential profiles (b) in various simulation steps in PIC simulation.

3.3 Treecode (TC) method

As has already been shown (see [58]), the reliability of the results obtained using the treecode method utilised in 1D simulation codes is as high as those of a direct simulation method. This feature is a property of our code as well. To test the grid-free treecode method, we developed a program in C language and compiled it on the Linux operating system. The program allows the user to define the main simulation parameters in the input file: densities, simulation system sizes, output variables, parameters for tree generation, grid for computing potential, etc.

A special feature of our code is the possibility to investigate the fine structure of the potential profile and its derivatives - the electric field as a function of position and time with higher reliability. This is important for resolving the plasma-sheath boundary in our future simulations of plain discharges with warm ions as they will be compared with the results from our PIC simulations [59]. Namely, the problem with PIC simulations on plain discharges arises due to the high plasma parameter's gradients near the plasma boundary, which are difficult to resolve without high grid densities. Unfortunately, the mesh in the existing PIC codes is uniform across the computing domain, while the simulation codes based on the treecode does not suffer from such a limitation.

The simulation code enables the computation of various plasma parameters: particle positions, densities, velocity distribution functions (VDFs), temperatures, fluxes, etc. with a high resolution in regions of strong plasma and field gradients. The results obtained from the present 1D version are precisely the same as the results from (very demanding regarding computer resources) the direct summation method. This feature arises from the fact that in 1D geometry, the underlying numerical methods used in the treecode do not have additional errors [14].

3.4 Results

3.4.1 Phase-space comparison for TC from MatLab and C programs

Our test case was a 1D virtual cathode problem, for which we compared the results from the treecode method with a MatLab-based code [14] and our C-based code. The MatLab program used for the comparison was developed in The Plasma Theory and Simulation Group (based at Michigan State University) solely to check the adequacy of the TC method in simulations of charged particles. It has many limitations, such as no input file for defining the simulation case, the capability to simulate only single

species and to handle just a few tens of particles in the system, to name just a few. We used the same simulation parameters (spatial region, initial values) and recorded results in a selected time, when the system was not yet in a quasi-stationary state. We selected $t = 0.45ns$ for the simulation time from the start of the simulation and Fig. 3.3 (MatLab code - 3.3a; C program - 3.3b) show phase-space diagram for the selected time. Once a quasi-stationary state is established, the system oscillates with a period of $T = 3.5ns$. When simulating the virtual cathode, the system comes to a quasi-stationary state and then oscillates.

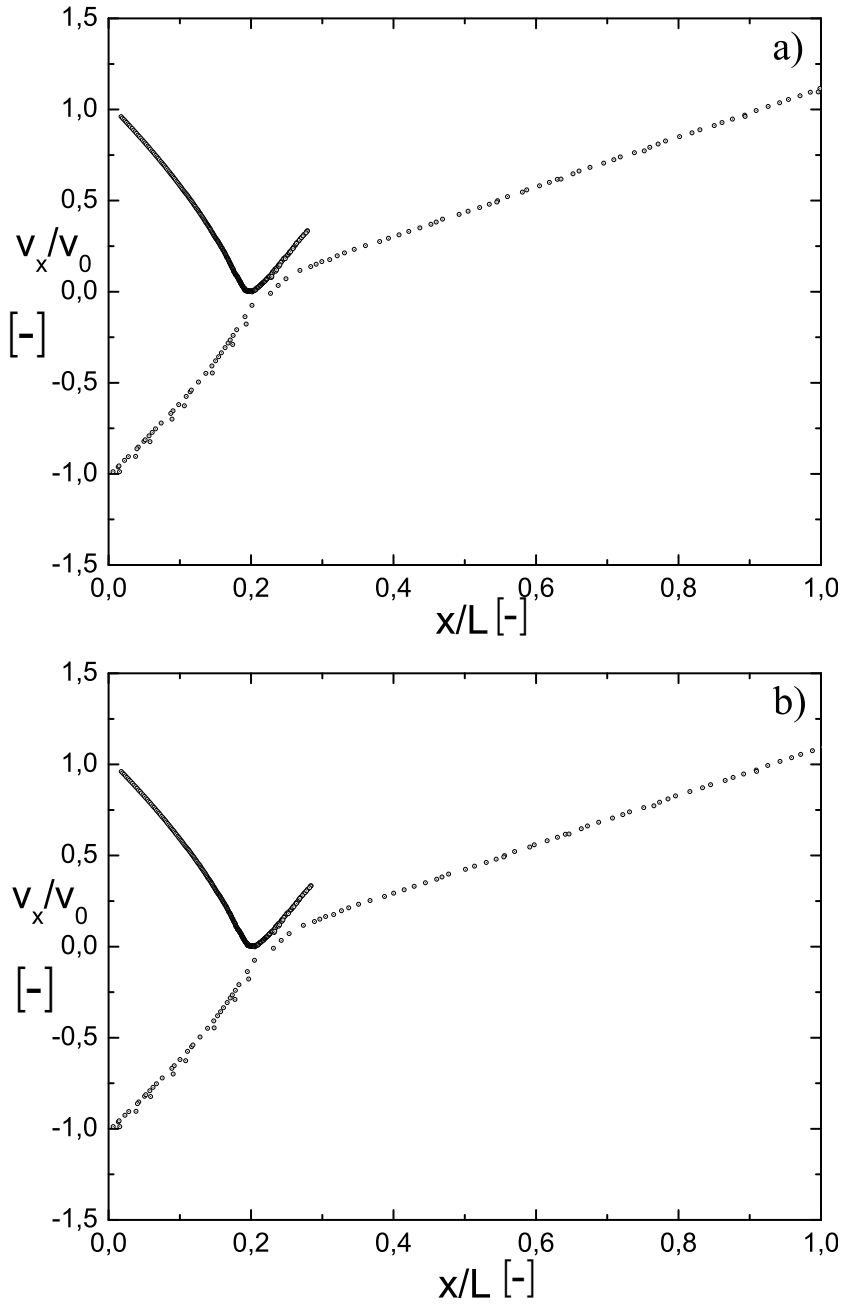

Figure 3.3: Comparison of phase-space diagrams at same simulation time (t=0.45ns) from MatLab (a) and our program in C (b).

Fig. 3.4 shows the values for the phase-space diagram, the potential profile and the density at various times during the oscillation cycle. The values for the density are normalised to the total number of particles in the system and the density peak is cut-off for readability reasons. The treecode method requires the definition of an arbitrary grid, usually done in the input file, which is used solely for computing the values of the potential at given points for the results post-processing. The potential was computed using a Green's function (see [14]) and was computed on a grid with 200 cells.

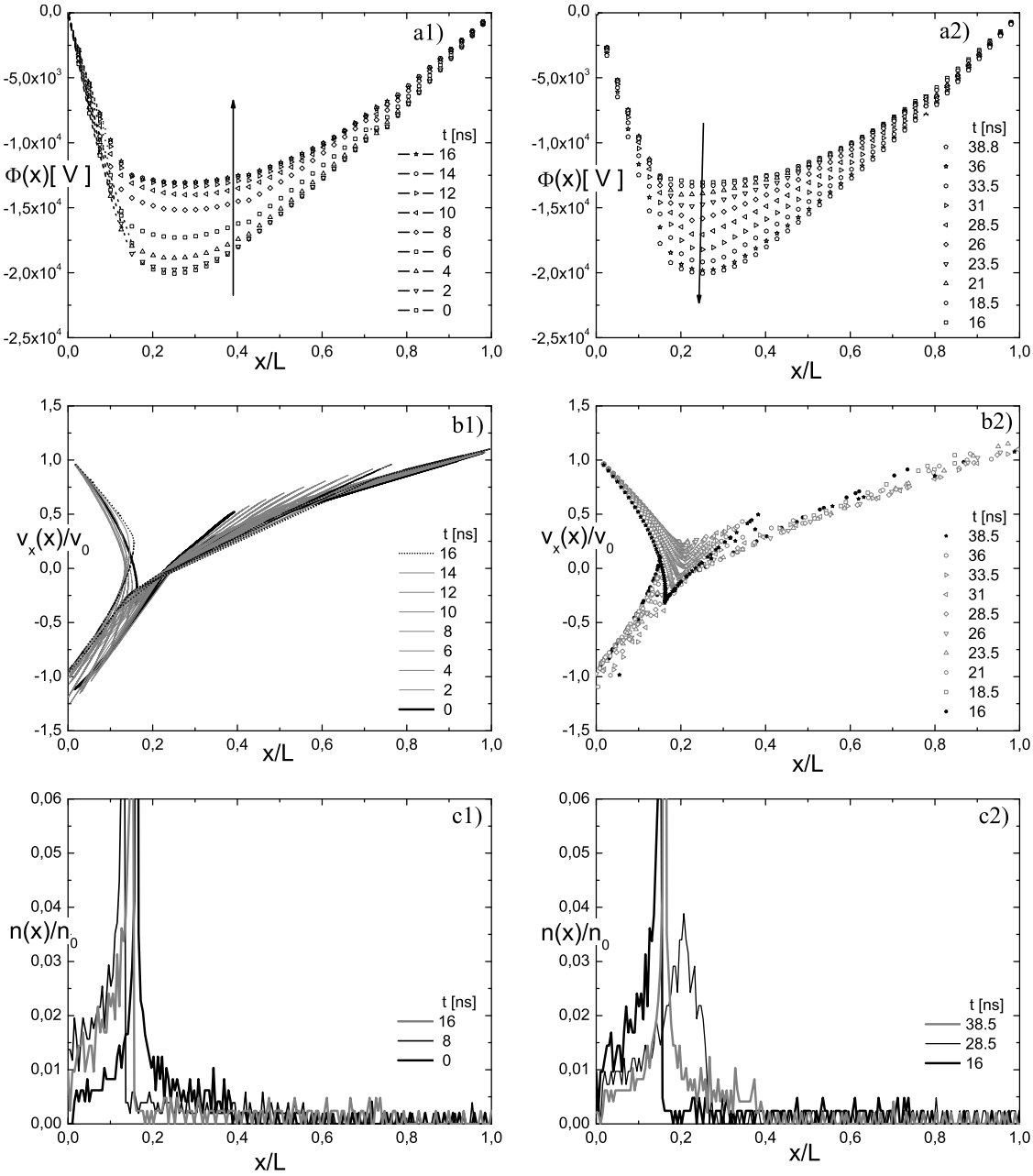

Figure 3.4: Potential (a1, a2), phase-space (b1, b2) and particle density (c1, c2) in one cycle. Left column when the potential is increasing and right column when it is decreasing.

The left column in Fig. 3.4 shows the potential profiles, densities and phase-space diagrams during the first stage of the oscillation cycle (increasing the potential from the minimum to the maximum value, i.e., during the decreasing number of particles in the system). The right column shows the same quantities during the opposite stage of the oscillation cycle (decreasing potential, i.e., increasing number of particles). It is a little tricky to interpret the simultaneous behaviour of the potential profile, the density and the phase-space in time on static figures, since the positions of the particles are not simply related to the instant potential profile, but are a consequence of the whole history during the period of the cycle. That is why we have to obtain and store a huge amount of data to make the appropriate time-dependent records to better observe the qualitative features of such time-delayed effects at any point of observation of the said quantities.

3.4.2 Two species diode scenario

In order to reduce or even eliminate the oscillations in a diode (as shown in Fig. 3.5), two species scenarios with injecting ions from the opposite side of the diode to the electrons was researched. Simulations were performed for various values of the ratio (denoted by R) between the injected electrons and the ions from 0% (no ions were injected) to 100% (same numbers of ions and electrons were injected). The number of injected electrons is the same for all values of the ratio R, only the number of ions is increased according to the selected ratio R. The injection mass, the charge and the velocity were selected to be the same for electrons and ions, only the sign of the charge was different.

Fig. 3.5 shows the onset of oscillations T_{onset} and the oscillation period T_{osc} for various ratios R (ratio between the number of injected of electrons and ions). We can observe that the onset of the oscillations (T_{onset}) moves away from the start of the simulation with an increasing ratio R between the injected electrons and the ions. The system reaches a stable state only with one value and one value only - when the number of injected ions is the same as the number of injected electrons, i.e., $R = 100\%$. With an increasing ratio R, the oscillation period (T_{osc}) shows a tendency to increase also, to the point for $R = 100\%$, when all the oscillations disappear.

It is necessary to point out that the oscillations presented in Fig. 3.5, for the ratio values 99.995% and 100%, do not originate from the numerical methods and their errors. Namely, the characteristic frequency of the system can be readily estimated as $T_{osc} \approx v_0/L$, where v_0 is the initial injection velocity of the particles and L is the length of the system. The detailed physical reasons concerning both instabilities, the onset and the change of frequency with an increased ion density, is a very intriguing feature, but one which is beyond the scope of this thesis. Fig. 3.6

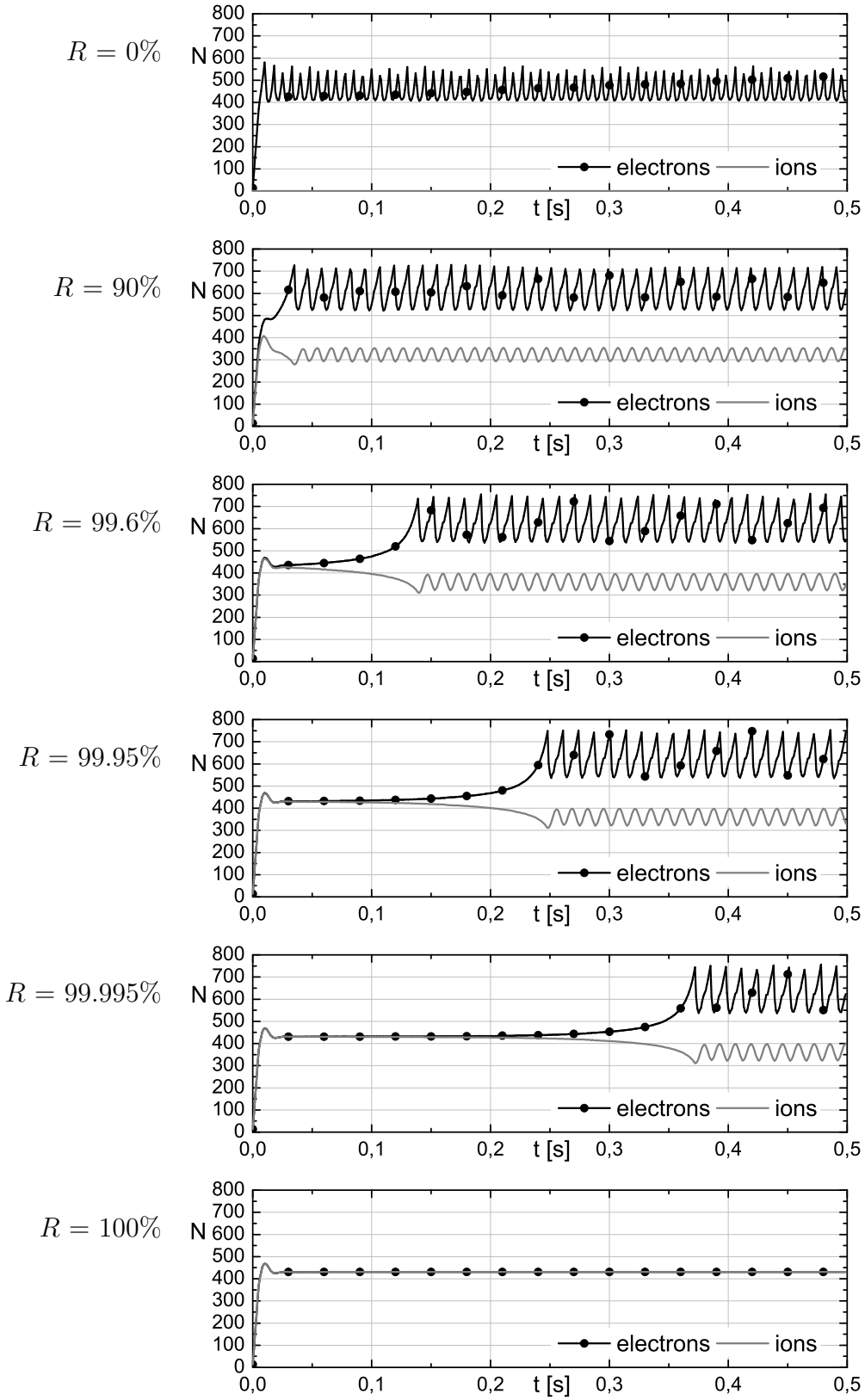

Figure 3.5: Illustration of the onset of oscillations (T_{onset}) and the oscillation period (T_{osc}) for various ratios of electrons and ions (R) as injected on the left- and right-hand side, respectively, with equal mass, charge and initial velocity.

shows the changing onset of oscillations (T_{onset}) and the oscillation period (T_{osc}) in relation to the injection ratio R. It is shown clearly that with an increase of the ratio R, both T_{onset} and T_{osc} increase, with a maximum value of infinity for $R = 100\%$.

However, these phenomena as well as the question why an infinitely small difference in the ratio of particles automatically leads to an unstable state, should be investigated by analytic means. Of course, in a real experiment it is hard to expect that we can adjust the ideal balance, so from this point of view, instability *cannot* be stabilised at all. However, the fact that the simulation employs ideally monoenergetic beams might be inherently a source of the presented scenario. Therefore, the last assumption should be relaxed via employing beams of a finite energy spread (e.g., shifted Maxwellian distributed particles). This is a task that will be fulfilled during the upgrade of our program, so it will be capable of dealing with more realistic simulations.

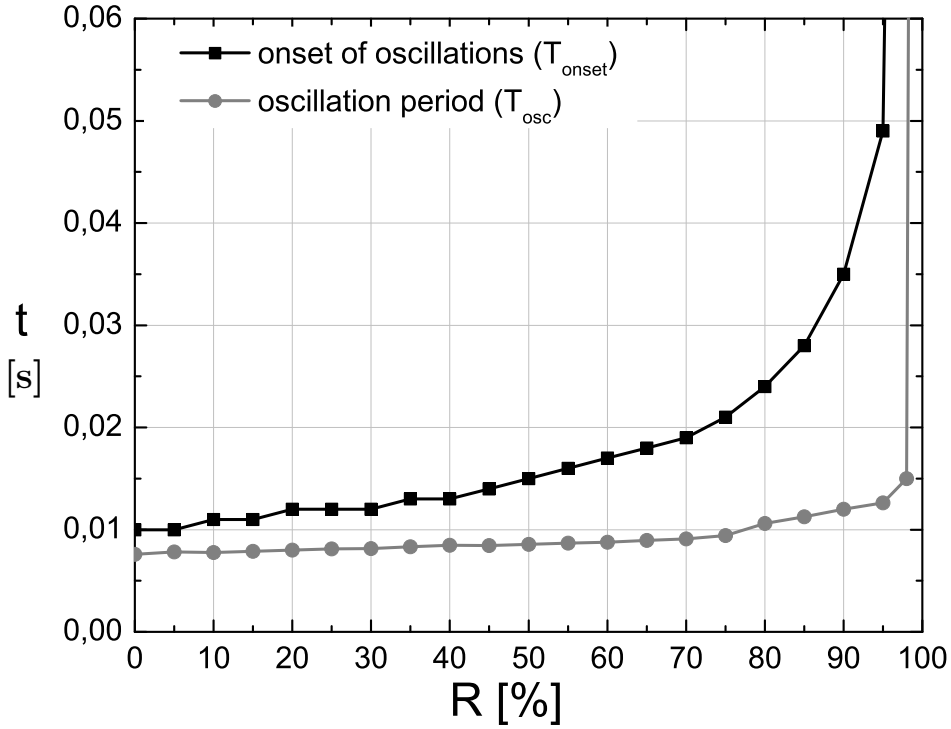

Figure 3.6: Illustration of T_{onset} and T_{osc} change depending on electrons and ions injection ratio R ranging from 0% to 100%.

Chapter 4

Theory and simulations of thermionic emissions in a simple biased diode[2]

The problem of biased diodes with thermionic emission was first presented by Langmuir [11] with a theoretical solution predicting the dependence of a diode current on a biased voltage in plane and cylindrical geometries. It was shown that an increase in the density of emitting particles naturally leads to a potential barrier with a non-monotonic potential profile. For many years, the value of the potential minimum and its position were considered as the free parameters of this problem. Nevertheless, analytical (explicit) expressions for these parameters were only found many years later [60]. However, the question of the stability of such a structure, with the potential bias as an external control parameter, has not yet been fully investigated. In this chapter, the gridless treecode (TC) method was used to address this problem, in a similar manner to Christlieb [14] and Krek [15] for the case of a short-cut diode (Chapter 3). Recent investigations were focused on confirming the high reliability of the treecode method (compared to the direct summation and PIC methods), while in the present investigation we apply the TC method to particular problems of engineering importance. Namely, we use the same cases that were presented in Refs. [11, 60], which, in addition, implies cases with arbitrary finite diode bias voltages, ranging from zero (short-cut) to bias values much higher that the emitted particle's thermal energy.

The simulation system is modelled by a plane-parallel diode, as shown in Fig. 4.1, with a vacuum inside. The distance between the diode electrodes (the walls of the system) is defined as d and the voltage on the cathode (left-hand-side electrode) is defined as V_0. The anode (right-hand-side electrode) is grounded ($V_1 = 0$). The

[2]Original/full text was presented in [44]

electrons have a Maxwellian distribution and are emitted from the cathode without an initial velocity ($v_0 = 0$) and with an initial temperature $T = 1eV$.

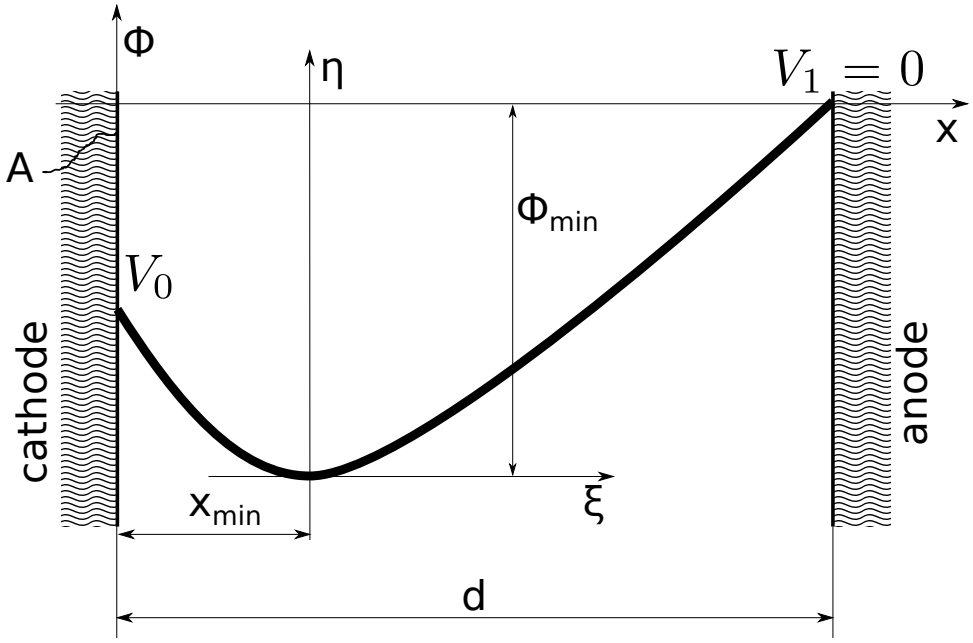

Figure 4.1: Simplified presentation of plain diode with global coordinate system $(x - \Phi)$ and coordinate system of introduced variables $(\xi - \eta)$.

4.1 Langmuir exact solution (theoretical solution)

The exact (theoretical) solution of the potential profile inside a plain diode in a hot-cathode discharge regime was first presented by Langmuir [11] as:

$$\xi(\eta) = \pm \int_0^{\eta} \left(e^t - 1 \mp e^t \operatorname{Erf}(t^{\frac{1}{2}}) \pm \frac{2t^{\frac{1}{2}}}{\pi^{\frac{1}{2}}} \right)^{-\frac{1}{2}} dt \tag{4.1}$$

where the dimensionless variables η and ξ and the Debye length λ are defined as:

$$\begin{aligned} \eta &= \frac{e\Phi}{kT}, \qquad \xi = \frac{x}{\lambda} e^{-\frac{\eta_c}{2}} \\ \lambda &= \sqrt{\frac{\varepsilon_0 kT}{2n_0 e^2}} \end{aligned} \tag{4.2}$$

The error function is defined as:

$$\operatorname{Erf}(x) = \frac{2}{\pi^{\frac{1}{2}}} \int_0^x e^{-t^2} dt \tag{4.3}$$

4.2 Semi-approximation solutions

Martin and Donoso [12] derived an equation for an approximation of the potential profile inside the diode on the right-hand side from the potential minimum (positive values of ξ in Fig. 4.1). Equation 4.4 gives excellent results compared to the exact solution in equation 4.1 (see Fig. 4.2):

$$\xi^{+}(\eta) = \frac{2\sqrt{2}}{3}\pi^{\frac{1}{4}}\left[\left(\eta^{\frac{1}{2}} + r_1\right)\left(\eta^{\frac{1}{2}} + r_1^2\right)^{\frac{1}{2}} - r_1 r_2\right] \tag{4.4}$$

where the constants p_0, r_1 and r_2 are defined as:

$$\begin{aligned} p_0 &= \frac{2}{\pi^{\frac{1}{2}}}\left[1 - \left(1 - \frac{\pi}{4}\right)^{\frac{1}{2}}\right] \\ r_1 &= \left(3 - \pi^{\frac{1}{2}} p_0\right) p_0 \\ r_2 &= \frac{1}{2^{\frac{1}{2}}}\pi^{\frac{1}{4}} p_0 \end{aligned}$$

Jelić [61] presented an approximate solution for the left-hand side from the potential minimum (negative values of ξ on Fig. 4.1) and provided the missing part for a full description of the potential profile with approximation methods:

$$\xi^{-}(\eta) = \left[q_0 \frac{\pi^{\frac{1}{2}}}{\sqrt{2}}\,\mathrm{Erf}\left(\frac{\eta^{\frac{1}{2}}}{\sqrt{2}}\right) + D_n(\eta^{\frac{1}{2}} e^{-\frac{\eta}{2}}) - d_0\right] \tag{4.5}$$

where

$$D_n(\eta^{\frac{1}{2}}) = \sum_{i=1}^{n} d_i \eta^{\frac{1}{2}}$$

A comparison of the results from the approximation solution to the Langmuir (equation 4.1) and the simulation results would be practically impossible without following an inverse approximate solution:

$$\begin{aligned} \eta_{NJ}^{+}(\xi) &= \left(\frac{\xi}{2}\right)^{\frac{3}{2}} \mathrm{Erf}\left(\frac{\xi^{\frac{1}{2}}}{\sqrt{2}}\right) \\ \eta_{NJ}^{-}(\xi) &= \frac{\xi^{\frac{3}{4}}}{\mathrm{Erf}(\frac{1}{2}(\xi + D)^{\frac{1}{2}})} \end{aligned} \tag{4.6}$$

where the constants $D = 2.5533$. Erf(), ξ and η are defined in equation 4.2.

4.3 Simulations

The simulations were performed using the Particle-In-Cell (PIC) and grid-free treecode simulation code (PEG-TC) on three simulation cases. Each simulation case had different cathode voltages, different minimum potentials and a grounded anode and a

vacuum inside the diode. The particles were electrons with a Maxwellian distribution, temperature $T = 1eV$ and without an initial velocity ($v_0 = 0$). The diode's cross-sectional area was $A = 10^{-4}m^2$.

The distance d between the diode electrodes (the system walls) depends on the selected potential minimum and the applied voltage at the cathode. To be able to compare the simulation and theoretical results, the distance d was computed for each simulation case using the universal exact potential profile solution shown in Fig. 4.2. The values for the selected parameters (potential, voltage and distance d) are presented in table 4.1.

Case	Φ_{min}	V_c	d	d
1	3V	-5V	8.344 ξ	1.8935 $\cdot 10^{-5}$m
2	6V	-20V	20.251 ξ	9.23 $\cdot 10^{-4}$m
3	10V	-24V	23.677 ξ	5.892 $\cdot 10^{-2}$m

Table 4.1: Simulation case parameters.

4.4 Results

First, we compare the agreement of the exact and the two approximation methods for the theoretical potential profile and the results are shown in Fig. 4.2. The figure shows excellent agreement between the exact method and the approximations in the selected range of ξ. Asymptotic behaviour on the left-hand side of the potential minimum is clearly seen.

For the case with a high potential difference between the cathode and the anode, potential profile comparisons from the exact method and the two simulation codes (PIC and TC) are presented in Fig. 4.3. It is clear that the PIC method does not give accurate results in the areas to the left of the potential minimum (negative values for ξ). Both simulation methods show an agreement with the exact solution in the area just to the right of the potential minimum (positive values for ξ).

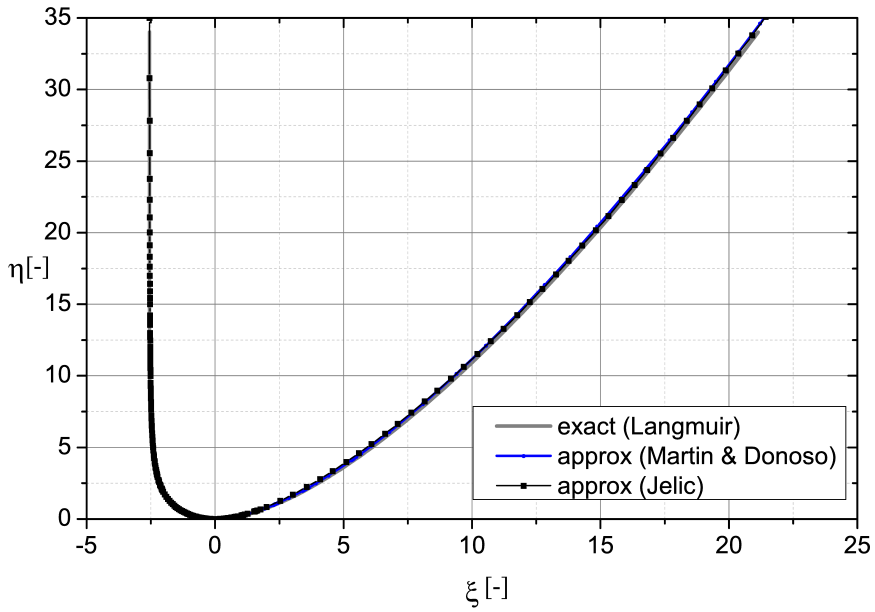

Figure 4.2: Universal potential profiles acquired from exact (equation 4.1) and approximate methods (equations 4.4, 4.5 and 4.6).

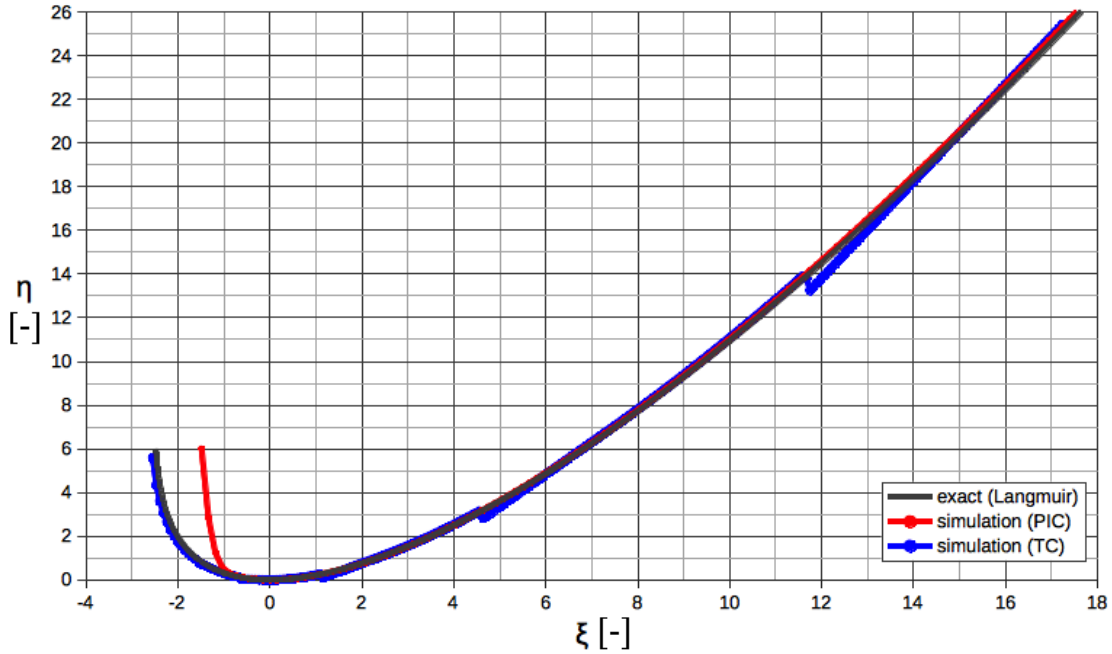

Figure 4.3: Comparison of simulation results acquired with PIC and TC methods with the exact solution (equation 4.1) - potential profiles for case with high potential difference between cathode and anode.

Chapter 5

PIC simulations on the plasma-sheath boundary in collisionless plasmas with warm ion sources[3]

Finding and defining the plasma-sheath boundary (also called the "plasma edge", "sheath edge" or "sheath entrance") is a problem of ubiquitous relevance and importance in plasma physics. In a conventional approach, this problem starts from Poisson's equation (2.6) with assumptions that: (i) the electron density distribution is a known function of the local potential, (ii) the ion source velocity distribution is known, and (iii) the potential profile is monotonic. The basic unknown quantities of the problem to be determined are the spatial potential profile $\Phi(x)$ (or, equivalently, the electric-field profile) and the final ion velocity distribution function (ion VDF) $f_i(\Phi, v)$ at any location of the discharge (or, equivalently, for any potential), where x (position) and v (velocity) are the usual phase-space diagram coordinates. Mathematically, this problem is defined by a coupled set consisting of the Boltzmann and Poisson equations, which in plane-parallel geometry (i.e., for the considerations of the present work) read as:

$$v\frac{\partial f_i}{\partial x} - \frac{e}{m_i}\frac{d\Phi}{dx}\frac{\partial f_i}{\partial v} = S_i(x, v) \tag{5.1}$$

$$\int_{-\infty}^{\infty} f_i(\Phi, v)dv = n_e(\Phi) - \frac{\varepsilon_0}{e}\frac{d^2\Phi}{dx^2}, \tag{5.2}$$

with e the positive elementary charge, m_i the ion mass, ε_0 the vacuum dielectric constant, and $S_i(x, v)$ the ion source term. The problem is closed, provided that the boundary conditions are well defined.

[3]Original/full text was presented in [59]

A formal solution of equation (5.1) is

$$f_i(\Phi(x), v) = \int_{\Phi'} \frac{dx'}{d\Phi'} \kappa(\Phi, \Phi', v) d\Phi' \tag{5.3}$$

where

$$\kappa(\Phi, \Phi', v) \equiv \frac{S_i\left(\Phi', v^2 - \frac{2e}{m_i}(\Phi' - \Phi)\right)}{\sqrt{v^2 - \frac{2e}{m_i}(\Phi' - \Phi)}} \tag{5.4}$$

so equation (5.2) takes the form of an integro-differential equation

$$\int_{\Phi'} \Psi(\Phi') \mathcal{K}(\Phi, \Phi') d\Phi' = n_e(\Phi) + \frac{\varepsilon_0}{e} \frac{dx/d\Psi}{|\Psi|^3} \tag{5.5}$$

where

$$\mathcal{K}(\Phi, \Phi') = \int_v \kappa(\Phi, \Phi', v) dv \tag{5.6}$$

is the known kernel of the integro-differential equation, if S_i is prescribed. The unknown function to be found from equation (5.5) is the negative value of the inverse electric field $\Psi \equiv dx/d\Phi \equiv -1/E$. Once this quantity is found the ion velocity distribution $f_i(\Phi(x), v)$ from equation (5.3).

Solving the above problem is a very demanding task, even with present-day numerical methods and computational resources. The first difficulty arises when choosing a particular source function, which has to be physically meaningful and at the same time amenable to analytic or numerical integration for obtaining the kernel. For the "regular" case of "warm" ion sources (when ions are generated with a distribution of finite initial velocities), the kinetic problem formulated above is of such complexity that it was never solved for the whole discharge region.

5.1 Defining the position of the plasma-sheath boundary

In 1929, Tonks and Langmuir [62] triggered this kinetic problem with a "cold" ("singular") ion source distribution, i.e., all the ions are generated with a zero initial velocity ($v_0 = 0$). Mathematically speaking, the ion source distribution in their model was defined as:

$$S_i(x, v) = s_i(\Phi)\delta(v) \tag{5.7}$$

$$\delta(x) = \begin{cases} \infty & x = x_0 \\ 0 & x \neq x_0 \end{cases} \tag{5.8}$$

where δ is the well-known Dirac δ function. However, at that time the problem of dealing with the complete "plasma and sheath equation" still appeared to be too difficult, as Tonks and Langmuir termed the model. In our terminology, they felt able to deal only with $\varepsilon \to 0$ plasmas, but not with *finite-ε* ones, where the smallness parameter ε is defined as $\varepsilon \equiv \lambda_D/L$, with L the pre-sheath (plasma) characteristic length and $\lambda_D \equiv \sqrt{\varepsilon_0 k T_e/n_e e^2}$, the electron Debye length. It is well known that the plasma state is defined for $\varepsilon \ll 1$, otherwise the ionised system is not a plasma, but just an ionised gas unable to establish quasi-neutrality. Tonks and Langmuir employed the condition $\varepsilon \to 0$ ("asymptotic two-scale limit"), i.e., neglecting the term originating from the second derivative of the potential. In this way they obtained the nowadays famous "plasma equation", which holds in the case of strict plasma quasi-neutrality. They solved the plasma equation using an analytic expansion method.

Harrison and Thompson, however, found an exact analytic solution for that in 1959 [63]. Furthermore, a rigorous mathematical formulation of the asymptotic two-scale plasma and sheath problem was given in 1962 by Caruso and Cavaliere on the basis of boundary-layer theory. Self in 1963 [18], on the other hand, solved the one-dimensional "plasma and sheath equation" numerically *without* splitting the discharge into the plasma and the sheath regions. One important consequence emerging from his work is that, for *finite-ε*, the plasma-sheath boundary is a rather arbitrary concept from the academic point of view *but that, anyway, it is important to define it for practical purposes*. The only situation for which the plasma-sheath boundary is unambiguous is the asymptotic, two-scale limit ($\varepsilon \to 0$), in which case it is defined by the famous Bohm criterion, which was originally obtained in 1949 by using a simple fluid model [26].

This criterion was upgraded to another famous formulation [63] known as the Harrison-Thompson plasma-sheath criterion (frequently also referred to as the generalised Bohm criterion), which is valid for arbitrary electron and ion velocity distributions. The Harrison-Thompson criterion for the case of Maxwellian distributed ion sources with non-negligible temperatures was confirmed explicitly by Bissel and Johnson [64] and Scheuer and Emmert [65]. Physical interpretations of this criterion were given in both fluid [66] and kinetic treatments [67]. There the plasma-sheath transition was interpreted as a surface where slow perturbations ($\omega/k \to 0$) originating from the sheath region are incapable of penetrating into the plasma.

In particular, it would be of great importance to *unify* the plasma and sheath descriptions for various discharge scenarios with finite ε. One way to do this is to find some universal rules that hold for the whole discharge region, i.e., some kind of "similarity variables" that reduce the dimensionality of the problem. This task has already been partially performed for plasmas modelled in the fluid [68]

and kinetic [69] approaches by using solutions that hold in the intermediate plasma region to match together the plasma and sheath solutions obtained in the asymptotic two-scale approach. While these scalings are well confirmed in both fluid and kinetic models with cold ion sources, scalings in kinetic models with warm ion sources were just *predicted* (see, e.g., [70, 71]) on the basis of rather general kinetic considerations, but never confirmed explicitly due to a lack of appropriate analytic and/or numerical solutions for the intermediate region.

From the practical point of view, unifying the plasma and sheath descriptions is frequently not of primary importance, but on the contrary *distinguishing* the plasma and the sheath regions is the issue at hand. In particular, for simulations of the Scrape-Off Layer (SOL) regions in tokamak devices with fluid codes (like, e.g., SOLPS and EDGE2D [72]) it is necessary to define the boundary conditions at the quasi-neutral plasma edge and not at the wall. The investigations of [73] and [74] indicate that the plasma-sheath boundary can be identified using the concept of the "local polytropic coefficient" $\gamma(x)$, which exhibits a characteristic kink-like behaviour at the transition between the quasi-neutral pre-sheath plasma and the non-neutral sheath. The ability to define γ enables a reliable calculation of the ion sound velocity $c_s(x) = \sqrt{(kT_e + \gamma kT_i)/m_i}$. It will be shown here how to find the plasma-sheath boundary and also the place where the ion sound velocity, with such a calculated ion polytropic coefficient, equals the ion fluid velocity.

5.2 Numerical (PIC) simulation

PIC (Particle-In-Cell) simulations were performed using the PIC simulation program BIT1, that has a special feature: it is capable of maintaining the electron velocity according to a Maxwellian distribution in the region of quasi-neutral plasma, even in the absence of collisions - just like in real experiments.

The initial (source) velocity distribution of both electrons and ions is Maxwellian. Electrons are "born" (added/injected to the system) with a fixed temperature $T_{e,src} = 1eV$ (index "src" means "source temperature"), while the ion initial temperature $T_{i,src}$ is changed in simulations, and representative results with equal electron and ion source temperatures are shown. In our simulations the electrons and ions are injected into the simulation domain in pairs, with injection positions randomly distributed over the simulation volume. After a steady state is established, the electron velocity distribution remains Maxwellian with a cutoff in the tail of the velocity distribution. The position of the cutoff of the electron VDF depends on the local plasma potential. However, this cutoff of the tail does not have a serious influence on the electron temperature, which is very close to $1eV$ in the steady state. On the contrary (as will be seen below), the final ion velocity distribution is

far from Maxwellian-like, in spite of the fact that the ion source distribution is also Maxwellian. In any case, the cutoff is an inherent result of the simulation itself and, unlike the theoretical models where it is usually ignored, it would be hard to avoid this effect (e.g., for the purposes of fitting some theoretical models).

The system of research is defined as a one-dimensional plane-parallel system with the electrodes positioned as shown on Fig. 5.1. The distance between the electrodes is $L = 0.03m$ and the inner-space is divided into 8192 cells. The simulations were performed with the enhanced and updated BIT1 (Berkeley-Innsbruck-Tbilisi) 1D simulation code [54]. The plates at $x \pm L/2$ are assumed to be perfect absorbers and electrically floating. The profile of the electrostatic potential $\Phi(x)$ is assumed to be monotonic, decreasing for $x > 0$, and is defined to be zero at $x = 0$, that is $\Phi(0) = 0$.

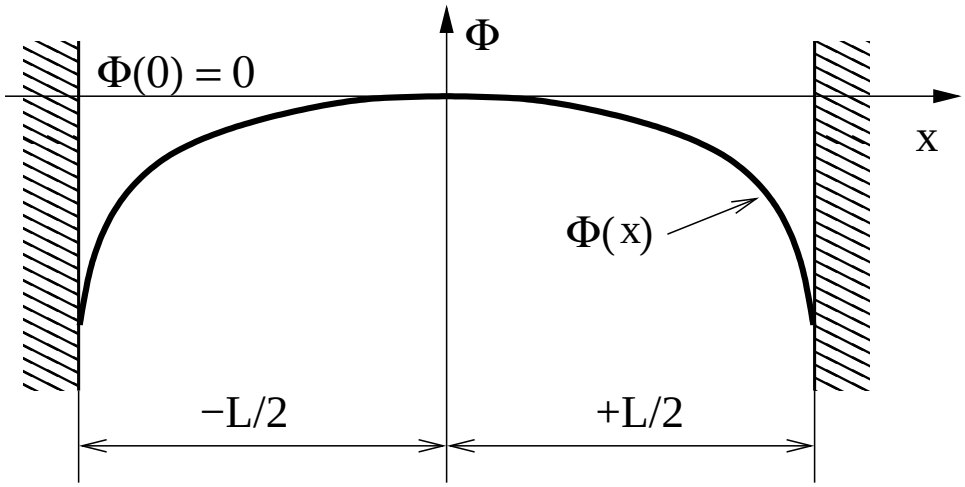

Figure 5.1: The geometry of the system with the position of the coordinate system and a sketch of the potential profile.

5.2.1 Changing the ion source profile during the simulation

The currently available version of BIT1 does not offer the possibility to change the ion source profile during the simulation. It is possible to define the ion source profile at the beginning of the simulation in the form of the input file, but not during the simulation. When new electrons are born, their position is selected randomly in the source area (which was in our case the whole system, from $x = -L/2$ to $x = L/2$, see Fig. 5.1). To "upgrade" BIT1 and to include the possibility to take into account the ion strength profile in the current simulation step, it was decided that the ion strength profile would be computed as

$$S_i(x) = e^{\alpha\Phi(x)} \tag{5.9}$$

where $\Phi(x)$ is the potential and α is the source strength factor.

The idea is that with a larger value of $S_i(x)$ in a given grid cell (at the position x), the probability that an electron is born in that cell is also larger. The easiest way to achieve this is to calculate the area below the function (presented in equation 5.9, see Fig. 5.2) and then use the calculated value in a function that defines (randomly selects) a new electron position. Because the integration is done numerically with a known grid in the direction x, the calculated area can also be expressed as a strip that is Δx wide and L'_{total} long. Here, Δx is the distance between the grid points (defined in simulation parameters) and L'_{total} is the sum of all the lengths below $S_i(x)$ for the whole system (equation 5.10 and Fig. 5.2).

$$\begin{gathered} L'_i = e^{\alpha\Phi(i)} \quad L'_k = e^{\alpha\Phi(k)} \\ L'_{total} = \sum_{i=0}^{N} L'_i = \sum_{i=0}^{N} e^{\alpha\Phi(i)} \end{gathered} \tag{5.10}$$

where N is the number of grid cells. The steps in computing the new particle-insertion position, i.e., the grid cell, are:

- select random value between 0 and L'_{total} and mark the value with L'_{sel},
- check the condition presented by equation (5.11) for each grid cell

$$L'_{i-1} < L'_{sel} <= L'_i \tag{5.11}$$

  where i is the grid-cell index from 1 to N and
- the first cell (defined with the grid cell index i) for which the condition in equation (5.11) is true, it is the grid cell for new particle.

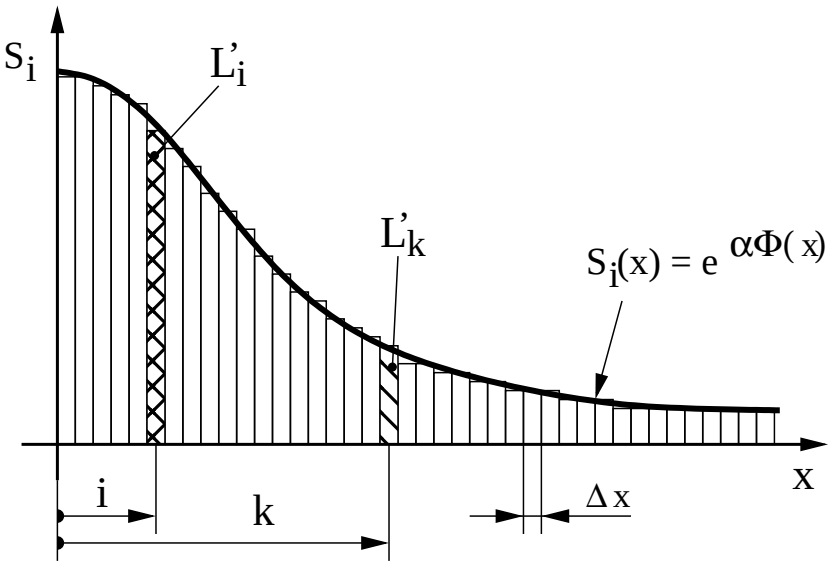

Figure 5.2: Graphical representation of how the area under function is calculated and divided into strips. The total length of the strips (L'_{total}) is used as the upper limit from which new particle positions are randomly selected.

New particles are injected (added) to the system at every simulation step, which includes computing the injection position of the new particles. With this, calculating the value of L'_{total} and defining the grid cells for the injected particles is performed for each simulation step. The "updated" BIT1 could perform worse compared to the "original" BIT1 because of the extra computing performed and the comparison of the simulation running time, and their difference is presented in Chapter 5.3.3.

5.3 Results

5.3.1 Influence of strength factor α on the particle distribution

The influence of strength factor α (equation 5.9) on the electron and ion distributions was tested for five cases, as presented in table 5.1. Fig. 5.3 shows to what extent the electrons and ions remain Boltzmann distributed during the simulation in relation to the potential. A logarithmic scale presentation was used for a better representation of the respective densities n_{01} - n_{05}, as defined at the plane of symmetry. Note that the reference potential $\Phi = 0$ in this presentation is taken in the middle of the system and the wall is at the right-hand side (Fig. 5.1). Straight lines with the same slope (slopes correspond to the electron temperature and are constant, independent of the plasma density) fit these curves well, at least in the plasma core, i.e., for small values of the potential.

Fig. 5.4 illustrates the ion velocity distributions obtained for the case when the source velocity distribution of both electrons and ions is Maxwellian. While the electron *final* velocity distribution remains Maxwellian, the ion final velocity distribution in the steady state was predicted to dramatically change in the whole volume [64, 65].

Case	n at L/2	λ_D	ε
1	$2 \times 10^{14}\ m^{-3}$	5.27×10^{-4}	3.513×10^{-2}
2	$1.08 \times 10^{15}\ m^{-3}$	2.27×10^{-4}	1.513×10^{-2}
3	$2.2 \times 10^{15}\ m^{-3}$	1.58×10^{-4}	1.053×10^{-2}
4	$1.14 \times 10^{16}\ m^{-3}$	7×10^{-5}	4.76×10^{-3}
5	$1.15 \times 10^{17}\ m^{-3}$	2.2×10^{-5}	1.47×10^{-3}

Table 5.1: Plasma densities (at the plane of symmetry of the discharge), Debye lengths at the centre of the plasma and the corresponding smallness ε-parameters used.

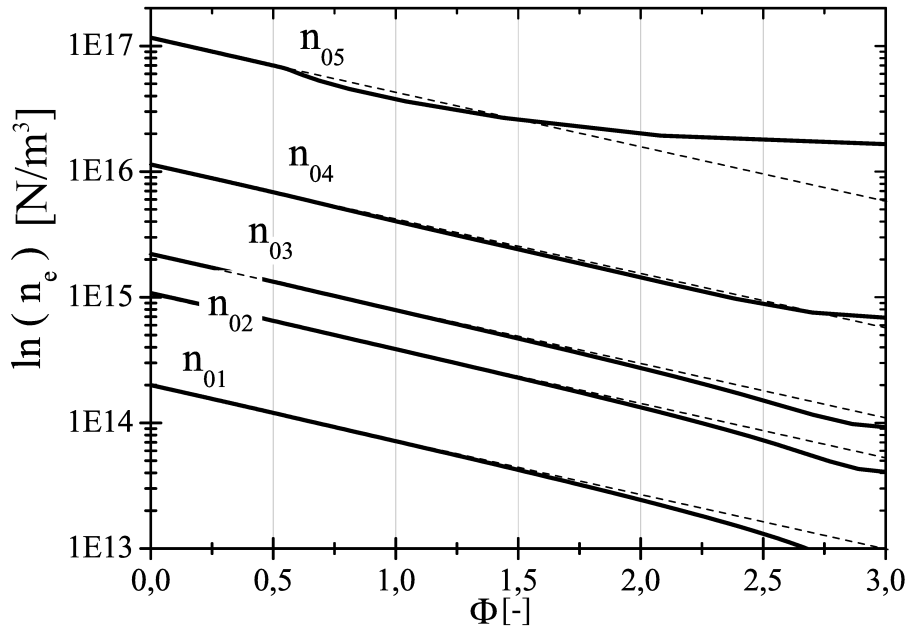

Figure 5.3: The electron density profile on a logarithmic scale as a function of the local plasma potential Φ as normalised to the electron temperature.

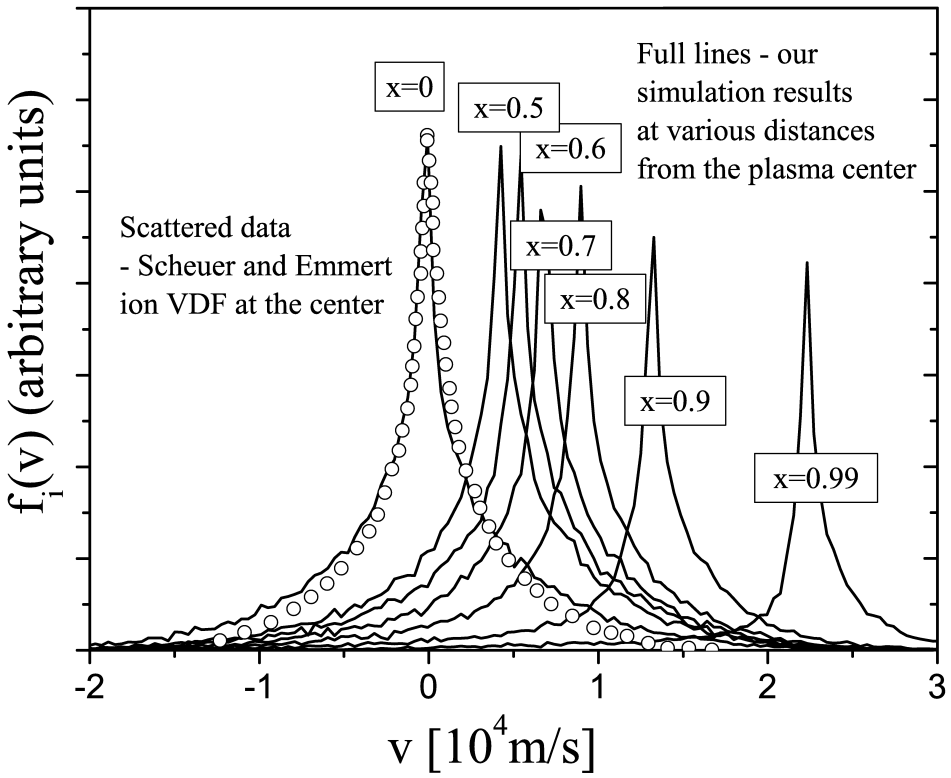

Figure 5.4: Velocity distribution as a function of the distance from the centre for the case of the smallest density that was simulated (i.e., $\varepsilon = 3.513 \times 10^{-2}$). The shape of the velocity distribution at the plane of symmetry of the system is compared with with the results obtained by Scheuer and Emmert.

Fig. 5.5 shows the ion temperature profiles and the corresponding local values of γ_i for various ε as functions of the normalised local plasma potential. This is a very important picture for understanding the behaviour of ions near the plasma-sheath boundary and in the sheath as well. Namely, there is clear evidence that γ_i has a maximum in a wide range of ε. In fact, this maximum is the only observable characteristic point in the full-scale model. From the mathematical point of view it corresponds to the place where the ion temperature has an inflection point. From the physical point of view these maxima correspond to the place where the ions

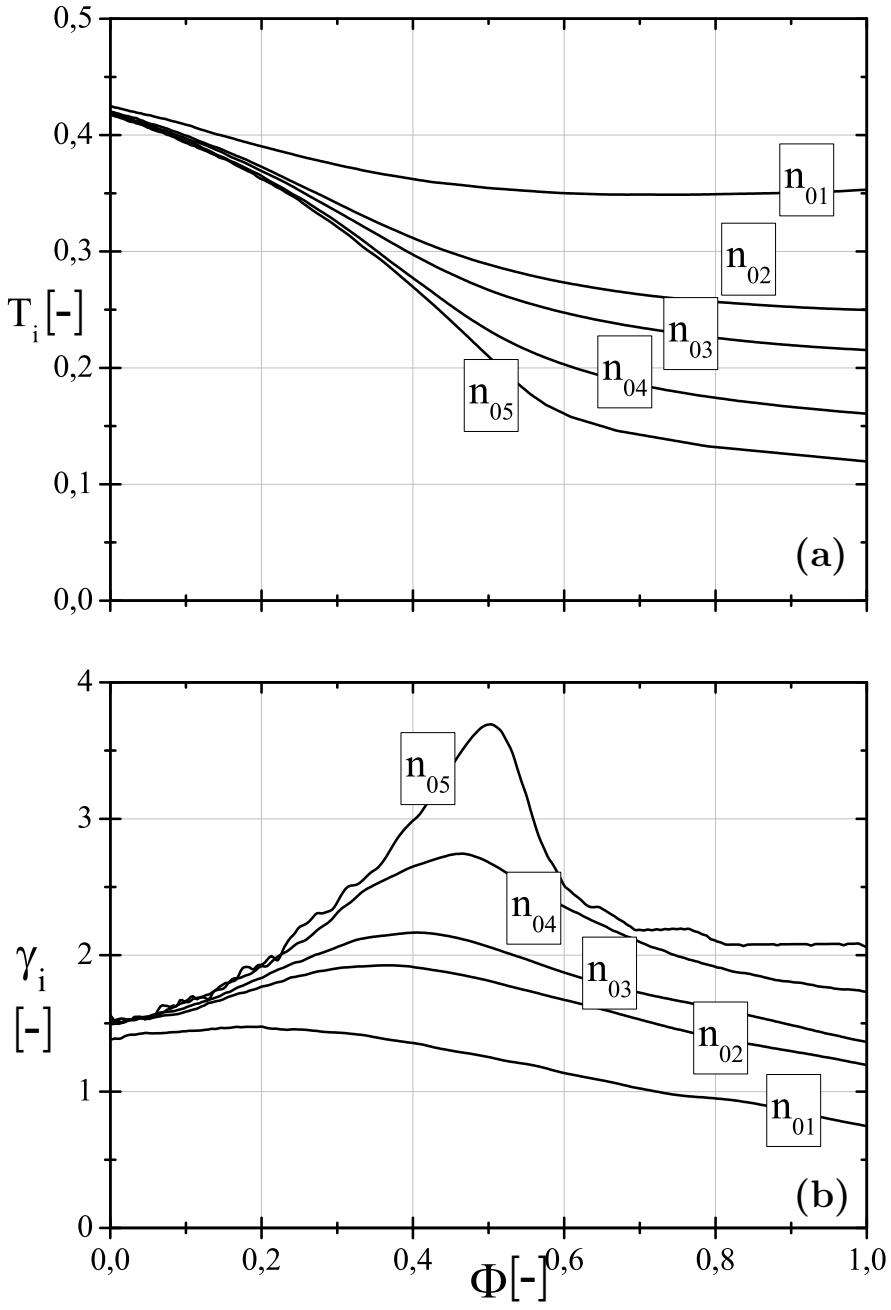

Figure 5.5: The ion temperature profiles (a) and the corresponding local values of γ_i (b) for various ε as functions of the local plasma potential. It is evident that the maximum of γ_i is strongly dependent on the value of ε.

become strongly accelerated towards the wall. This implies that the electric field gradient is the strongest here. Unlike the cold-ion source models, in the warm-ion source model this place does not coincide with the place where the so-called marginal Bohm criterion holds. It turns out to be a better measure of the unknown plasma-sheath boundary $\Phi_s - x_s$ than the place of the marginal Bohm criterion, as taken from the two-scale approach.

Note that the ion temperature increases in the sheath (next to the point of the temperature inflection) maximum of γ, as we approach the wall. This is a common feature in both cold and warm ion sources models, confirmed both in numerical solutions and computer simulations [see also 74]. This has a simple explanation that in the full-scale approach (both plasma and sheath regions) the ions are created in the sheath in a wide range of local sheath potentials, so the final velocity distribution and the corresponding ion temperature depend strongly on the sheath width. The ion temperature in the sheath is wider as the sheath is thicker (increased ε). However, this mechanism fortunately does not "mask" or "delete" the inflection point of the ion temperature, at least in the collisionless plasmas that we are considering here.

Nevertheless, we consider our results rather reliable for determining the plasma-sheath boundary based on the theory of [73]. The so-called "sonic point" has to be found for the known local ion polytropic coefficient, determining the local ion sound velocity. Then one has to find the point where the ion sound velocity equals the ion average directional velocity towards the physical plasma boundary. This method is illustrated in Fig. 5.6 for various plasma densities. Once the potential Φ_s is known, the remaining task is to find the location corresponding to such a potential for each particular density. We show in Fig. 5.7 the method for determining the plasma sheath's physical locations x from simulated $\Phi(x)$ curves with values Φ_s determined from Fig. 5.6.

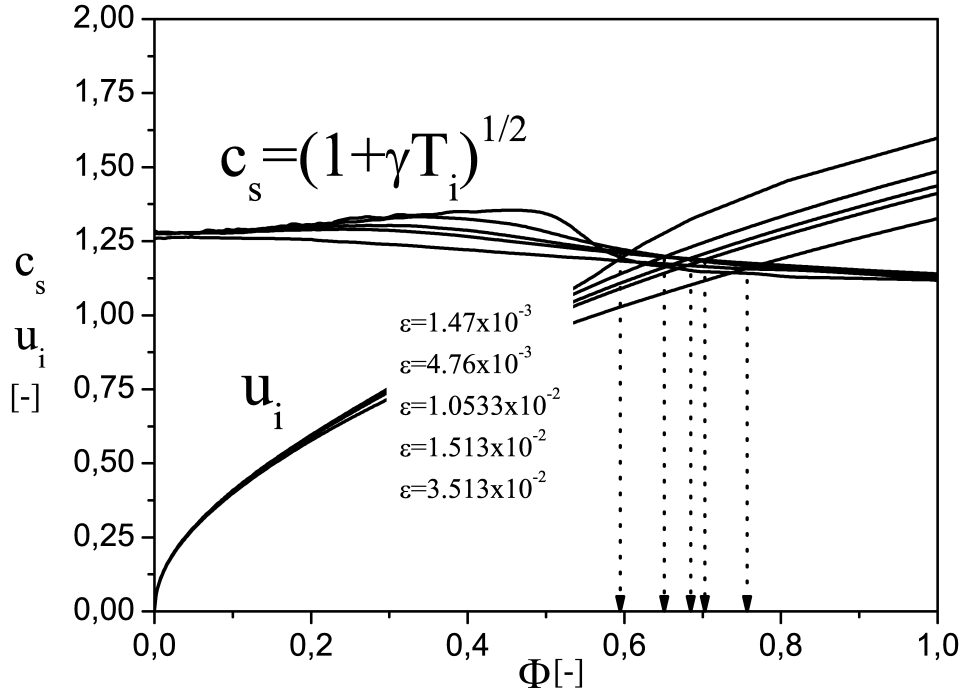

Figure 5.6: Determination of the plasma-sheath potential as a point in which the ion fluid velocity u_i equals the ion sound velocity $\sqrt{1+\gamma T_i}$.

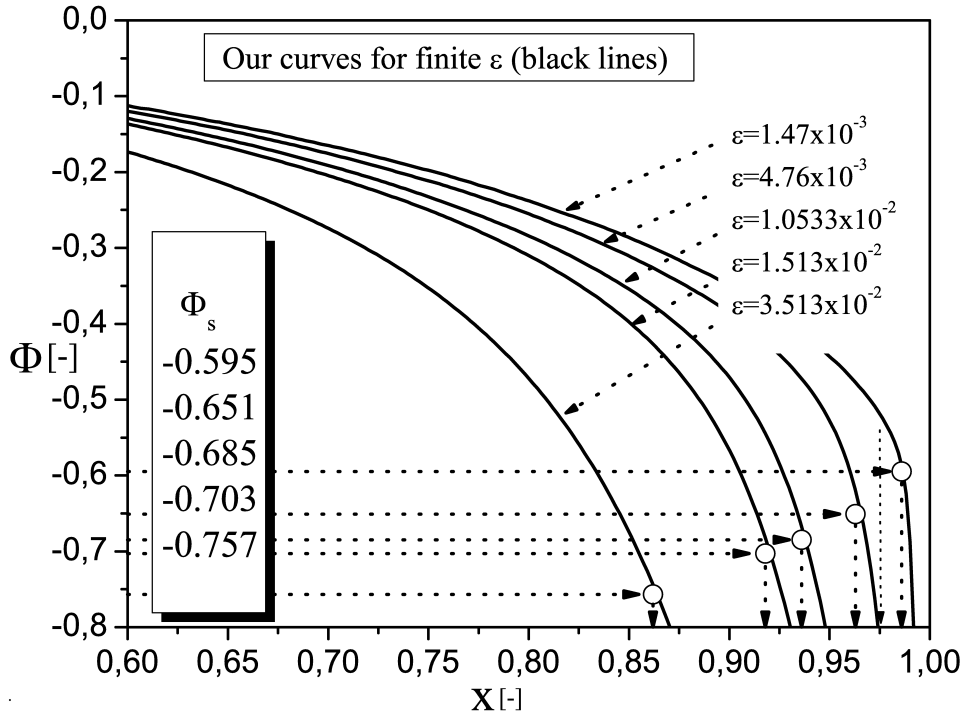

Figure 5.7: Illustration of the method for determining the plasma sheath physical locations from $\Phi(x)$ curves with values Φ_s determined from Fig. 5.6.

5.3.2 Influence of the strength factor α on the particle distribution

As stated before, both electrons and ions are born with a fixed temperature $T_{e,src} = T_{i,src} = 1eV$. The first simulations were performed with $\alpha = 0$ ("flat" ion source profile) and the potential profile was compared with the potential profile obtained by Scheuer and Emmert (S&E), as shown in Fig. 5.8. Fig. 5.8 shows surprisingly good agreement, in spite of the fact that S&E claimed that their theoretical curve was obtained with $\alpha = 1$. The difference is obvious only in the sheath region, where the PIC method is superior in the sense that the PIC method also describes the sheath region in addition to the quasi-neutral plasma.

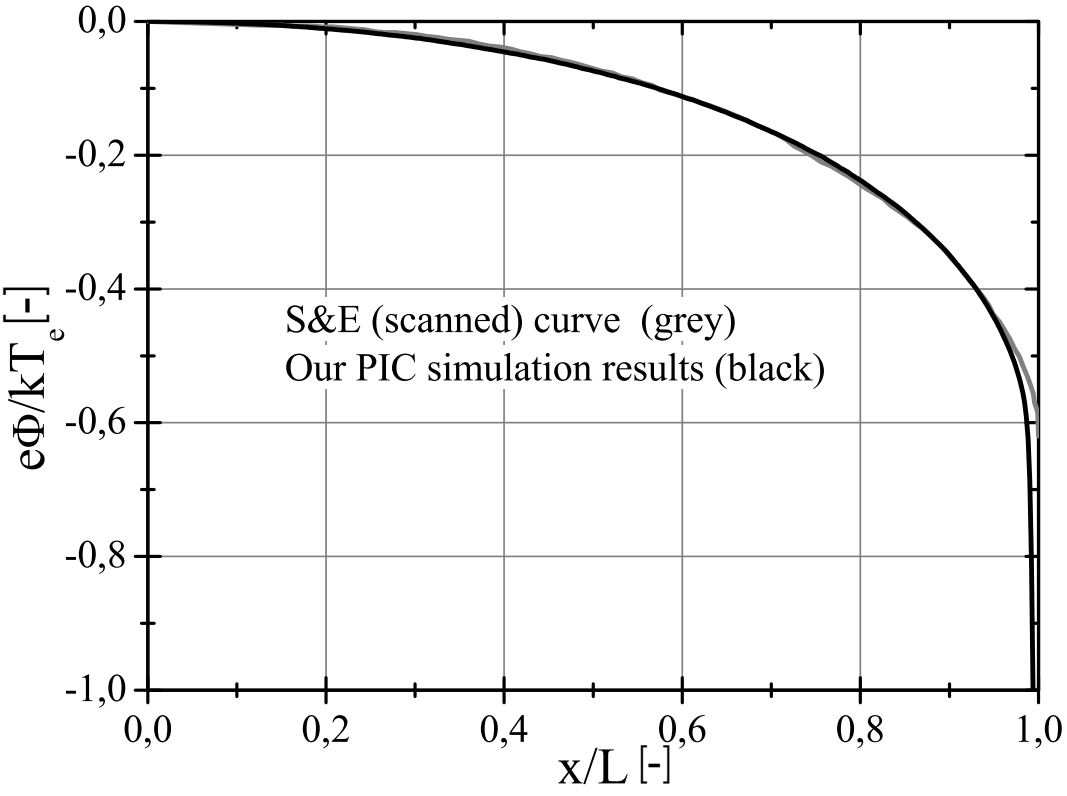

Figure 5.8: Comparison of our PIC simulation results with the results of Scheuer and Emmert.

Now we compare our PIC simulation results obtained using $\alpha = 1$ with theory, developed in [57]. The theoretical potential profile utilises the limit value for ε: $\varepsilon = 0$. With this in mind, the theoretical results are valid for plasmas with small values of λ_D and very high densities. Because in the PIC simulation ε is small, but not 0, the density is always limited and can never be as high as in theory. Fig. 5.9 presents a comparison of the potential profiles resulting from PIC simulations and theory for the same source term $S_i \approx e^{\Phi}$. It is shown that in simulations with higher densities, the potential profile is approaching the theoretical potential profile.

This suggests that running simulations with very high densities, potential profiles from both the theory and simulation would coincide. That would require huge computational resources or even better, some kind of multiprocessor (OpenMP or MPI) version BIT1 that is capable of utilising all the available memory and CPUs in clusters. Of course, the OpenMP version would be used for running the simulation on "smaller" crunching machines (machines with multiple processors and multiple cores per processor), the MPI version would be used on "big" computing clusters with a large number of nodes.

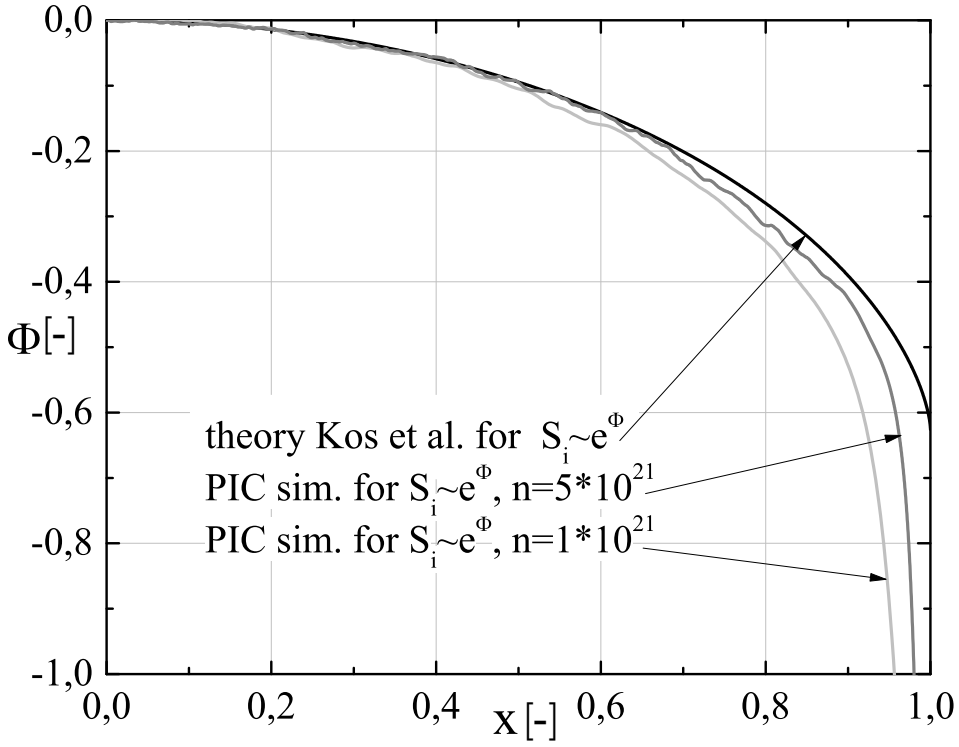

Figure 5.9: Comparison of the potential profile from PIC simulations and theoretical results.

5.3.3 Comparing running times of two BIT1 versions

When compared to the original BIT1 simulation ($S_i = const$), the PIC simulation in the updated BIT1 code ($S_i \approx e^{\Phi}$) requires some additional computation time for integrating S_i and defining the grid cell for injected particles. The purpose of the comparison was to check how much these additional features add to the total simulation computer time. The compared simulations were the same in all parameters (initial conditions, temperatures, system geometry and dimensions, etc.), except for the ion source strength profiles: one being constant and the other with a profile proportional to Φ. The simulations were stopped after 1×10^6 simulation steps and were only run to compare the simulation times (not part of any other simulation and at stop time they were not even close to the steady state). Fig. 5.10

shows the difference in the simulation times that were recorded every 4096 simulation steps, which is the frequency of writing dump and data files in BIT1. Although the computation of the ion source strength values takes some additional time in every simulation step, one can observe from Fig. 5.10 that the ion source strength profile does not influence much on the overall simulation time and can be neglected compared to the overall simulation computation time. The average difference in computer times is around 1.5% and stays constant even with a larger number of simulation steps.

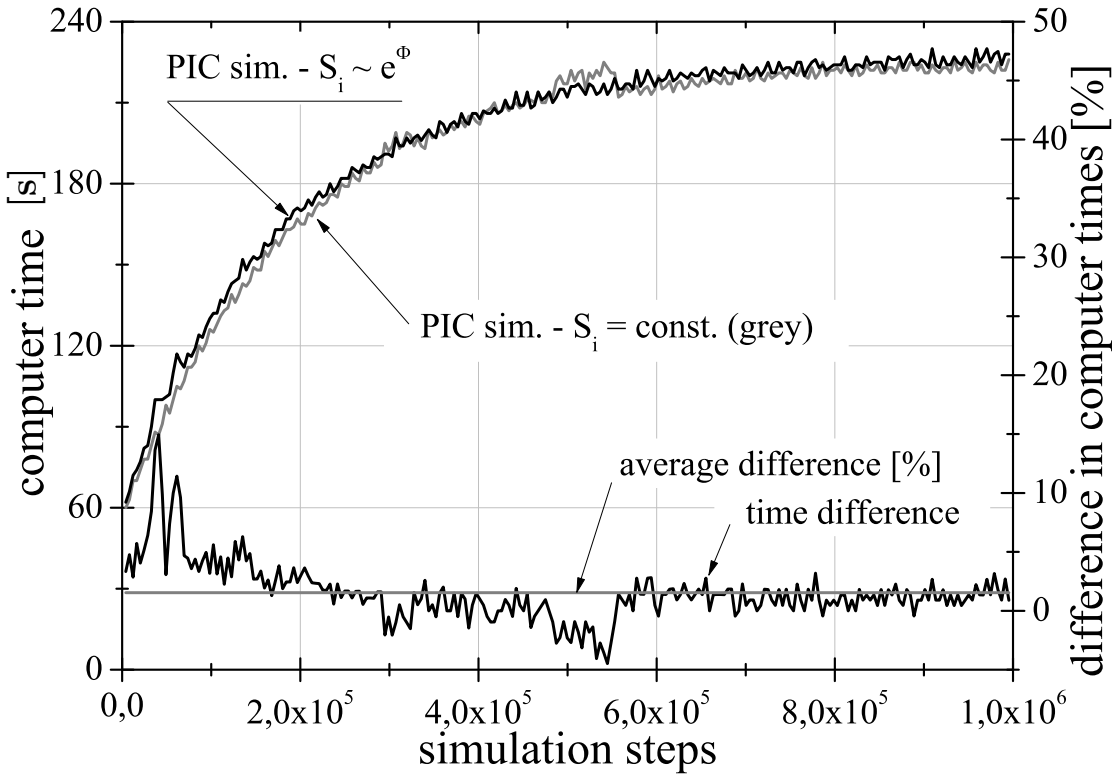

Figure 5.10: Comparison of simulation computer times needed to run for various simulation steps for $S_i = const$ and $S_i = e^{\Phi(x)}$.

Chapter 6

Gradients in a gas-filled diode during electrical breakdown[4]

In comparison to pure DC discharges in the steady state, the transition stage leading towards a breakdown situation is an even harder problem to solve. Problems involving transition stages are relatively purely investigated via kinetic codes, especially in cases when extremely dense plasmas are present. This was the main motivation for doing an investigation with a particular scenario of the discharge ignition using an ideal DC current generator. 2D simulations [75] were made using the 2D simulation code XOOPIC, which is based on the 2D Particle-In-Cell (PIC) method with the included Monte Carlo Collision (MCC) method [76] (Fig. 2.1).

The simulations are essentially based on solving a self-consistent system of Newtonian equations for a system of particles, with each particle defined by the index i, at positions $\vec{r}_i$:

$$m_i\ddot{\vec{r}}_i = e_i[\vec{E}(\vec{r}_i,t) + \dot{\vec{r}}_i \times \vec{B}(\vec{r}_i,t)] + \vec{F}_i, \tag{6.1}$$

with $i = 1, 2, \ldots, N$ (N is number of particles) and the total electric ($\vec{E}$) and magnetic ($\vec{B}$) fields acting on a particle i [77] defined as:

$$\vec{E}(\vec{r}_i,t) = -\left[\nabla\Phi(\vec{r},t) + \frac{\partial\vec{A}}{\partial t}(\vec{r},t)\right]_{\vec{r}=\vec{r}_i} \tag{6.2}$$

$$\vec{B}(\vec{r}_i,t) = \left[\nabla \times \vec{A}(\vec{r},t)\right]_{\vec{r}=\vec{r}_i} \tag{6.3}$$

[4]Original/full text was presented in [36]

with:

$$\Phi(\vec{r}_i, t) = \frac{1}{4\pi\varepsilon_0} \sum_{j=1}^{N-1} \frac{e_j \delta(\vec{r}_i - \vec{r}_j)}{|\vec{r}_i - \vec{r}_j|} \tag{6.4}$$

$$\vec{A}(\vec{r}_i, t) = \frac{1}{4\pi\varepsilon_0 c^2} \sum_{j=1}^{N-1} \frac{e_j \dot{\vec{r}}_j \delta(\vec{r}_i - \vec{r}_j)}{|\vec{r}_i - \vec{r}_j|} \tag{6.5}$$

The flowchart for numerically solving the above equations is shown in Fig. 2.1 [78], which, together with the proper boundary conditions (BCs), represents a fully self-consistent approach. However, a universal implementation of the approach is a difficult task and the approach that neglects the magnetic vector potential $\vec{A}$ is used here with an evaluation of its possible importance a posteriori.

6.1 Numerical simulation parameters

Starting with the assumption that in a small chamber (diode) containing neutral gas atoms of density $n_a \sim 10^{23}$ there could be sufficient ionisation to yield an ion-current density (of single ionised ions) $j = en_i u_i \sim 10^8 A/m^2$ (with a characteristic for a cold non-isothermal plasma with $T_e \sim 1eV \gg T_i$ ion velocity u_i, caused by ambipolar flow at the plasma edge, of the order 10^4). From an engineering point of view this is represented by a small, disk-shaped plasma volume of the order of $V_D = S_D L_D \sim 10^{-6} m^3$ with an inner-electrode distance of the order of one millimetre. In the steady state, the maximum ion current in such cases can be estimated to be of the order of $I \sim 10^2 A$. Of course, it could be considerably higher when either the ion-directional velocity is much higher or during the periods when the currents consist only of electrons.

The simulations were performed with a constant DC current (option G_C on Fig. 1.1) the value of which is much below the value stated above. The reason for such a current value selection is that the idea was to obtain a DC regime, even if the ionisation degree is as small as 10^{-3}. The computational domain is presented in Fig. 6.1 and a system with the coordinate system is displayed in Fig. 6.5. As shown in Fig. 6.5, the system is a disk-shaped (azimuthally symmetrical about z) gas-filled diode with the following parameters: disk diameter $d_D = 1$ cm, inner-electrode distance $L_D = 1$ mm and biased electrodes at a constant external current-generator $I = 0.01$ A. The external resistivity, inductance and capacitance are neglected. A small number of initial electrons and argon ions are created in a basic argon gas background at a pressure that is sufficiently high (4 Torr) to initiate an electron avalanche. The anode (A) is grounded, while the initial cathode (C) voltage is $V_C = -1000$ V. Each ion reaching the cathode is neutralised there and during its impact with the cathode, a new (secondary) electron will be delivered (with a certain

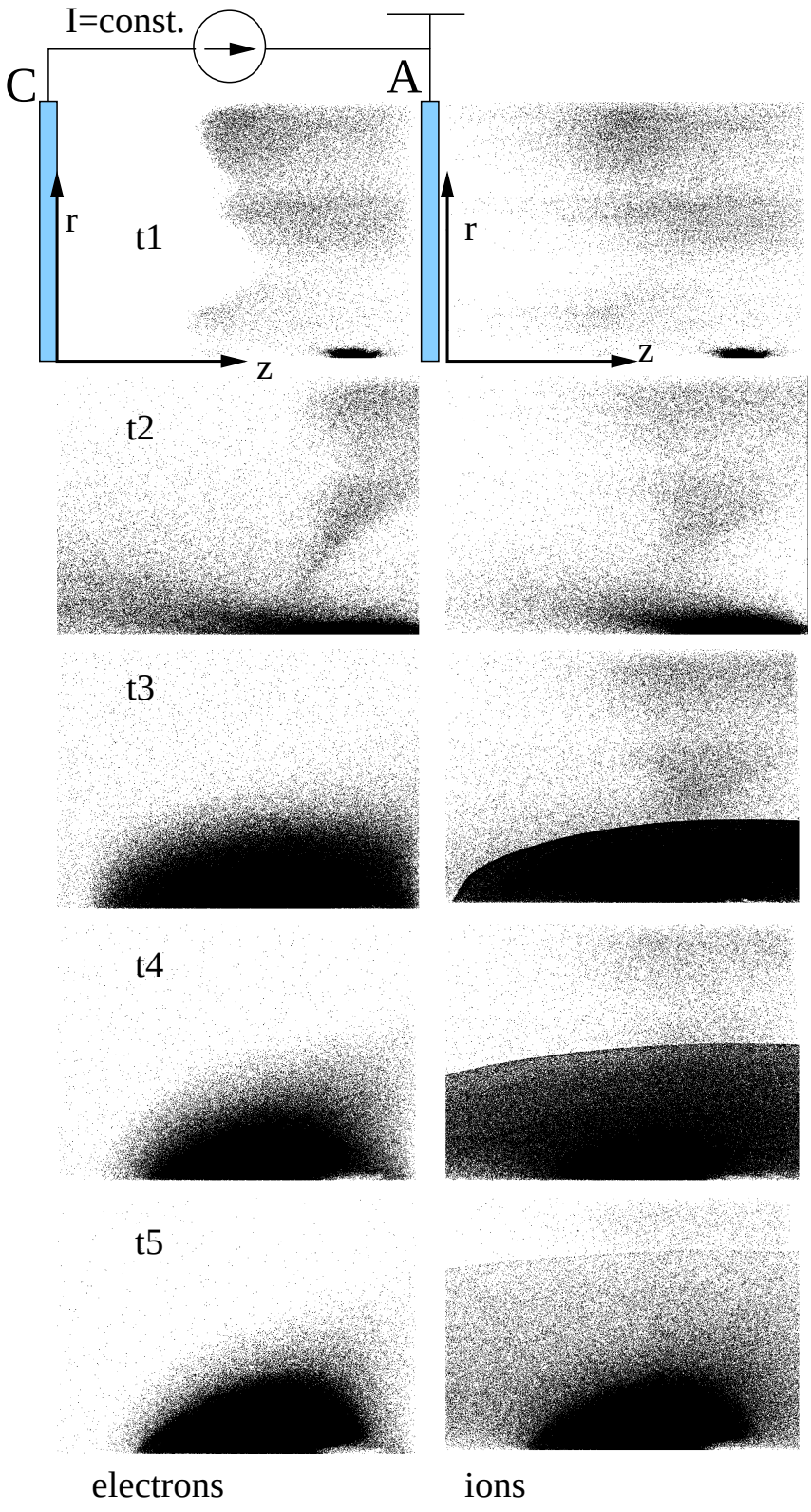

Figure 6.1: Number of electrons (first column) and ions (second column) during several characteristic moments (times) of the discharge development. Due to the azimuthal symmetry only the upper half of the disk cross-section in the central $z-r$ plane is shown and the system is visually stretched in the z-direction for a better visual resolution of the obtained results.

probability, typically 0.2) and accelerated within the plasma sheath into the diode gap, performing there its own avalanche.

The simulation results in Fig. 6.1 are presented by plotting the "snapshots" (images capturing particle positions in the system at a given time) of electrons (first column) and ions (second column) during several characteristic moments t_1 - t_5 of the discharge development, as indicated in Fig. 6.2a. Fig. 6.2a displays the total number of ions and electrons originating from the volume ionisation as a function of time. Secondary electrons are mainly delivered from that localised part of the cathode that is most frequently impacted by ions originating from the nearest local plasma-bunch. Such a "normal" situation appears after the discharge reaches the time t_1, when the ion-rich plasma "attacks" the cathode. Then the cathode "spot" spreads over the cathode (times t_4, t_5 and later). Before that time, strong electron and ion particle current bursts can be obtained. Since the total external current $I = 0.01A$ should be conserved it follows that extreme displacement currents play a role that compensates the particle (conductive) currents. Unlike 1D simulations [79] where the displacement currents are aligned in one direction [80], in the present situation, obviously, internal electric and kinetic 2D effects, field-particle-field interaction, play a special role. Namely, it is expected from the trend of currents and fields that a steady-state situation is established during a characteristic ion-flight time, which can be estimated from $t \sim d_D/u_i$ to be of the order of $10^{-7}s$. It should be noted that with so many particles in the system, such a time (for reaching the steady-state) would be difficult to reach using the present method and reaching the steady state exceeds the scope of the present investigation.

6.2 Results of numerical simulations

At each time step during the simulation run, a huge number of relevant data (results) are saved into "dump" files for post-processing. It is clear from the time-history in Fig. 6.2 that there are stages in which the electron or ion dynamics dominates the diode's internal behaviour, while the external circuit at that stage *temporarily* does not play an important role (could be temporarily disconnected). The same holds for the secondary electrons. Namely, the total ion current at the diode plates, after time t_1 is of the order of $10^3 \gg I = 0.01A$. The same as with the internal local potential at time t_2, where its value is of the order of $\Phi \sim 10^6 V$, which is even considerably above the diode bias voltage ($V_{Cathode} \sim 10^5 V$). An instant power accumulated within the diode gap during the ion-dominated current stage (t_2) is thus of the order of several GW. During the ion-dominated stage (i.e., $t_1 < \Delta t < t_3$, approximately $0.5ns$) the energy stored within the plasma can be crudely estimated to be of the order of 1 Joule.

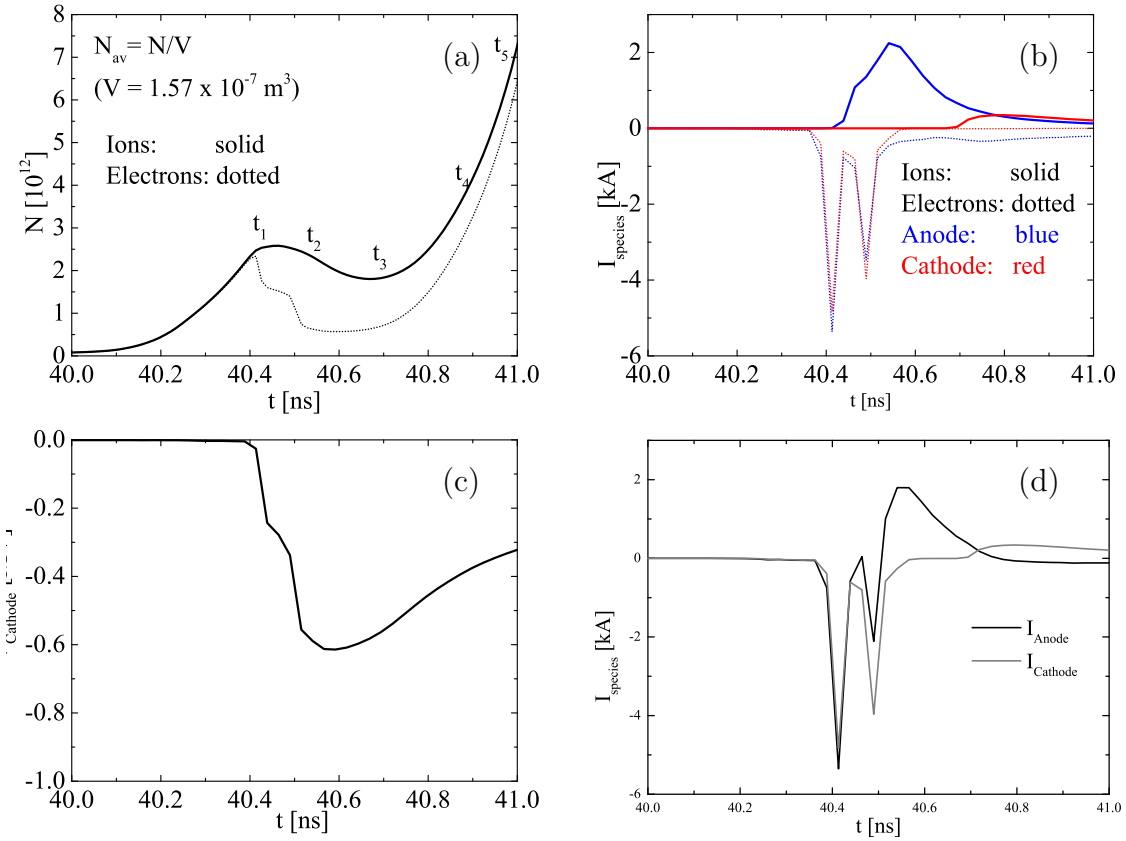

Figure 6.2: Total number of ions and electrons (a), ion and electron conduction electric currents to cathode and anode (b), cathode potential (c) and total conduction electric current at electrodes.

Since the order of magnitude of the above quantities is known, it is necessary to perform a detailed analysis of the "macroscopic" behaviour of the relevant quantities, i.e., the moments of the velocity distributions (densities, average random and directional velocity components and related fluxes, energy and heat fluxes components, and the distribution of the scalar and vector fields components). Here, it is necessary to first look into the distributions of the electrostatic field values (Fig. 6.3), presented via its radial $E_r(r,z)$ and axial $E_r(r,z)$ component distributions, at times t_3 and t_4.

For estimating the displacement current density distributions defined as

$$j_{D,z} = \varepsilon_0 \frac{\partial E_z}{\partial t}(z,r,t) \quad \text{and} \quad j_{D,r} = \varepsilon_0 \frac{\partial E_r}{\partial t}(z,r,t)$$

a crude (post-processing) approximation

$$j_{D,r,z}(z,r) = \varepsilon_0 \frac{E_{r,z}(z,r,t_4) - E_{r,z}(z,r,t_3)}{(t_4 - t_3)}$$

and the values of the displacement current distributions from Fig. 6.3 were used.

The results plotted in Fig. 6.4 show that the local magnitudes of both the radial and axial displacement current densities take values of the order of $10^7 A/m^2$. Since

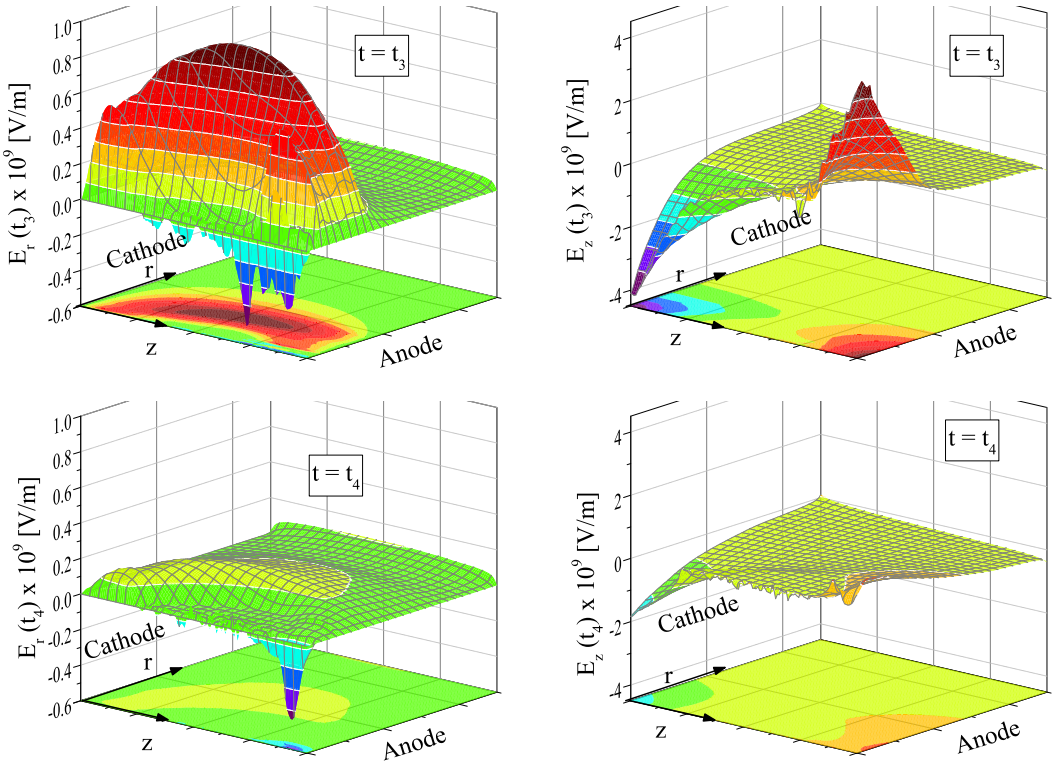

Figure 6.3: Profiles of electric fields $E_r(z,r,t)$ (first column) and $E_z(z,r,t)$ (second column) at times t_3 (first row) and t_4 (second row).

the characteristic diode surface is of the order of $10^{-4}m^2$ it turns out that local displacement currents of the order of $10^{11}A$ could be recognised as high as the conduction currents diagnosed at the boundaries.

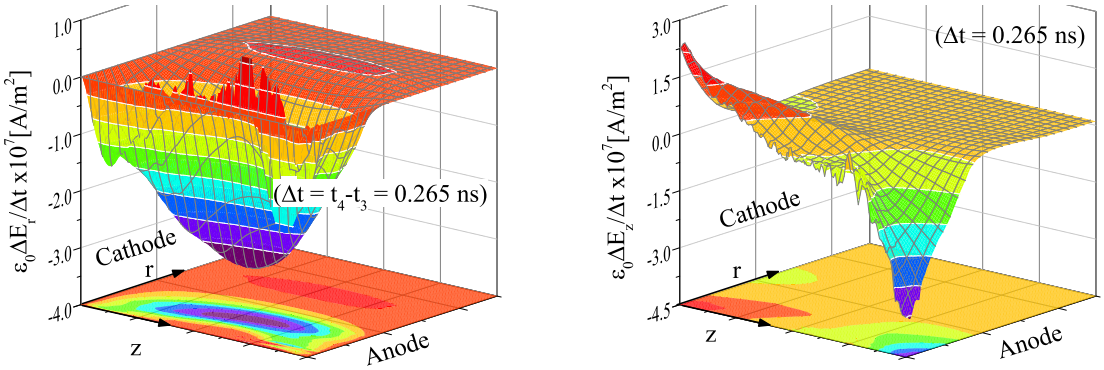

Figure 6.4: Estimation of radial and axial displacement current density distributions $\varepsilon_0 \partial E_r(z,r,t)/\partial t$ and $\varepsilon_0 \partial E_z(z,r,t)/\partial t$ in (z,r)-plane, done within the time-interval from t_3 to t_4.

The described estimations demonstrate explicitly the same orders of magnitudes of conduction and displacement and indicate that the simulation results may perfectly satisfy the electric current continuity $\nabla(j_e + j_i + \varepsilon_0 \partial E_r(z,r,t)/\partial t) = 0$ through-

out an arbitrarily small (in the numerical sense) closed surface, i.e., that there is no reason to doubt that the results and related phenomena are *globally* physically correct, up to an arbitrary constant $\nabla(I/S_D)$ where I is in this case our external current.

However, *inside* the diode the three currents from the continuity equation could be *in principle* distributed over a surface in infinite numbers of detailed variations. The presented example, however, does not seem to be quite arbitrary. Namely, the shape of the radial displacement of the current density in Fig. 6.4 (left-hand graph) is obviously a rather well localised *torus* and it is not immediately evident with which component of the conduction current the continuity is satisfied. At the moment we can only plot our estimated $\varepsilon_0 \partial \vec{E}(z, r, t)/\partial t$ vector field (Fig. 6.5), indicating an instant converging of the huge displacement current towards the toroidal axes. For satisfying the continuity current over an arbitrary surface with each position of the torus a *complete phase-space information of particles should be extracted and post-processed*, and it does not seem that the available PIC codes are properly equipped for this task. In any case, the presented simulation clearly indicates that a rather well self-organised torus-like global plasma-structure has some influence on the simulation, through which parameters and to what extent is a task for future research.

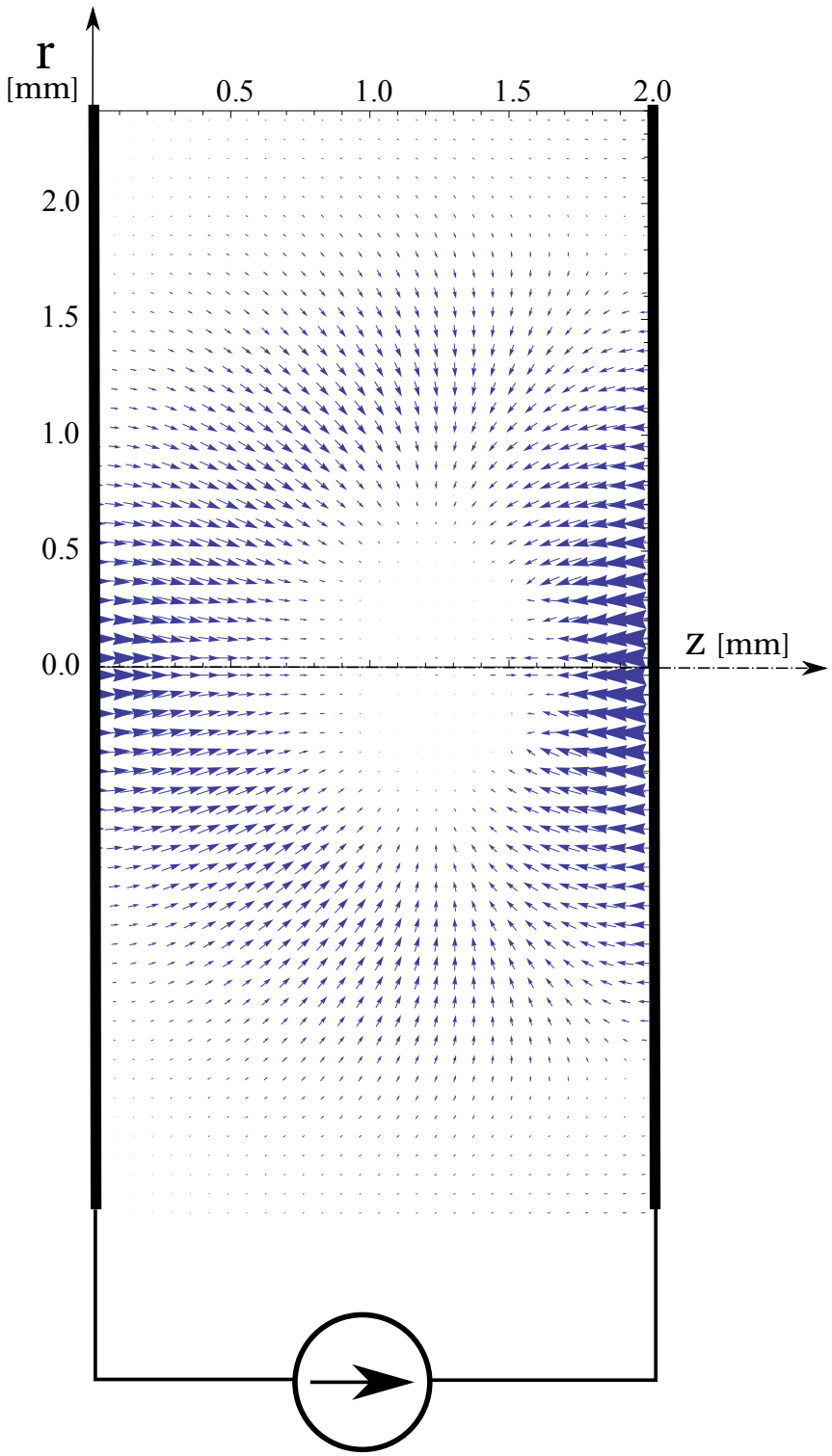

Figure 6.5: Approximate $\varepsilon_0 \partial \vec{E}(z,r,t)/\partial t$ vector-field (between times t_3 and t_4).

Chapter 7

Discussion and conclusion

This thesis presents an overview of the existing research on diode systems and the author's own research on the possibility of using the gridless treecode method in diode-systems research. The gas-discharge systems that are presented as part of the research in this thesis can be distinguished by many physical parameters, with the most important ones being: system geometry, layout of the external circuit, working media (type of gas), working regime (pressure and temperature), surface and volume processes (primary and secondary emission, ionisation, elastic and nonelastic collisions of ions, electrons and neutrons) and gas ionisation level.

The main objective of the thesis was to research conditions that enable the creation of a virtual cathode in diode systems. The virtual cathode generally does not appear at the same position as the physical cathode and its appearance depends on the primary heating (emission) or secondary processes, such as a strong electric field (Fowler-Nordheim effect) or ion neutralisation on the cathode. The exact conditions for the virtual cathode's appearance differ from various diodes and are influenced by the diode's main usage. The research was focused on diode use where the plasma is formed in the diode, either intentionally or due to the "failure" of the diode when an external gas breaks into the system. A large number of simulation-parameter combinations can result in the formation of a plasma in the system and from all possible combinations, the following most common scenarios are presented in the thesis: diode with a vacuum inside (zero-pressure system), a noncollisional plasma (relatively low-pressure system) and a gas-discharge tube (relatively high-pressure system). The model of the discharge tube with different gas pressures, either with of without the presence of a plasma in the system, was used to conduct the research on these three scenarios. In the majority of cases the steady state is not achieved, but we can observe oscillations of the volume distributions for most parameter combinations, which are also transferred to an external circuit. These oscillations are the result of a virtual cathode forming, and the simulation results show that the kinetic-

simulation codes used in simulations are not able to amply describe the transient states of the system. This is even more clearly presented in systems where a plasma is present. For kinetic-simulation codes based on the Particle-In-Cell (PIC) method, one has to use more fine computational grids to adequately describe the simulation quantities (states) in areas where high gradients are present, which eventually results in longer simulation times. To overcome the limitation of the PIC method, a new gridless treecode (TC) method is presented. It was already used and proven in other fields (e.g., astronomy), but is relatively new in the field of charged-particle simulations.

The thesis includes four simulation cases in total, where the first two cases present a comparison of the PIC and TC methods for various simulation cases and system configurations, the third case is focused on defining the plasma-sheath boundary and the fourth case on a more complicated geometry (2D system) and high gradients. The first comparison of the PIC and TC methods was made in a vacuum system without ionised gas or plasma and with diode electrodes at the same potential (shortcut diode). A comparison of the results from both methods shows a good match and the treecode method presents a good alternative for the currently widely used PIC method. The second comparison was made in a geometrically similar system, but with biased electrodes having an arbitrary (and variable) potential difference between the electrodes, and with thermal emission of the particles from the cathode. The results of both methods are compared with the results of the theoretical (semi-approximative) method and show a good match in areas with low-profile gradients. In areas with high potential gradients, a comparison of the results shows a discrepancy between the PIC and TC results. Surprisingly, the results of the TC method show some nonlinearities in the potential profiles in areas with low potential gradients, for which there is no explanation at the moment.

The third case presents a system where a sufficiently high particle ionisation causes the formation of a collisionless plasma via a complicated scenario that could be observed only in the transient regimes. The theoretical model is also complicated and only an approximative model is available. The focus of the research was on defining the position of the boundary between the plasma (the middle of the system) and the sheath (the narrow zone at the system wall). Defining the position of the boundary is a rather important task as it represents the boundary condition for simulations of the core of the system, which is usually done with fluid-simulation codes, and a plasma sheath, which is usually done with kinetic-simulation codes. The last case presents a more complicated system in the geometrical and physical sense - a highly collisional plasma in a 2D system, where the steady state was not reached due to the large number of particles in the system. The simulations were performed using the 2D PIC simulation code XOOPIC and the results show the presence of extremely high gradients of plasma quantities (e.g., ion density, see

Fig. 6.3). Because the PIC method requires dense grids to describe areas with a high gradient of plasma quantities, the simulation should be performed again with the TC method to compare the results from both the PIC and TC methods.

Simulations with the grid-free treecode (TC) method were made using what are basically development versions of the simulation codes that were written specifically for research on the usability of the TC method for plasma-related simulations. Nevertheless, the simulation results show good agreement with existing and already-proven PIC codes, and also with the theoretical results. The results presented in the thesis indicate that the TC method could be used as an alternative kinetics-simulation method for plasma-related simulations (research) where high gradients are present. This also opens up a wide range of possibilities for developing and updating the simulation codes, either for 1D or 2D systems. The first step of this development was already done with the TC method partially included into the 1D simulation code OOPD1 and its Python-based version PyPD1, both developed in The Plasma Theory and Simulation Group at Michigan State University. The results also indicate that one development should proceed in the direction of improving the description of the external circuits and self-adaptive boundary conditions, to name just a few.

Bibliography

[1] H. Sundar, R. S. Sampath, S. S. Adavani, C. Davatzikos, G. Biros: *Low-constant parallel algorithms for finite element simulations using linear octrees*. V: *SC '07: Proceedings of the 2007 ACM/IEEE conference on Supercomputing*. ACM, New York, NY, USA, 2007, ISBN 978-1-59593-764-3 str. 1–12 doi:http://doi.acm.org/10.1145/1362622.1362656.

[2] S. C. Brown: *Introduction to Electrical Discharges in Gases*. Wiley, New York, 1966.

[3] A. Von Engel: *Ionized Gases*. Clarendon, Oxford, 1965.

[4] M. A. Lieberman, J. Licthenberg Allan: *Principles of Plasma Discharges and Materials Processing*. druga izdaja John Wiley & Sons, 2005.

[5] G. A. Mesyats: *Similarity laws for pulsed gas discharges*. Physics-Uspekhi **49**:10 (2006) str. 1045.

[6] M. M. Pejovic, C. S. Milosavljevic: *The estimation of static breakdown voltage for gas-filled tubes at low pressures using dynamic method*. IEEE Trans. Plasma Sci. **31**:4 (2003) str. 776 doi:10.1109/TPS.2003.815815.

[7] M. Frignani: *Simulation of gas breakdown and plasma dynamics in plasma focus devices*: Phd, University of Bologna, 2007 URL http://amsdottorato.cib.unibo.it/414/1/Michele_Frignani_XIXciclo.pdf.

[8] G. Miley, UlmG., H. Leon, P. Shrestha, H. Hora: *Cylindrical IEC neutron source design for driven research reactor operation*. Journal of Radioanalytical and Nuclear Chemistry **282**(2009) str. 193–197 ISSN 0236-5731 doi:10.1007/s10967-009-0261-x URL http://dx.doi.org/10.1007/s10967-009-0261-x.

[9] T. J. Dolan: *Magnetic electrostatic plasma confinement*. Plasma Phys. Control. Fusion **36**:10 (1994) str. 1539 doi:10.1088/0741-3335/36/10/001 URL http://stacks.iop.org/0741-3335/36/i=10/a=001.

[10] G. Petraconi, H. Maciel, R. Pessoa, G. Murakami, M. Massi, C. Otani, W. Uruchi, B. Sismanoglu: *Longitudinal magnetic field effect on the electrical breakdown in low pressure gases*. Brazilian journal of physics **34**:4B (2004) str. 1662–1666 doi:10.1590/S0103-97332004000800028.

[11] I. Langmuir: *The Effect of Space Charge and Initial Velocities on the Potential Distribution and Thermionic Current between Parallel Plane Electrodes*. Plasma Rev. :21 (1923) str. 419–435.

[12] P. Martin, G. Donoso: *A new Langmuir–Child equation including temperature effects*. Physics of Fluids B: Plasma Physics **1**(1989) str. 247 doi:http://link.aip.org/link/doi/10.1063/1.859098.

[13] N. Jelic, R. Schrittwieser, S. Kuhn: *Revised generalized Child-Langmuir law*. Physics Letters A **246**:3–4 (1998) str. 318 – 324 ISSN 0375-9601 doi:10.1016/S0375-9601(98)00435-6 URL http://www.sciencedirect.com/science/article/pii/S037596019800435.

[14] A. J. Christlieb, R. Krasny, J. P. Verboncoeur: *Efficient Particle Simulation of a Virtual Cathode Using a Grod-Free Treecode Poisson Solver*. IEEE Transactions on plasma science **32**:2 (2004) str. 384–389.

[15] J. Krek, N. Jelić, J. Duhovnik: *Grid-free treecode method in diode simulation*. Nuclear Engineering and Design (2012) doi:http://dx.doi.org/10.1016/j.nucengdes.2012.09.035.

[16] S. Dushman: *Electron Emission from Metals as a Function of Temperature*. Phys. Rev. **21**(1923) str. 623–636 doi:10.1103/PhysRev.21.623 URL http://link.aps.org/doi/10.1103/PhysRev.21.623.

[17] L. Tonks, I. Langmuir: *A General Theory of the Plasma of an Arc*. Phys. Rev. **34**:6 (1929) str. 876–922 doi:10.1103/PhysRev.34.876.

[18] S. A. Self: *Exact Solution of the Collisionless Plasma-Sheath Equation*. Physics of Fluids (1958-1988) **6**:12 (1963) str. 1762–1768.

[19] R. C. Bissell, P. C. Johnson: *The solution of the plasma equation in plane parallel geometry with a Maxwellian source*. Phys. Fluids **30**:2 (1987) str. 779–786 doi:10.1063/1.866328.

[20] V. Godyak, V. Meytlis, H. Strauss: *Tonks-Langmuir problem for a bi-Maxwellian plasma*. Plasma Science, IEEE Transactions on **23**:4 (1995) str. 728–734 ISSN 0093-3813 doi:10.1109/27.467995.

[21] K.-U. Riemann, J. Seebacher, D. D. Tskhakaya, (Sr.), S. Kuhn: *The plasma–sheath matching problem*. Plasma Phys. Control. Fusion **47**:11 (2005) str. 1949–1970 doi:10.1088/0741-3335/47/11/006 URL http://stacks.iop.org/0741-3335/47/1949.

[22] K.-U. Riemann: *Plasma-sheath transition in the kinetic Tonks-Langmuir model*. Phys. Plasmas **13**:6 (2006):063508 doi:10.1063/1.2209928 URL http://link.aip.org/link/?PHP/13/063508/1.

[23] J. E. Allen: *The plasma–sheath boundary: its history and Langmuir's definition of the sheath edge*. Plasma Sources Sci. Technol. **18**:1 (2009) str. 014004 doi:10.1088/0963-0252/18/1/014004 URL http://stacks.iop.org/0963-0252/18/i=1/a=014004.

[24] L. Kos, D. D. T. (sr.), N. Jelić: *Potential profile near singularity point in the kinetic Tonks-Langmuir discharges as function of the ion sources temperature*. Phys. Plasmas (2010), (to be published).

[25] D. D. Tskhakaya, L. Kos, , N. Jelić: *A unified analysis of plasma-sheath transition in the Tonks–Langmuir model with warm ion source*. Phys. Plasmas **21**(2014) str. 073503 doi:10.1063/1.3587112 URL http://scitation.aip.org/content/aip/journal/pop/21/7/10.1063/1.4885638.

[26] D. Bohm: *The Characteristics of Electrical Discharges in Magnetic Fields*. McGraw-Hill, 1949.

[27] E. R. Harrison, W. B. Thompson: *The Low Pressure Plane Symmetric Discharge*. Proc. Phys. Soc. **74**:2 (1959) str. 145–152 doi:10.1088/0370-1328/74/2/301.

[28] P. C. Stangeby, J. E. Allen: *Plasma boundary as a Mach surface*. J. Phys. A **3**:3 (1970) str. 304 doi:10.1088/0305-4470/3/3/017 URL http://stacks.iop.org/0022-3689/3/i=3/a=017.

[29] K.-U. Riemann: *Bohm's Criterion and Plasma-Sheath Transition*. Contrib. Plasm. Phys. **36**:S1 (1996) str. 19–27 ISSN 1521-3986 doi:10.1002/ctpp.19960360105 URL http://dx.doi.org/10.1002/ctpp.19960360105.

[30] J. Krek, N. Jelić, J. Duhovnik: *Particle-in-cell (PIC) simulations on plasma–sheath boundary in collision-free plasmas with warm-ion sources*. Nucl. Eng. Des. **241**(2011) str. 1261–1266 doi:j.nucengdes.2010.04.005.

[31] W. Li, J. Ma, J.-j. Li, Y.-b. Zheng, M.-s. Tan: *Measurement of virtual cathode structures in a plasma sheath caused by secondary electrons*. Physics of Plasmas (1994-present) **19**:3 (2012) str. 030704.

[32] J. S. Townsend: *Electricity in Gases*. Clarendon, Oxford, 1915.

[33] J. S. Townsend, V. A. Bailey: *The motion of electrons in gases*. Phil. Mag. **42**(1921) str. 873–891.

[34] N. Leoni, B. Paradkar: *Numerical Simulation of Townsend Discharge, Paschen Breakdown and Dielectric Barrier Discharges Tehnično poročilo HPL-2009-234* HP Laboratories 2009 URL http://www.hpl.hp.com/techreports/2009/HPL-2009-234.pdf.

[35] P. F. Kurbatov: *The positive-column plasma in low-pressure noble gas d.c. discharge as an integral plasma-field system*. AIP Advances **1**:2 (2011):022115 doi:10.1063/1.3592525 URL http://link.aip.org/link/?ADV/1/022115/1.

[36] N. Jelić, L. Kos, J. Krek, J. Kovačič, T. Gyergyek, A. J. Christlieb, J. P. Verboncoeur: *Ionization front in a gas-filled diode during electrical breakdown*. V: A. Žemva, P. Šorli, I. Šorli (ur.): *49th International Conference on Microelectronics, Devices and Materials*. MIDEM, Kranjska Gora, Slovenia, 2013, str. 109–114.

[37] N. Jelic, M. Cercek, M. Stanojevic, T. Gyergyek: *An investigation of the collisionless discharge in the presence of an electron beam*. J. Phys. D: Appl. Phys. **27**:12 (1994) str. 2487 doi:10.1088/0022-3727/27/12/008 URL http://stacks.iop.org/0022-3727/27/i=12/a=008.

[38] C. Li, J. Teunissen, M. Nool, W. Hundsdorfer, U. Ebert: *A comparison of 3D particle, fluid and hybrid simulations for negative streamers*. Plasma Sources Science and Technology **21**:5 (2012) str. 055019 URL http://stacks.iop.org/0963-0252/21/i=5/a=055019.

[39] J. Hammel, J. Verboncoeur: *DC Discharge Studies Using PIC-MCC Tehnično poročilo* Plasma Theory and Simulation Group, Berkeley 2004 URL http://ptsg.berkeley.edu/~jhammel/report.pdf.

[40] J. Krek, N. Jelić, D. Jože: *Particle-In-Cell (PIC) simulations on plasma-sheath boundary in collision-free plasmas with warm-ion sources*. Nucl. Eng. Des. **241**:4 (2011) str. 1261–1266 doi:10.1016/j.nucengdes.2010.04.005.

[41] J. Barnes, P. Hut: *A Hierarchical O(NlogN) Force-Calculation Algorithm*. Nature **324**(1986) str. 446–449 doi:10.1038/324446a0.

[42] K. Matyash, R. Schneider, R. Sydora, F. Taccogna: *Application of a Grid-Free Kinetic Model to the Collisionless Sheath*. Contributions to Plasma Physics **48**:1-3 (2008) str. 116–120.

[43] P. Gibbon, W. Frings, S. Dominiczak, B. Mohr: *Performance analysis and visualization of the N-body tree code PEPC on massively parallel computers*. Proceedings of Parallel Computing (2005).

[44] N. Jelić, K. Krek, J. Duhovnik: *Theory and simulations of a thermionic emissions in a plain diode*. V: *Plasma Science (ICOPS), 2013 Abstracts IEEE International Conference on*, zvezek 40, 2013, str. 1–1.

[45] J. Krek, N. Jelić, J. Duhovnik: *Grid-Free Treecode Method in Particle-In-Cell (PIC) Simulations*. Nucl. Eng. Des. **261**(2012) str. 238–243 doi:j.nucengdes.2012.09.035.

[46] C. K. Birdsal, A. B. Langdon: *Plasma Physics via Computer Simulation*. McGraw-Hill, 1985.

[47] C. Li, U. Ebert, W. Hundsdorfer: *Spatially hybrid computations for streamer discharges: II. Fully 3D simulations*. Journal of Computational Physics **231**:3 (2012) str. 1020–1050.

[48] J. P. Verboncoeur, A. B. Langdon, N. T. Gladd: *"An object-oriented electromagnetic PIC code"*. Computer Physics Communications **87**(1995) str. 199–211 doi:10.1016/0010-4655(94)00173-Y.

[49] B. Jeon, J. D. Kress, L. A. Collins, N. Granbech-Jensen: *Parallel TREE code for two-component ultracold plasma analysis*. Computer Physics Communications **178**:4 (2008) str. 272 – 279 ISSN 0010-4655 doi:10.1016/j.cpc.2007.09.003.

[50] S. Pfalzner, P. Gibbon: *A 3D hierarchical tree code for dense plasma simulation*. Computer Physics Communications **79**:1 (1994) str. 24 – 38 ISSN 0010-4655 doi:DOI:10.1016/0010-4655(94)90227-5.

[51] S. E. Olson, A. J. Christlieb: *Gridless DSMC*. J. Comput. Phys. **227**:17 (2008) str. 8035–8064 ISSN 0021-9991 doi:http://dx.doi.org/10.1016/j.jcp.2008.04.038.

[52] J. K. Salmon, M. S. Warren: *Skeletons from the treecode closet*. Journal of Computational Physics **111**:1 (1994) str. 136–155.

[53] J. P. Verboncoeur: *Particle simulation of plasmas: review and advances*. Plasma Physics and Controlled Fusion **47**(2005) str. A231–A260.

[54] J. Tskhakaya, R. Schneider: *Optimization of PIC codes by improved memory management*. J. of Comp. Phys. :225 (2007) str. 829–839.

[55] K. Matyash, R. Schneider, F. Taccogna, A. Hatayama, S. Longo, M. Capitelli, D. Tskhakaya, F. X. Bronold: *Particle in Cell Simulation of Low Temperature Laboratory Plasmas*. Contrib. Plasma Phys. **47**(2007).

[56] K. Matyash, R. Schneider, R. Sydora, F. Taccogna: *Application of a Grid-Free Kinetic Model to the Collisionless Sheath*. Contrib. Plasma Phys. **48**(2008) str. 116–120.

[57] L. Kos, N. Jelić, S. Kuhn, J. Duhovnik: *Extension of the Bissel-Johnson plasma-sheath model for application to fusion-relevant and general plasmas*. PhysPlasmas **16**:9 (2009).

[58] A. J. Christlieb, R. Krasny, J. P. Verboncoeur, J. W. Emhoff, I. D. Boyd: *Grid-Free Plasma Simulation Techniques*. IEEE Transactions on Plasma Science **34**:2 (2006) str. 149–165.

[59] J. Krek, N. Jelić, J. Duhovnik: *Particle in Cell (PIC) Simulations on Plasma-Sheath Boundary In Collision-Free Plasmas With Warm Ion Sources*. Nuclear Engineering and Design **241**:4 (2010) str. 1261–1266 doi:doi:10.1016/j.nucengdes.2010.04.005.

[60] N. Jelić, R. Schrittwieser, S. Kuhn: *Revised generalized Child-Langmuir law*. Physics Letters A **246**:3 (1998) str. 318–324.

[61] N. Jelić, J. Krek: *Self-consistent problem of external circuits with a hot-cathode gas-filled diode, during the transition from high space-charge dominated to temperature-limited regimes. Tehnično poročilo* University of Ljubljana, Faculty of Mechanical Engineering, LECAD laboratory 2013.

[62] L. Tonks, I. Langmuir: *A general theory of the plasma of an arc.* Physical Review **34**:6 (1929) str. 876.

[63] e. R. Harrison, W. B. Thompson: *The Low Pressure Plane Symmetric Discharge.* Proc. Phys. Soc. London **74**:2 (1959) str. 145.

[64] R. C. Bissell, P. C. Johnson: *The solution of the plasma equation in plane parallel geometry with a Maxwellian source.* Phys. Fluids **30**(1987) str. 779.

[65] J. T. Scheuer, G. A. Emmert: *Sheath and presheath in a collisionless plasma with a Maxwellian source.* Phys. Fluids **31**(1988) str. 3645.

[66] P. C. Stangeby, J. E. Allen: *Plasma boundary as a Mach surface.* J. Phys. A: Gen. Phys. **3**(1970) str. 304.

[67] J. E. Allen: *A note on the generalized sheath criterion.* J. Phys. D: Gen. Phys. **3**(1970) str. 304.

[68] K. U. Riemann, J. Seebacher, D. D. Tskhakaya, S. Kuhn: *The plasma–sheath matching problem.* Plasma physics and controlled fusion **47**:11 (2005) str. 1949.

[69] K. U. Riemann: *Plasma-sheath transition in the kinetic Tonks-Langmuir model.* Plasma Phys **13**:6 (2006), 063508.

[70] K. U. Riemann: *The Bohm criterion and sheath formation.* Journal of Physics D: Applied Physics **24**:4 (1991) str. 493.

[71] K. U. Riemann: *Theory of the plasma-sheath transition.* J. Tech. Phys., Special Issue **41**(2000) str. 89.

[72] P. C. Stangeby: *The Plasma Boundary of Magnetic Fusion Devices.* IOP Publishing Ltd, Bristol and Philadelphia, 2000.

[73] S. Kuhn, K. U. Riemann, N. Jelić, D. D. Tskhakaya (sr.), D. Tskhakaya (jr.), M. Stanojevič: *Link between fluid and kinetic parameters near the plasma boundary.* Phys. Plasmas **13**:013503 (2006).

[74] N. Jelić, K. U. Riemann, T. Gyergyek, S. Kuhn, M. Stanojevič, J. Duhovnik: *Fluid and kinetic parameters near the plasma-sheath boundary for finite Debye lengths.* Physics of Plasmas **14**(2007).

[75] V. Vahedi, G. DiPeso: *Simultaneous Potential and Circuit Solution for Two-Dimensional Bounded Plasma Simulation Codes.* J. Comput. Phys. **131**:1 (1997) str. 149 – 163 ISSN 0021-9991 doi:10.1006/jcph.1996.5591 URL http://www.sciencedirect.com/science/article/pii/S0021999196955916.

[76] C. Birdsall: *Particle-in-cell charged-particle simulations, plus Monte Carlo collisions with neutral atoms, PIC-MCC*. Plasma Science, IEEE Transactions on **19**:2 (1991) str. 65 –85 ISSN 0093-3813 doi:10.1109/27.106800.

[77] J. D. Jackson: *Classical Electrodynamics*. druga izdaja John Wiley & Sons, New York, 1975.

[78] J. P. Verboncoeur: *Particle simulation of plasmas: review and advances*. Plasma Physics and Controlled Fusion **47**(2005) str. A231–A260.

[79] J. P. Verboncoeur, M. V. Alves, V. Vahedi, C. K. Birdsall: *Simultaneous Potential and Circuit Solution for 1D Bounded Plasma Particle Simulation Codes*. J. Comput. Phys. **104**:2 (1993) str. 321–328 ISSN 0021-9991 doi: http://dx.doi.org/10.1006/jcph.1993.1034.

[80] B. P. Wood: *Displacement current and multiple pulse effects in plasma source ion implantation*. J. Appl. Phys. **73**:10 (1993) str. 4770–4778 doi:10.1063/1.353841 URL http://link.aip.org/link/?JAP/73/4770/1.

Dodatek A

Slovenski povzetek

A.1 Uvod

Plašč plazme volumsko predstavlja majhen, vendar zelo pomemben del industrijskih, laboratorijskih ali fuzijskih plazemskih naprav, saj se v plašču dogajajo velike časovne in prostorske spremembe parametrov plazme (električno polje, potenciali, itd.). V magistrskem delu je za modeliranje plazemskega plašča in pogojev nastanka virtualne katode uporabljen model planarne diode. S plinom napolnjene diode so skupina naprav, ki je, kljub svoji enostavni sestavi, zgodovinsko gledano med najbolj raziskanimi napravami. Zaradi zmožnosti delovanja v različnih obratovalnih režimih, določenih z geometrijo sistema, uporabljen plin in parametere plina za polnitev komore ter parametrov zunanjega tokokroga, plinski odvodnik ponuja veliko število načinov uporabe: kot eden od osnovnih elementov v elektronskih vezjih, napravah visokih moči, laserjih, proizvodnji novih materialov, vzdrževanju jedrskih reakcij pri proizvodnji izotopov, proizvodnji curka nevtronov in ionov, itd. Napravo navadno sestavljata dve elektrodi (plan- ali osno- paralelni), ki sta od zunanjih vplivov ločeni s komoro v katero sta vstavljeni. Komora je napolnjena s plinom z določenim tlakom, ki je navadno veliko nižji od atmosferskega in ustvarja vnaprej določene pogoje pod katerimi se dogajajo različni pojavi.

A.2 Izvleček vsebine

Procese in stanja v komori, napolnjeni s plinom ali plazmo, je možno popisati na dva (glavna) načina oziroma fizikalna modela: kot tekočino (*fluid model*) ali kot množico delcev (*kinetic model*). Računalniške simulacijske metode, in s tem simulacijske programske kode, lahko za simulacije uporabljajo enega od naštetih modelov ali kombinacijo obeh. Popis pogojev za nastanek navidezne katode zahteva podrobo

poznavanje zunanjih in notranjih procesov v danem sistemu, ki jih je možno določiti le z uporabo simulacij s kinetičnimi metodami (kinetični simuilacijski programi). Taki simulacijski programi (kode) so bili uporabljeni tudi za simuliranje v nalogi predstavljnih primerov.

S primerom planarne diode v 2D (Slika A.3, predstavljena v sklopu zunanjega tokokroga), ki predstavlja simulacijski model za simulacijo s plinom napolnjenega plinskega odvodnika (npr. za protinapetostno zaščito), je bila predstavljena problematika nastanka in okarektirizacija premikalnih tokov znotraj diode. Predstavljena je bila problematika različnih tipov zunanjega tokokroga in vpiv tokokroga na različne delovne režime diode (Slika A.1). S prikazanim primerom, za simulacijo je bila uporabljena simulacijska koda XOOPIC (kinetična koda za simulacije 2D modelov), je bila prikazana zapletenost različnih delovnih režimov diode in potreba po možnosti določitve idealnega tokovnega generatorja za potrebe simulacij. Tega v trenutni simulacijski kodi ni možno preprosto nastaviti.

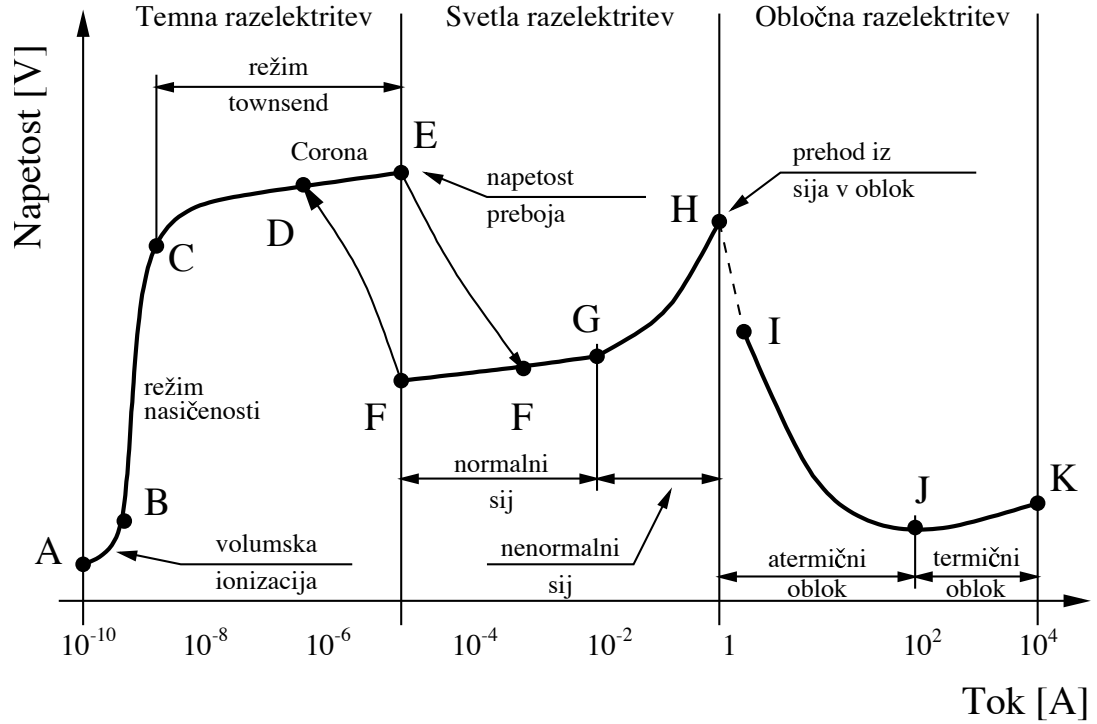

Slika A.1: Predstavitev različnih delovnih režimov plinskega odvodnika.

V diodi nastanejo področja, kjer se pojavljajo veliki gradienti električnih polj, kar predstavlja težavo pri uporabi metode *Particle-In-Cell* (PIC), saj mora biti računska mreža za ustrezen popis stanja v teh področjih ustrezno gosta. S povečanjem gostote računske mreže se, med drugim, podaljša čas računanja. Ena od rešitev "težave" z gostoto mreže, ki je bila uporabljena v nalogi, je predstavljena (in uporabljena) brezmrežna metoda *TreeCode* (TC). Metoda TC temelji na uporabi drevesne strukture zapisa položajev delcev v sistemu v določenem trenutku simulacije. Metoda pred izračunom vrednosti v določenem simulacijskem koraku izdela drevesno strukturo

trenutne razporeditve delcev v sistemu (od tod naziv metode *treecode*, Slika A.2) in na področjih večje gostote v drevesni strukturi ustvari več vozlišč. S tem se porazdelitev delcev v sistemu popiše bolj učinkovito in se tako zmanjša zahtevano število računskih operacij z $O(N^2)$ (metoda z direktnim seštevanjem - *direct summation method*) na $O(Nlog(N))$ (metoda TC).

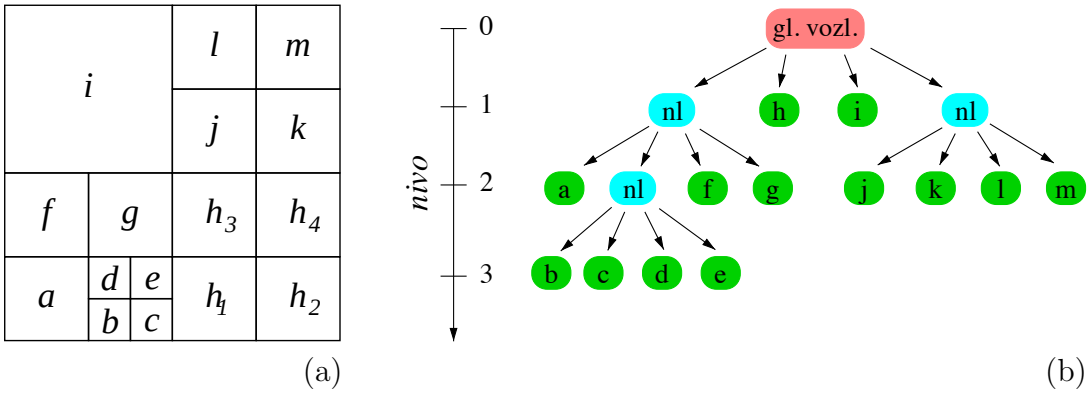

Slika A.2: Primer kvadratne računske domene (a) in predstavitev celic v drevesni strukturi (slika iz [1]).

Bolj zahteven primer diode z visokimi gradienti in s primerjavo z znanimi teoretičnimi rezultati, je predstavljen s primerom termične emisije delcev s katode. Izdelana in predstavljena je primerjava profilov potenciala, pridobljenimi s teoretično rešitvijo (Langmuir [11]), poenostavljeno aproksimativno rešitvijo (*semi-approximation method* - Martin in Donoso [12], Jelić [61]) in rešitve simulacij z metodo PIC (simulacijska koda BIT1) ter metodo TC ([44]). Ujemanje med rezultati prikazanih metod je dobro.

V plazemskih sistemih plašč plazme predstavlja del sistema med jedrom plazme in mejo sistema (steno naprave) in v katerem nastajajo največje spremembe parametrov plazme (npr. električnega polja). Določitev meje med plazmo in plaščem plazme je pomembno vprašanje za področje simulacij *tokamak*[5] naprav, saj omogoča izračun vrednosti parametrov na meji in s tem določitev robnih pogojev za oba dela simulacijskega območja, in sicer: (a) jedro naprave, kjer se navadno uporabljajo modeli za tekočinski popis plazme (*fluid model*) in (b) plašč plazme, ker se za simulacije uporabljajo kinetične programske kode (*kinetic model*). Prikazana je primejava izračunanega profila potenciala nadgrajene verzije programske kode BIT1 (s funckijo izvora delcev $S_i = e^{\alpha\Phi(x)} \approx e^{\Phi(x)}$), teoretičnimi rezultati [57] in originalno programsko kodo BIT1 (s funkcijo izvora delcev $S_i = konst$).

S primerom simulacije 2D sistema, kot je predstavljen v poglavju 6, je predstavljen primer velikih notranjih premikalnih tokov. Uporabljeni simulacijski program

[5]'tokamak' - okrajšava ruskih besed *toroidalnaja kamera magnitnaja katushka*, ki pomenijo toroidno komoro z magnetnimi jedri.

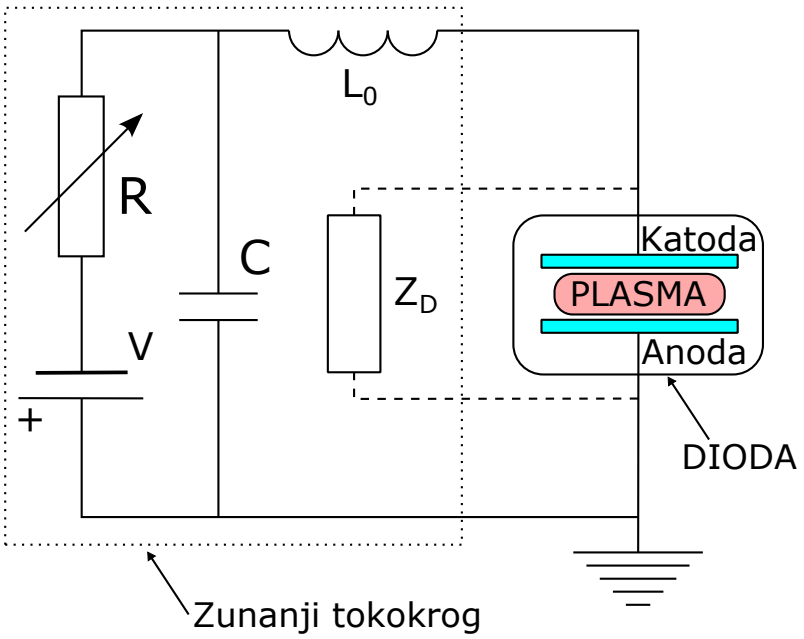

Slika A.3: Predstavitev enostavne planarne diode z zunanjim tokokrogom.

XOOPIC omogoča simuliranje 2D sistemov s kinetično metodo PIC. Predstavljen primer je zapleten tako z dimenzijskega (2D sistem) kot tudi fizikalnega stališča, saj obravnava visoko-kolizijsko (*highly-collisional*) plazmo z velikim številom delcev. Stacionarno stanje pri tem primeru ni bilo doseženo zaradi zapletenosti primera in nakazuje, da bi bila uporaba drugačne metode za primere predstavljenega tipa zelo dobrodošla.

A.3 Sklepi

Naloga obravnava nastanek pojava virtualne katode v enostanih elementih (diode), ki se v različnih velikostih in za različne namene, množično uporabljajo na velikem številu področij - od elektronskih vezij do prednapetostne zaščite in elemetov v laserskih sistemih. Želja za popis pogojev nastanka navidezne katode je pomembna tako s stališča za preprečevanja njenega nastanka kot tudi za primere, ko se želi ustvariti navidezno katodo. V nalogi predstavljeni primeri prikazujejo trenutne sposobnosti kinetičnih simulacijskih programskih kod in hkrati tudi nekatere njihove pomankljivosti. Za posamezne primere so predstsavljene primerjave med analitičnimi, aproksimativnimi in simulacijskimi rezultati (tako za metodo PIC kot tudi TC). Iz predstavljenih rezultatov je razvidno, da metoda TC prinaša prednosti v primerih velikih gradientov in sistemov, v nastopajo velike razlike v gostoti delcev med posameznimi področji v sistemu.

Za simulacije so bile uporabljeni preverjeni simulacijski programi, ki se za izvajanje simulacij v različnih primerih uporabljajo že dalj časa (XOOPIC, BIT1) in za ta

namen razvita simulacijska programa, ki deluje na osnovi brez-mrežne metode TC (*treecode*): LTC in novejša PEG-TC. Čeprav sta uporabljena similacijska programa na osnovi metode TC trenutno v zgodnjih fazi razvoja in daleč od "produkcijske" stopnje razvoja, se je brez-mrežna metoda TC izkazala za primerno za uporabo v primerih visokih gradientov, kar je prikazano v primerih v nalogi.

Po prvih rezultatih se je metoda TC izkazala za obetajočo, kar kaže tudi interes za vključitev metode TC v obstoječe simulacijske kode. Metoda TC (*treecode*) je v zaključni fazi vključitve v priznano 1D simulacijsko programsko kodo OOPD1 (in Python različico PYPD1), ki je bila razvita v Plasma Theory and Simulation Group (PTSG) pod vodstvom prof. Johna Verboncoeurja na Michigan State University (MSU). Za 2D simulacijsko kodo XOOPIC, prav tako razvito v PTSG (MSU), je bila dodana možnosti izračuna gradientov električnih polj (v fazi zapisa rezultatov v datoteke z rezultati), kar se je uporabilo pri simulaciji primera v poglavju 6.

Vita

Janez Krek was born in Ljubljana, Slovenia, on 24th of April 1972. He attended primary school in Pivka, Ljubljana and Grosuplje between years 1978 and 1985. He finished Secondary School for Mechanical Enginnering in 1990 and enrolled in Faculty of Mechanical engineering, University of Ljubljana the same year. He graduated in 1996 with thesis titled "Solid modeller based on CSG and BREP" under supervision of prof. Jože Duhovnik. After graduation he worked in LECAD laboratory as a teaching asisstant in field of Computer Aided Design and as a researcher on various fields. He was member of staff on international project E-GPR between 2002 and 2006 and was involved, with some hiatus, in projects from field of plasma simulations with emphasis on development of computer simulation codes between 2005 and 2013. He is involved in several projects on development of web applications with connection to mobile devices from 2008. He is actively involved in international projects on developing computer simulation codes from field of plasma physics from 2013.

Življenjepis

Janez Krek se je rodil 24. 4. 1972 v Ljubljani. Med leti 1978 in 1985 je obiskoval osnovno šolo v Pivki, Ljubljani in Grosuplju. Srednjo šolo za strojništvo je opravil leta 1990 in se nato istega leta vpisal na Fakulteto za strojništvo Univerze v Ljubljani. Tam je leta 1996 pod mentorstvom prof. Jožeta Duhovnika diplomiral z zagovorom diplomske naloge z naslovom "Prostorski modelirnik z BREP in CSG predstavitvijo". Po končani diplomi je deloval v laboratoriju LECAD kot asistent pri predmetih s področja računalniško podprtega konstruiranja in kot raziskovalec na različnih področjih. Med letoma 2002 in 2006 je sodeloval na projektu E-GPR kot del tehnične ekipe in kot organizator. Med letoma 2005 in 2013 je s krajšimi vmesnimi prekinitvami sodeloval v projektih s področja fizike plazme s poudarkom na razvoju simukacijskih računalniških aplikacij. Od leta 2008 sodeluje na različnih projektih s področja razvoja spletnih aplikacij in baz podatkov v povezavi z mobilnimi napravami. Od leta 2013 aktivno sodeluje v mednarodnih projektih, povezanih z izboljšavami in dopolnitvami simulacijskih aplikacij na področju fizike plazme.

Author's statement

The present Master Thesis, or Dissertation, is an extended written treatise that presents original results and interpretations of a unique investigation by the degree candidate under the supervision of his mentor doc. dr. Leon Kos and his co-mentor prof. dr. Jožef Duhovnik.

Izjava

Magistrsko delo predstavlja rezultate lastnega znanstveno-raziskovalnega dela na osnovi sodelovanja z mentorjem doc. dr. Leonom Kosom in somentorjem prof. dr. Jožefom Duhovnikom.

Janez Krek